

Ocean Engineering

Output of a tidal farm in yawed flow and varying turbulence using GAD-CFD

--Manuscript Draft--

Manuscript Number:	OE-D-22-04888R1
Article Type:	Review Article
Section/Category:	CME article
Keywords:	FloWave; GAD-CFD; Blade Element Momentum; TidalEnergy; Tidal Turbine; Horizontal Axis Turbine
Corresponding Author:	Charles Erzan Badoe, MSc, PhD, MRina University of Swansea Swansea, UNITED KINGDOM
First Author:	Alison Williams
Order of Authors:	Alison Williams Charles Badoe Xiaorong Li Ian Masters
Abstract:	<p>Tidal stream turbine arrays will be subject to a range of flow conditions throughout the tidal cycle and it is important for developers to have an understanding of the impact of these on array performance when planning site design. A generalised actuator disk-computational fluid dynamics model is used to conduct simulations on a three and fourteen turbine array arranged in two different configurations. Performance predictions for the three turbine array in straight flow conditions are in close agreement with previous studies. In the fourteen turbine array, wake recovery to free-stream conditions was better in the modified formation compared to the regular formation and the total power output was increased by over 10%. The influence of yaw angle and upstream turbulence intensity on both array performance was also studied. Strong sensitivity of overall farm power and thrust was found to exist in small variations in yaw angle. However, the overall wake structures were similar irrespective of the yaw angle. Simulations of different turbulence intensities showed rapid decay shortly downstream of the inlet. Turbulence intensity had little effect on the thrust and power of the upstream set of devices for the considered TI range but greatly influenced the individual downstream devices.</p>
Suggested Reviewers:	<p>Alex Phillips, Dr Head of MARS Development Group, National Oceanography Centre abp@noc.ac.uk Much of Alexander's work has concentrated on the development of numerical tools to predict the hydrodynamic performance of maritime vehicles and tidal energy devices. This can then be utilised to: reduce power consumption, improve manoeuvrability and be used to develop enhanced control strategies.</p> <p>Rachel Nicholls-Lee, Dr Research Fellow, University of Exeter R.F.Nicholls-Lee@exeter.ac.uk Rachel is a postdoctoral researcher investigating dynamic submarine power cables supporting the EPSRC Supergen ORE Hub. Her research interests lie in the field of fluid structure interactions in relation to marine renewable energy and clean transportation, including:</p> <ul style="list-style-type: none">- Subsea power cable numerical analysis and experimental testing- Novel device and floating platform development (offshore wind, wave and tidal)- Electric and hybrid vessel design

Charles E Badoe

Engineering and the Environment Research Group
Zienkiewicz Centre for Computational Engineering
College of Engineering
Swansea University
SA1 8EN
Email: c.e.badoe@swansea.ac.uk, charlesbadoe@yahoo.co.uk
28th March 2022

To Ocean Engineering Editorial Board

Dear Sir/Madam,

I am writing to submit our manuscript entitled, "Output of a tidal farm in yawed flow and varying turbulence using GAD-CFD," for consideration for publication in Ocean Engineering Journal. This study compares the influence of yaw angle and upstream TI (turbulence intensity) on tidal stream array performance. A generalised actuator disk-computational fluid dynamics (GAD-CFD) model is used to conduct simulations on a three and fourteen turbine array arranged in two different configurations. Firstly, simulations of both arrays are conducted in straight flow conditions to understand the hydrodynamics around devices and evaluate their performance. The influence of yaw angle and upstream TI (turbulence intensity) on both array performance was then studied.

Performance predictions for the three turbine array in straight flow conditions are in close agreement with previous studies. In the fourteen turbine array, wake recovery to free-stream conditions was better in the modified formation compared to the regular formation and the total power output was increased by over 10%. Strong sensitivity of overall farm power and thrust was found to exist in small variations in yaw angle. However, the overall wake structures were similar irrespective of the yaw angle.

Finally, simulations of different turbulence intensities showed rapid decay shortly downstream of the inlet. In all arrays, turbulence intensity had little effect on the thrust and power of the upstream set of devices for the considered TI range but greatly influenced the individual downstream devices.

This manuscript describes original work and is not under consideration by any other journal. All authors approve the manuscript and this submission. Thank you for receiving our manuscript and considering it for review. We appreciate your time and look forward to your response.

Sincerely

Charles Badoe

Highlights of paper entitled “Output of a tidal farm in yawed flow and varying turbulence using GAD-CFD”

Authors: Charles E. Badoe, Xiaorong Li, Alison J. Williams and Ian Masters

Highlights

- Presented is a new GAD-CFD model for simulating tidal arrays subject to yawed inflow as well as various upstream turbulence.
- Strong sensitivity of tidal-farm power exists even to small variations of inflow direction.
- Yaw has minimal effect on the individual wakes.
- Turbulence intensity helps in recovery of axial velocity in the wake.
- Results can help understand/improve array configurations.

Declaration of interests

The authors declare that they have no known competing financial interests or personal relationships that could have appeared to influence the work reported in this paper.

Reviewer #1: Comments addressed

We thank the reviewer for the positive and constructive comments.

1. 3.1: In line 21-22, the authors state “However, few works have been reported on tidal turbines under yaw conditions”. However, In fact, there are many researchers studying this question, Note that although some researchers discuss this question in their papers, they do not add “yaw conditions” to the titles of their papers. therefore, authors should take these work into consideration.

The progress in computational and experimental studies on tidal turbines under yaw condition has been made clear in the manuscript. This can be seen in lines 21-82 of the new version.

3.2: In line 605-607 and line 621-623, Ref. [18] and Ref. [13] seem to be the same.

We thank the reviewer for spotting this and has been corrected.

3.3: In line 53-54, authors use a phrase “energy source model”, should it be “momentum source model” ?

This has been corrected in the new version o the paper. Lines 53-54 now line 65-66 reflect the changes.

2. In line 73-84, authors introduce a new model “GAD-CFD”, however, authors do not clearly explain the difference between the actuator disc model built in OpenFOAM and the GAD model. And according to Ref. [26], the GAD model seem to be a variant of BEM model rather than actuator disc model, the name “Generalised Actuator Disc” is confusing. 4.2 Similarly, in line 111-119, the descriptions about GAD model let me regard this model as the actuator disc model built in OpenFOAM at beginning, and the latter can not generate circumferential flow in the weak and do not need the parameters such as TSR and the design detail of the blade. It may let readers misunderstand the method and thus question the reliability of this study.

Momentum source term approaches to modelling turbines (of which BEM-CFD is a part) can provide a good estimate of turbine power and thrust. These models provide an approximation of the downstream wake and this is where the estimates vary. Actuator disks models are the most simple to set up, but do not impart swirl on the wake. BEM-CFD models correctly predict swirl, but as the effect is rotationally averaged, cannot produce a tip vortex. Actuator line approaches show a tip vortex and the characteristic corkscrew wake pattern. In all cases, the tip treatment is important for performance and wake extent; performance losses and creation of turbulence in the wake edge must both exist and be numerically consistent. With this in mind, the GAD-CFD model includes new improved features such as a more concise downwash distribution computation, variation of foil section, application of tip radius correction, variation of lift/drag curves with Reynolds number and surface roughness. The use of analytical methods to successfully and effectively predict the distribution of lift towards the tip of finite wing, have been demonstrated to produce reasonable estimates of thrust and power [24]. Allowing for the variation of foil section shape within the model adds to the refinements including the distribution of forces along the foils. This helps produce slightly better characteristics closer to the rotor hub, and

also improved prediction in the stall region of the TSR range. A more detailed description of the GAD-CFD model including the extended downwash distribution method and coupling strategy to OpenFOAM's "simpleFoam" solver/validation is presented in reference [24] and [25]. This has been included in the new version of the paper in lines 103-118 and lines 138-146.

4.3 Authors should give more information about the boundary layer mesh.

The GAD-CFD approach do not model the actual turbine geometry but uses momentum source terms to represent the turbine. Details of the grid was given in lines 176-189 of the old version, now lines 204-224 of the new version.

4.4 Authors should declare the solver they used

The GAD-CFD has been implemented in OpenFOAM CFD steady state solve 'simpleFoam'. This has already been discussed in lines 142-151 of the old version, now lines 138-146 in the new version.

3. 6.1 The structure should be improved. The consistency of this paper seems to be weak. To some degree, it may be better to let the two cases correspond to two first class heading respectively. Then, the case descriptions and the results of the same cases should be under the same first class heading.

The structure and consistency of the paper has been improved as requested by the reviewer.

4. In line 305-306 and line 338-342, the decrease in CP due to the misalignment seem to be too large.

An under prediction of power was observed in the CP curve as well as slight over prediction of thrust in Figure 4 in straight flow, $\beta = 0^\circ$ and this could increase in yaw. The GAD-CFD model only reports thrust acting directly on the rotor, thus a correction needs to be calculated considering the fluid drag acting on the assembly. This issue has been examined in [24], [30] and demonstrates good correlation for the combined results of thrust. RANS based models including the GAD- CFD model are known to under-predict how much of the energy exerted on the turbine will be converted into rotation on the blades and hence useful power. This has also been reported by [35]. With this in mind the power characteristics due to the misalignment correlates well and show similar trends to other yawed flow investigations [10].

Reviewer #2: Comments addressed.

We thank the reviewer for the positive and constructive comments.

1. This article has a lot of space and charts to analyze the impact of turbulent flow, but the introduction needs to see the summary of such research; readers can not rely on the research background to think about the necessity of turbulent flow research. Yawed inflow has been a research direction for nearly 10 years. The author only gave three application examples of actuator line approaches in the CFD review link, but the logic needs to be clarified. As far as I understand, the three examples are not the progress of the research method, but if It is to deepen the understanding of physical phenomena, the conclusions of the three studies need to be described in the introduction part.

The examples given by the author on turbine modelling was to deepen the understanding of physical phenomena. As requested by the reviewer, the conclusions of these studies have been added in the introduction in lines 65-82 of the new version.

2. There are doubts about the setting of experimental conditions. One of the article's conclusions is that the stagger configuration can enable tidal arrays to obtain higher power. However, the two configurations for comparison do not control the same layout area. Compared with the regular one, the stagger configuration expands the width of the tidal field from 3D to 4D, and the length expands from 30D to 38D. Such an experimental setting may reduce the convincingness of the conclusion. Please explain to the author.

The numerical simulation work was first compared with physical tank testing at $\beta = 0^\circ$ for a three turbine arrangement and then additional simulation carried out at $\beta = 4^\circ$ & 8° to study yaw effects. Based on the findings of the three turbine arrangement, the GAD-CFD was used to simulate a full-scale 14-turbine array in varied configuration at $\beta = 0^\circ$, 2° and 8° to understand the performance of the individual devices within the array and the hydrodynamic flow structure between rotors. No physical tank testing was conducted for the full-scale 14 rotor array in the two configurations. First, a standard hypothetical staggered arrangement of four rows with constant lateral and longitudinal spacing of 3.0 diameters and 10.0 diameters respectively (regular formation), was modelled. Then the array layout was altered based on observations from the evaluation of the influence of spacing between devices on performance in our earlier work in [29]. Both configurations were simulated in the same computational domain and the results for $\beta = 0^\circ$, 2° and 8° showed the total power output to be higher in the modified array compared to the regular one. It is important to stress that each of the results have been obtained using a fixed TSR and a time averaged representation of the flow. It is likely that using the local TSR's at the turbines as well as a transient model could influence the results.

3. For the three turbine array, it is mentioned in the article that the actual turbulence intensity of the incoming flow at the front turbine is 7%, 10%, and 10.5%, which is very important for readers to understand the actual working conditions. After all, in actual engineering, the measurement is also The intensity of turbulence at the installation location. In the fourteen-turbine array case, the actual turbulence intensity of the front turbine also needs to be explained.

In the physical tank testing experiments for the three turbine array, there was no facility to control the turbulence intensity of the currents generated and was around 7% for the flow velocity used in the experiments. This is approximately representative of some real world tidal sites for periods of fast flows [26].

As already stated, there was no physical tank testing for the 14 turbine arrangement. The turbulence intensities used at the inlets were 1%, 5% and 10%. These low values of turbulence intensities are applicable here as the turbine arrays are placed in a wide channel and therefore only extract a small fraction of the energy available to them. Future large-scale generation will undoubtedly require the deployment of hundreds of devices at high-energy locations. A couple of lines have been put in the paper to make this clear in lines 192-194 and 355-357 of the new version.

4. For lines 18-22, the author calculated C_p data are 2.0%, 4.0%, 3.0%, and 5.0%. It may be a coincidence, but please confirm that the calculation results are correct.

The overall power was reduced by 3.0% and 5.0% for $\beta = 4^\circ$ and 8° respectively compared to the $\beta = 0^\circ$ case. Additionally, the thrust also reduced by 2.0% and 4.0% for $\beta = 4^\circ$ and 8° respectively compared to the $\beta = 0^\circ$ case. This has been made clear in lines 261-264 of the new version.

5. For lines 40-43, "A possible reason could be that the blockage by the two upstream turbines straightens part of the flow to the primary turbine", the analysis here is rather vague, and it should be explained based on the velocity composition.

When tidal arrays experience misalignment in flow conditions, the flow of water is no longer aligned with the array but develops a crossflow across the plane of the array. This will alter the thrust and torque as well as changing the effective direction of the turbine race. The net sideforce will vary more than during straight ahead conditions resulting in a decrease in effective inflow angle, especially to the downstream turbine. At the same time the upstream turbines can also block and straighten the flow to the downstream turbine, leading to a recovery in effective inflow angle to the downstream turbine. Lines 40-43, now 278-285 has been modified to reflect this.

6. For lines 471-472, power and thrust are different research scopes, they are affected by yaw inflow angle, so there is no need for comparison.

Comments addressed. Lines 471-472 now line 498 in the new version.

7. For lines 485-486, "the overall farm power of the modified array was increased by over 10%.

"What conditions should be stated, is all yawed inflow and TI can be increased by 10%?"

Compared to the regular staggered configuration at $\beta = 0^\circ$, the total power output of the modified array was increased by over 10%. Wake recovery to freestream was also better in the modified formation compared to the regular staggered configuration. This has been made clear in lines 510-513 of the new version.

8. The solid lines should be also illustrated on the Figures 18-19.

As suggested by the reviewer, the solid lines in Figures 18-19 have been illustrated.

9. I found some minor mistakes in the language. Please remember to correct them, for example, "the influence of yaw in the is" at lines 35-36; "as a results of" at lines 50-51.

We thank the reviewer for spotting this. We have corrected them in the new version.

Output of a tidal farm in yawed flow and varying turbulence using GAD-CFD

Charles E. Badoe, Xiaorong Li, Alison J. Williams[†] and Ian Masters

Energy and Environment Research Group, Zienkiewicz Centre for Computational Engineering, College of Engineering, Bay Campus, Swansea University, SA1 8EN, Wales, UK.

[†] *Corresponding author: alison.j.williams@swansea.ac.uk*

Abstract

Tidal stream turbine arrays will be subject to a range of flow conditions throughout the tidal cycle and it is important for developers to have an understanding of the impact of these on array performance when planning site design. A generalised actuator disk-computational fluid dynamics (GAD-CFD) model is used to conduct simulations on a three and fourteen turbine array arranged in two different configurations. Firstly, simulations of both arrays are conducted in straight flow conditions to understand the hydrodynamics around devices and evaluate their performance. Performance predictions for the three turbine array in straight flow conditions are in close agreement with previous studies. In the fourteen turbine array, wake recovery to free-stream conditions was better in the modified formation compared to the regular formation and the total power output was increased by over 10%. The influence of yaw angle and upstream TI (turbulence intensity) on both array performance was also studied. Strong sensitivity of overall farm power and thrust was found to exist in small variations in yaw angle. However, the overall wake structures were similar irrespective of the yaw angle.

Finally, simulations of different turbulence intensities showed rapid decay shortly downstream of the inlet. In all arrays, turbulence intensity had little effect on the thrust and power of the upstream set of devices for the considered TI range but greatly influenced the individual downstream devices.

Keywords: FloWave, GAD-CFD, Blade Element Momentum, Tidal Energy, Tidal Turbine, Horizontal Axis Turbine

1
2
3
4
5
6
7
8
9
10 **1. Introduction**

11 Tidal stream power generation is currently undergoing rapid progress-
12 ing as a reliable form of renewable energy due to the predictability of tidal
13 periods and magnitudes [1]. A number of sites across the world are being
14 identified and tidal current turbines installed in small arrays to generate and
15 export electricity to local networks [2]. However, a lot of the sites that have
16 been identified for installation of these devices exhibits some degree of mis-
17 alignment in incident flow, more especially in nearshore environments where
18 bathymetric and seabed frictional effects are significant. Misalignment in
19 incident flow or yawed inflow may also occur due to turbine support struc-
20 tures and the presence of upstream bluff bodies [3]. When a tidal current
21 turbine experiences misalignment in incident flow or yawed inflow, the flow
22 of water is no longer aligned with the turbine and crossflow is developed
23 across the turbine plane. This will alter the turbine’s thrust and power as
24 well as changing the effective direction of the turbine race. The net side-
25 force due to the turbine will vary more than during straight flow conditions.
26 Wake behaviour will also vary compared to straight flow conditions. Yaw
27 misalignment effects therefore play an important role and quantification of a
28 turbine’s performance and wake details under such condition is essential for
29 the design layout of a tidal farm for maximizing the power output [4].

30 A number of experimental studies have been conducted to improve under-
31 standing of yawed inflow influence on tidal turbines. For example, Galloway
32 et al. [5] studied the power and thrust performance of a scaled tidal current
33 turbine operating at yaw and in waves in a tow tank. The authors observed
34 that less power and rotor thrust was captured by the turbine and resulted
35 in reduced performance as yaw angle increased. Galloway et al. [6] followed
36 on his earlier work by conducting experiments to study the cyclic loading
37 and fatigue effects due to dynamic yaw on a rotor caused by wave-current
38 interaction. They found that yaw angles below 7.5 degrees had negligible
39 effect on the rotor. Maganga et al. [7] conducted experimental studies to
40 quantify the effects of flow characteristics (yaw and velocity gradient) on the
41 performance and loading on a tidal turbine. The authors observed that the
42 turbine’s performance was sensitive to the quality of the incoming flow and
43 a misalignment of a fixed turbine can cause significant losses. Zhang et al
44 [8] studied the effects of a turbine operating under varying yaw conditions.
45 Their results showed that increasing yaw angle results in a decrease in the
46 turbine’s streamwise force and an increase in spanwise force. Velocity distri-
47
48
49
50
51
52
53
54
55
56
57
58
59
60
61
62
63
64
65

1
2
3
4
5
6
7
8
9
10
11
12
13
14
15
16
17
18
19
20
21
22
23
24
25
26
27
28
29
30
31
32
33
34
35
36
37
38
39
40
41
42
43
44
45
46
47
48
49
50
51
52
53
54
55
56
57
58
59
60
61
62
63
64
65

butions also showed that the wake deflection and velocity deficit recovery rate increased at a rate proportional to the yaw angle. Modali et al [9] studied turbine performance and wake deflection within $\pm 15^\circ$ yawed conditions and showed that when an upstream turbine is yawed, the downstream turbine can extract more than 50% higher energy in a staggered layout than in an aligned layout. All of the above experimental work provides an opportunity to evaluate the performance of the tidal devices in a relatively low-cost, controlled laboratory environment, which can also be used to complement and validate numerical models.

Computational fluid dynamics (CFD) has also been used, through a number of approaches to study the performance and wake details of tidal devices under yawed inflow conditions. Each approach has advantages and disadvantages, with the main balance being a trade off between detailed simulation of the physics and the computational time and resources required to achieve a result. At the smallest and most detailed scale, fully resolved tidal current turbine geometry models have been used to provide insight into the development of the wake structures downstream of a device [10], [11], [12]. Turbulence was resolved using either Reynolds-averaged Navier-Stokes [13] or Large Eddy Simulations [14]. However, these approaches require small time steps due to restrictions imposed by explicitly solving the turbine flow, thus placing a high demand on computation. As such, they are not feasible when considering simulation of large arrays of full-scale turbines. In addition, high computational cost restricts simulation of a wide range of incident environmental conditions, which are known, for tidal energy sites, to be highly variable resulting from complex combinations of waves, currents and turbulence. Computations of this nature are often performed using momentum source models.

Momentum source models are able to compute the force distributions along the rotor blades, and determine the overall performance of a turbine. Significantly lower computational requirements and fast processing time can be exploited where many analyses are required. Howland et al. [15] used an actuator disk model, to investigate wake deflections of a turbine under yawed conditions. Their findings suggest that when a turbine is yawed for the benefit of downstream turbines, the curled shape of the wake and its asymmetry must be taken into account since this affects how much of it interacts with the downstream turbines. Baratchi et al. [16] used an actuator line method to study the performance and wake of the tidal turbine in both straight and yawed flow. Their results showed good agreement with the measurements

1
2
3
4
5
6
7
8
9
10 76 published in [17]. Gao et al. [18] coupled an actuator line method to large
11 77 eddy simulations to study the wake characteristics of a turbine under various
12 78 yaw conditions. They showed that wake skew exacerbates the instability of
13 79 the tip vortex and causes the wake region to narrow. At lower yaw angles,
14 80 nacelle vortex radially diffuses and blends with the tip vortex in the far wake
15 81 whilst at higher yaw angles, the nacelle vortex intercepts the tip vortex in
16 82 the near wake due to the different spatial distribution of thrust.

17
18 83 Despite the valuable insight from these experimental and numerical stud-
19 84 ies, there is still a gap in the performance and wake details of tidal current
20 85 turbines in arrays as most of these studies were carried out for either one or
21 86 two turbines. The wake generated by for example, the front set of turbines
22 87 in a large tidal turbine farm can cause disturbance to the rear set of turbines
23 88 in straight flow conditions and significantly increase in angled incoming flow
24 89 conditions [19]. Very large computational resources are also needed to cap-
25 90 ture and understand such flow detail. There are also open questions about
26 91 the wake details, for example, its propagation and extent of recovery in yaw
27 92 conditions.

28
29
30
31 93 One particular area of research which has gained momentum in recent
32 94 years and has been used to compute multiple tidal current turbines in arrays
33 95 is the Blade Element Theory combined with Computational Fluid Dynamics
34 96 simulation techniques (BEM-CFD) [20], [21]. The BEM-CFD models utilises
35 97 radially varying set of turbine blade characteristics, distributed uniformly in
36 98 an axial direction. Hence, computational cells at the same radius from the
37 99 turbine centre have the same properties, however, as the flow varies from cell
38 100 to cell, the resultant forces on the fluid also vary. The model can allow the
39 101 local environment to be simulated providing a comprehensive study of a tidal
40 102 farm and wake at a reduced computational cost [22]. The application of tip
41 103 loss corrections and downwash pertinent to a CFD type model representa-
42 104 tion takes the BEM-CFD approach further. This extension, the Generalised
43 105 Actuator Disk (GAD-CFD), has provided confidence when applied to labo-
44 106 ratory scale flume studies [23]. The GAD-CFD model includes new improved
45 107 features such as a more concise downwash distribution computation, varia-
46 108 tion of foil section, application of tip radius correction, variation of lift/drag
47 109 curves with Reynolds number and surface roughness. The use of analytical
48 110 methods to successfully and effectively predict the distribution of lift towards
49 111 the tip of finite wing, have been demonstrated to produce reasonable esti-
50 112 mates of thrust and power [24]. Allowing for the variation of foil section
51 113 shape within the model adds to the refinements including the distribution

1
2
3
4
5
6
7
8
9
10
11
12
13
14
15
16
17
18
19
20
21
22
23
24
25
26
27
28
29
30
31
32
33
34
35
36
37
38
39
40
41
42
43
44
45
46
47
48
49
50
51
52
53
54
55
56
57
58
59
60
61
62
63
64
65

114 of forces along the foils. This helps produce slightly better characteristics
115 closer to the rotor hub, and also improved prediction in the stall region of
116 the TSR range. The benefit of the GAD-CFD approach, with respect to
117 computational cost, is unequivocal and allows us to move into the realms of
118 array interaction modelling and site design at a more reasonable level of cost
119 [25].

120 In this work, the effectiveness of the GAD-CFD approach in accurately
121 capturing fluid-machine interaction for multiple tidal energy converters sub-
122 ject to yawed flow conditions is assessed. The GAD-CFD model is first used
123 to simulate a three-turbine array in straight flow, $\beta = 0^\circ$, and the results
124 compared with physical tank-testing conducted at the FloWave facility [26],
125 [27], [28]. Additional simulations are then conducted at yawed angles, $\beta =$
126 4° and 8° to study yaw effects. A second simulation is conducted to further
127 assess the performance of the approach, in terms of the capacity to model
128 multiple full-scale turbines in more varied configuration. The current work
129 extends our previous work in [29], [30] to provide a better understanding of
130 the influence of rotor spacing on the hydrodynamics around devices, leading
131 to optimised performance for large arrays.

132 Finally, as turbulence intensity also impacts the fluid-machine interac-
133 tions associated with the turbine energy production, simulations under straight
134 flow conditions with varying incoming turbulence intensities are also per-
135 formed and analyzed. This demonstrates how the GAD-CFD tool can be
136 useful to developers in real projects.

2. Numerical Methodology

2.1. Governing equations

The OpenFOAM toolbox [31] is utilised for the model implementation. The OpenFOAM toolkit provides a range of standard solvers which can be modified for use with the additional turbine physics. The additional GAD source terms are implemented in the steady state Reynolds Averaged Navier Stokes (RANS) “simpleFoam” solver. A more detailed description of the GAD-CFD model including the extended downwash distribution method and coupling strategy is presented in [24-25]. Within the assumption of an incompressible fluid, the set of equations may be written in the form:

$$\frac{\partial \bar{U}_i}{\partial x_i} = 0 \quad (1)$$

$$\frac{\partial \bar{U}_i}{\partial t} + \frac{\partial \bar{U}_i \bar{U}_j}{\partial x_j} = -\frac{1}{\rho} \frac{\partial \bar{P}}{\partial x_i} + \frac{\partial}{\partial x_j} \left(\nu \left(\frac{\partial \bar{U}_i}{\partial x_j} + \frac{\partial \bar{U}_j}{\partial x_i} \right) \right) - \frac{\partial \overline{u_i u_j}}{\partial x_j} + f_i, \quad (2)$$

where x_i represents the Cartesian coordinates (X, Y, Z), U_i is the Cartesian mean velocity components ($\bar{U}_x, \bar{U}_y, \bar{U}_z$) and f_i includes an additional source representing the disc rotor characteristics. The Reynolds stress is $\overline{u_i u_j}$ and must be modeled to close the governing equations by employing an appropriate turbulence model.

The k - ϵ RNG turbulence model [32] has been used for this work. In this model two equations are solved; k represents the energy contained within the turbulent fluctuations, and ϵ represents the dissipation rate of this energy. The equations for the transport of these variables are similar in form to the momentum equations. The model has been credible when applied to flows involving large rotating downstream wakes [33], [34] which is one of the key aspects of the present application. However, the models are also known to sometimes over-predict wake lengths, mainly due to the turbulence dissipation turbulent kinetic energy which can influence the loadings on downstream turbines [35].

3. Case Study 1: Three Turbine Array Turbine

3.1. Turbine arrangements

Using the GAD-CFD model, a three turbine array as shown in Figure 1 is simulated. The hubs of these two upstream turbines are 1 D upstream and

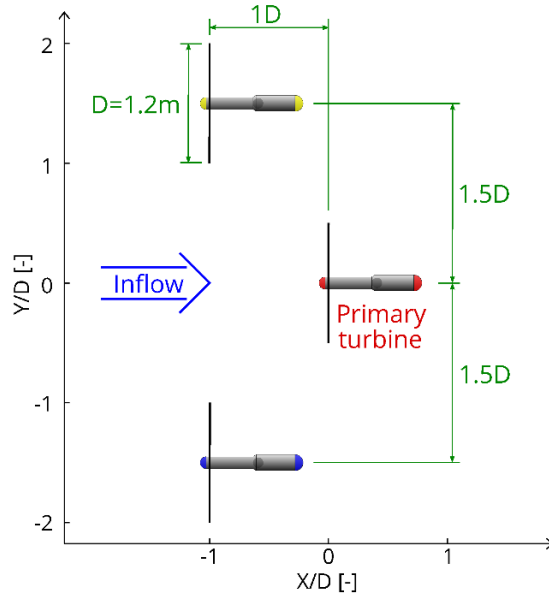


Figure 1: Schematics of the three-turbine array layout (not to scale). Turbine 1 denotes the primary turbine, Turbines 2 and 3 denote the right and left upstream turbines in the inflow direction respectively.

167 1.5 D either side of the primary turbine, giving a transverse separation of 3
 168 D. This configuration was shown in [25] to accelerate the flow experienced
 169 by the rear turbine and improve its performance. Additionally, the front
 170 row being only 1 D in front of the primary turbine, means that the rear
 171 turbine is not in the wake of the front two turbines. The turbines are generic
 172 bed-mounted, fixed-pitch, three-bladed horizontal axis design. The turbine
 173 models are 1:15 scale, corresponding to an 18 m diameter prototype. Table
 174 1 summarizes the principal dimensions of the turbines. Turbine rotational
 175 speed is set to be the same for all turbines, so that they have a tip speed ratio
 176 (TSR), of 7.0 relative to the inlet velocity. The turbine geometries were based
 177 on the NACA63812 and 63815 aerofoil sections and a separate CFD study
 178 was conducted to determine a set of lift and drag curves curves at a range of
 179 Reynolds numbers and turbulence levels required for these sections to use for
 180 this study. The chord-length Reynolds numbers vary between 0.5×10^5 (root)
 181 and 2.5×10^5 (tip). Physical tank testing experiments have been conducted
 182 in straight flow conditions, $\beta = 0^\circ$. Full details of the experiments can be
 183 found in [26].

Table 1: Three-turbine array dimensions

<i>Parameter</i>	<i>Dimension[m]</i>
Rotor diameter	1.2 (1D)
Nacelle length	1.03
Nacelle diameter, hub to tower	0.12
Nacelle diameter, beyond tower	0.16
Hub height	1.0 (0.83D)
Tower diameter	0.102
Distance from rotor plane to tower axis	0.486 (0.4D)

3.2. Domains and boundary condition

The entire flow field was considered as a result of asymmetry of the flow induced by the oblique motion and rotation induced by the turbines. Turbine yaw angle was achieved by keeping the inflow/domain fixed and rotating the turbines as per the required yaw angle. This technique was automated by employing a script which, when called upon, allows rotation of the turbines within the domain to the required yaw angle. The domain size represents the Flowave tank dimensions, see also Figure 2. The nominal inflow velocity of 0.8 m/s was set at the inlet. This corresponds to a full-scale flow speed of 3.1 m/s. Flow rates are set at the inlet vents. In the physical tank testing experiments, the turbulence intensity at the turbine location was recorded to be approximately 7% for the flow velocity used [26]. The tank walls are set to zero velocity and wall functions used for k , ϵ , and nut . The top of the domain is set to a full slip condition representing the open fluid surface. The initial conditions are mapped to the boundary conditions in all but velocity. The initial velocity condition is set to zero. The kinematic viscosity ν of this problem is set to $1.6667e^{-6}m^2.s^{-1}$. No roughness parameter was added and the bottom boundary assumed a smooth wall. Table 2 summarizes the computational parameters adopted for this study. Five flow configurations have been investigated, as illustrated in Table 3.

3.3. Grid Generation

The grids were created utilizing both blockMesh and snappyHexMesh in OpenFOAM. First, an initial structured hexahedral background mesh consisting of a block topology structure was generated which captures the domain extents of thirty metres square and four metres deep. The domain is

1
2
3
4
5
6
7
8
9
10
11
12
13
14
15
16
17
18
19
20
21
22
23
24
25
26
27
28
29
30
31
32
33
34
35
36
37
38
39
40
41
42
43
44
45
46
47
48
49
50
51
52
53
54
55
56
57
58
59
60
61
62
63
64
65

Table 2: Computational Parameters

<i>Parameter</i>	<i>Settings</i>
Computing	Astute Linux Cluster ^a
Mesh type	Unstructured hexahedral
Turbulence model	<i>k</i> - ϵ RNG
Pressure velocity coupling	SIMPLE
y^+ average (nacelle)	30
Grad (U) scheme	Gauss linear
Convergence criteria	RMS residual $< 10^{-3}$

Note: Run type and Parallel run (14 partitions run on $2 \times$ dual core nodes). ^a <http://enhpc-wiki.swan.ac.uk>.

Table 3: Simulation Flow Conditions

<i>Yaw, β ($^\circ$)</i>	<i>Turbulence Intensity, TI (%)</i>
0	15
0	25
0	30
4	15
8	15

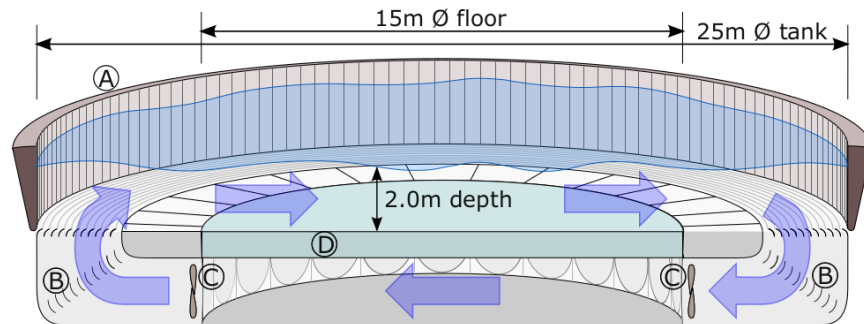


Figure 2: Sectional schematic of FloWave basin showing: (A) wavemaker paddles around circumference; (B) turning vanes and flow conditioning filters; (C) current drive impeller units; (D) buoyant raisable floor (15 mØ) below test area [27].

209 then subdivided using divisions defined in Table 4. With reference to Figure
 210 3, refinement of the mesh around the turbines and wake region is achieved
 211 using the snappyHexMesh utility. The wake region is defined as a cylinder
 212 0.7 metre radius, extending from the rotor to 9 metres downstream, i.e. to
 213 the domain outflow. The refinement level in this region is specified as level
 214 2, the base cell/mesh is subdivided twice in this region (Note 2 in Figure 3).
 215 The rotor assembly and bladebox is set with a refinement level of 5, i.e. Note
 216 5 in Figure 3. The region around the rotor assembly (Note 3 in Figure 3) is
 217 set at level 3 up to 0.1 metres from the assembly. A reasonable level of detail
 218 of the nacelle and support is included in the model as shown in Figure 3.

219 For the mesh independence study an examination of the coefficients of
 220 power, C_P and coefficients of thrust C_T is performed for a single rotor in
 221 straight inflow conditions, $\beta = 0^\circ$. It can be seen in Figure 4 that the
 222 coefficients tend to not change significantly after mesh density G4. Based
 223 on the study, mesh G4 (see Table 4), representing a reasonable compromise
 224 in accuracy and computational cost, was chosen to perform the remaining
 225 studies.

226 3.4. Results

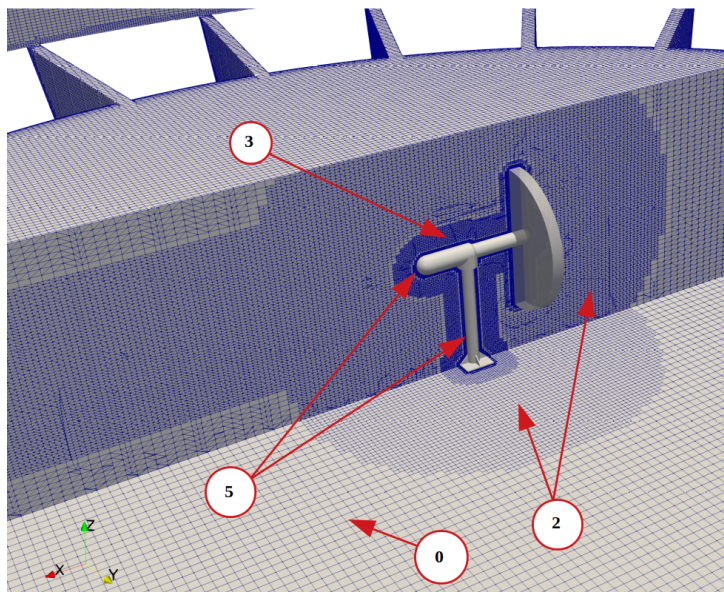
227 3.4.1. Performance at different yaw angles

228 The tidal stream configuration performances at yaw was quantified by
 229 comparing the yaw results with the straight flow cases. Two yawed inflow
 230 cases were considered, i.e. $\beta = 4^\circ$ and 8° . As already pointed out, the turbines
 231 have been fully tested experimentally at $\beta = 0^\circ$ and the results have been

1
2
3
4
5
6
7
8
9
10
11
12
13
14
15
16
17
18
19
20
21
22
23
24
25
26
27
28
29
30
31
32
33
34
35
36
37
38
39
40
41
42
43
44
45
46
47
48
49
50
51
52
53
54
55
56
57
58
59
60
61
62
63
64
65

Table 4: Table of initial mesh subdivisions for the set of meshes studied. The total cell count is post refinement using the snappyHexMesh utility

<i>Mesh</i>	<i>Subdivisions</i>	<i>Total no of cells</i>
G1	100×100×30	95686
G2	200×200×60	766968
G3	300×300×90	2590032
G4	400×400×120	6146016
G5	500×500×150	11998116
G6	600×600×180	20740456



(a)

Figure 3: Mesh topology generated using a combination of “blockMesh” and “snappy-HexMesh” utilities. Note 0 shows the outer/base distribution of cells, while Note 2 shows the level 2 refinements made in the wake region. Note 3 identifies the assembly area refinement, and Note 5 identifies the level 5 assembly region.

232 included for comparison purpose. Figure 5 demonstrates the performance
 233 of all turbines in the array model in terms of C_P and C_T at $TSR = 7$.
 234 Compared to the experiment, GAD-CFD predicts the thrust and power of
 235 the primary rotor (Turbine 1) within 3.5% and 9.5% respectively for $\beta =$
 236 0° . The GAD-CFD model only reports thrust acting directly on the rotor,

1
2
3
4
5
6
7
8
9
10
11
12
13
14
15
16
17
18
19
20
21
22
23
24
25
26
27
28
29
30
31
32
33
34
35
36
37
38
39
40
41
42
43
44
45
46
47
48
49
50
51
52
53
54
55
56
57
58
59
60
61
62
63
64
65

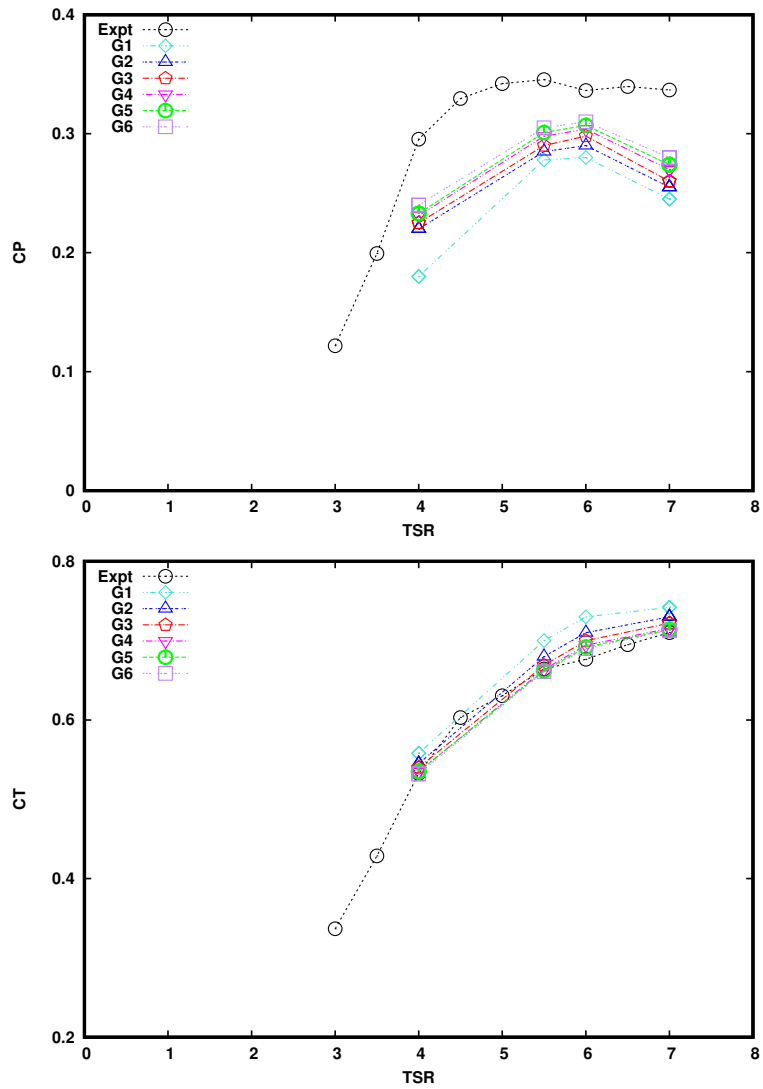


Figure 4: Coefficients of power, C_P (top) and thrust, C_T (bottom) plotted against mesh number from coarsest (G1) to finest (G6).

237 thus a correction needs to be calculated considering the fluid drag acting
238 on the assembly. This issue has been examined in [30] and demonstrated
239 good correlation for the combined results of thrust. RANS based models
240 including the GAD-CFD model are known to under-predict how much of the
241 energy exerted on the turbine will be converted into rotation on the blades

1
2
3
4
5
6
7
8
9
10
11
12
13
14
15
16
17
18
19
20
21
22
23
24
25
26
27
28
29
30
31
32
33
34
35
36
37
38
39
40
41
42
43
44
45
46
47
48
49
50
51
52
53
54
55
56
57
58
59
60
61
62
63
64
65

242 and hence useful power. This has also been reported by [35], [36]. C_P under
243 prediction may also be attributed to variations in local flow directions at
244 the blades and numerical rounding in the model. With this in mind the
245 thrust and power characteristics correlate well and show a similar trend to
246 the observations of the experimental results (see also Figure 4). Compared
247 to the other turbines, the primary rotor (Turbine 1) also produces the most
248 power. This is because it benefits from the accelerated approaching flow
249 from the two upstream turbines (Turbines 2 and 3). Having higher velocities
250 approaching the turbine can result in an increase in the extractable power.

251 The trend in both power and thrust curves for the different angles of
252 yaw are also identical. C_P and C_T decreases as yaw angle increases. This
253 is because as the incoming flow is no longer aligned to the turbine blades, a
254 crossflow is developed across the turbine plane and as the yaw angle increases,
255 the axial component of the velocity reduces, leading to less lift and hence
256 torque. Another problem regarding the reduction in C_P with increase in
257 yaw angle may be attributed to the separation of the nacelle and the flow in
258 the vicinity of the rotor. As yaw increases, the separation at the nose of the
259 nacelle becomes greater. This causes the flow in the vicinity of the turbine to
260 be more turbulent. Lastly, the blockage by the turbines to the flow can be felt
261 upstream, leading to greater deficit in the wake region and a corresponding
262 decrease in power. The overall power was reduced by 3.0% and 5.0% for $\beta =$
263 4° and 8° respectively compared to the $\beta = 0^\circ$ case. Additionally, the thrust
264 also reduced by 2.0% to 4.0% for $\beta = 4^\circ$ and 8° respectively compared to the
265 $\beta = 0^\circ$ case. Figure 6 shows the differences in the wake structure structure
266 for the various yaw angles. There is a slight increase in the skewness in
267 the wake as well as a slight decrease in the recovery distance as yaw angle
268 increases. This has also been reported by [10] at a similar TSR value. As
269 the wake propagates downstream, it also deviates slightly from the direction
270 of yaw.

271 Line samples of the velocities were taken downstream (Figure 7) of the
272 primary rotor to capture the fluid characteristics exiting the array for the
273 different yaw angles. The samples were taken at six x/D locations. Results
274 for the $\beta = 0^\circ$ case demonstrates that the wakefield generated by the array
275 compares well with experimental values. For yaw influence, the profiles are
276 different for turbines 2 and 3 compared to the primary turbine in the near
277 wake, i.e $x/D \leq 2.5$. In turbines 2 and 3, there is a shift in the profiles
278 compared to the $\beta = 0^\circ$ profile. However, for the primary turbine (or tur-
279 bine 1), the profiles show similar behaviour. When tidal arrays experience

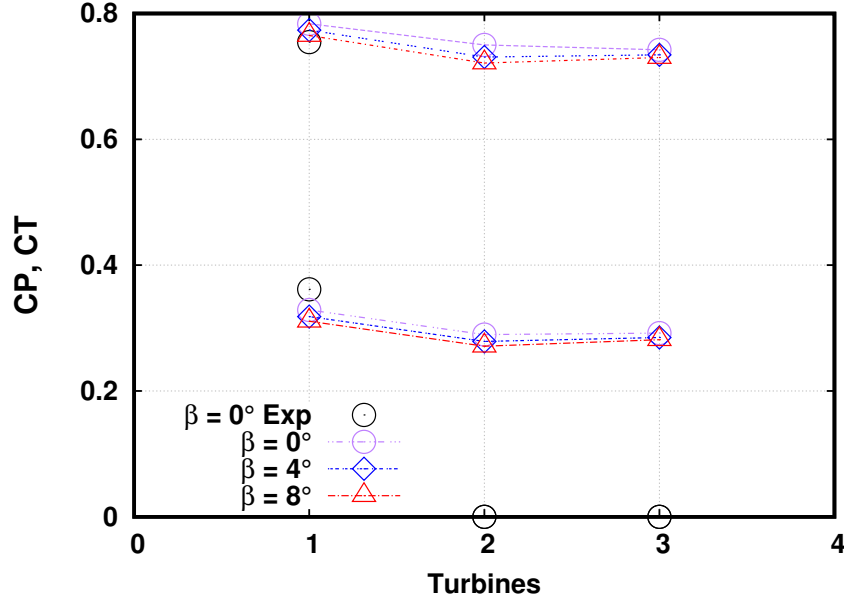


Figure 5: Comparison of coefficient of power C_P (bottom) and coefficient of thrust C_T (bottom) at different yaw angles, $TI = 15\%$, $TSR = 7$.

280 misalignment in flow conditions, the net sideforce will vary more than dur-
 281 ing straight ahead conditions resulting in a decrease in effective inflow angle,
 282 especially to a downstream turbine. At the same time an upstream turbine
 283 can block and straighten the flow to the downstream turbine, leading to a
 284 recovery in effective inflow angle to the downstream turbine. It is possible
 285 that the blockage by the two upstream turbines may have contributed to the
 286 behaviour of the primary turbine profile. Interestingly, for the two upstream
 287 turbines, the plots also show that $\beta = 0^\circ$ has the largest velocity deficit for
 288 turbine 3 whereas it has the smallest velocity deficit for turbine 2.

289 At $x/D > 2.5$ (Figures 7d-f, see also Figure 6), the peak velocity deficits
 290 in the combined or individual wakes is higher for $\beta = 0^\circ$ compared to the
 291 yaw cases. This may be as a results of the higher turbulence levels in the
 292 yawed flow cases.

1
2
3
4
5
6
7
8
9
10
11
12
13
14
15
16
17
18
19
20
21
22
23
24
25
26
27
28
29
30
31
32
33
34
35
36
37
38
39
40
41
42
43
44
45
46
47
48
49
50
51
52
53
54
55
56
57
58
59
60
61
62
63
64
65

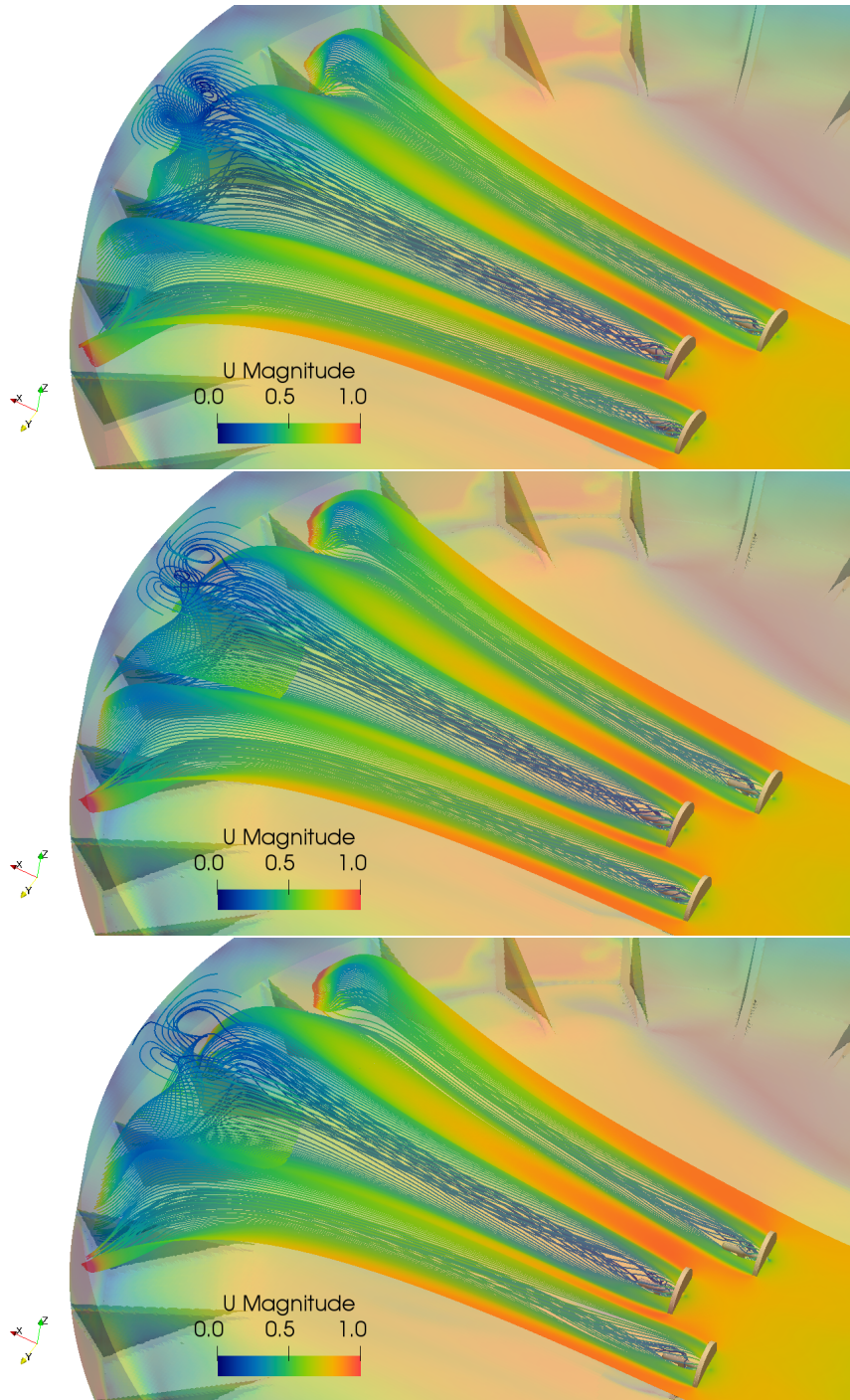
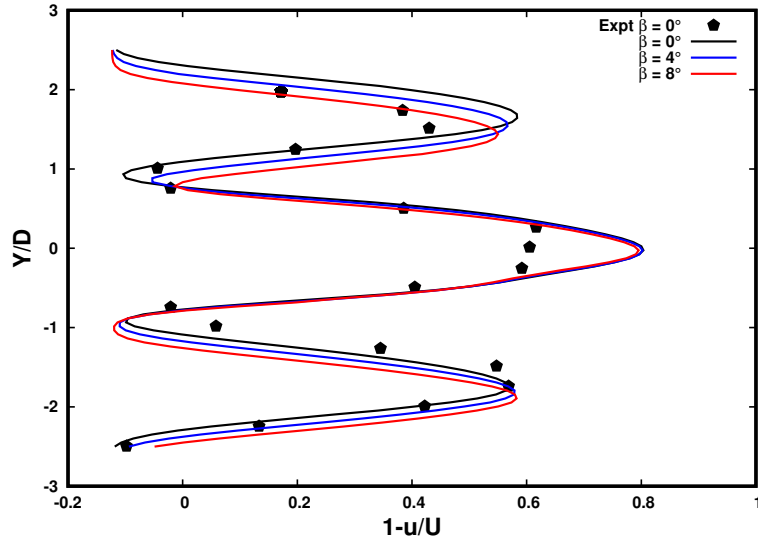
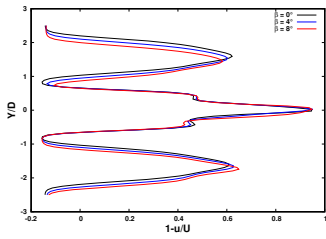


Figure 6: Wake velocity for the three turbine array at different yaw angles. Top to bottom: $\beta = 0^\circ, 4^\circ, 8^\circ$. Note: Increase in yaw angle is in a clockwise direction.

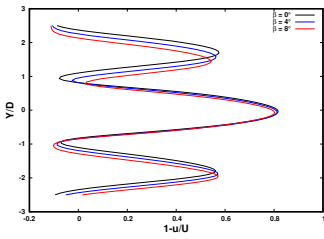
1
2
3
4
5
6
7
8
9
10
11
12
13
14
15
16
17
18
19
20
21
22
23
24
25
26
27
28
29
30
31
32
33
34
35
36
37
38
39
40
41
42
43
44
45
46
47
48
49
50
51
52
53
54
55
56
57
58
59
60
61
62
63
64
65



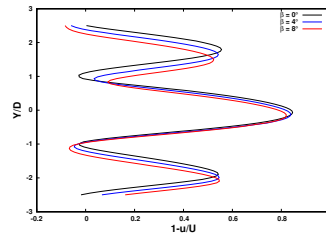
(a) $x/D = 2$



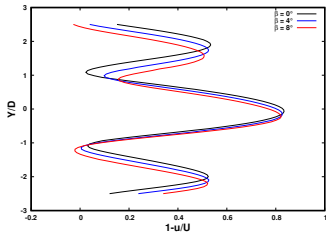
(b) $x/D = 1.0$



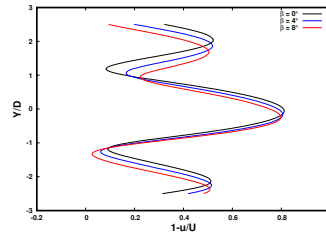
(c) $x/D = 2.5$



(d) $x/D = 3.5$



(e) $x/D = 4.5$



(f) $x/D = 5.0$

Figure 7: Transverse profiles of normalized downstream axial velocities at three different yaw angles, $\beta = 0^\circ, 4^\circ, 8^\circ$.

1
2
3
4
5
6
7
8
9
293 *3.4.2. Performance at different upstream turbulence intensities, TI 's*

294 Interaction of turbulence with tidal turbines is important if accurate fa-
295 tigue predictions are to be made and turbine reliability optimised. To con-
296 sider the effects of turbulence intensity, the three turbine array is compared
297 with three inlet turbulence intensities, TI 's of 15%, 25% and 30% at $\beta = 0^\circ$.
298 Figure 8 shows turbulence intensity decay variation as they progress down-
299 stream to the turbines. The two upstream turbines (Turbines 2 and 3) are
300 located at $x = -1.2$ m whilst the located of the primary turbine (Turbine 1)
301 is at $x = 0$ m. The plot shows a rapid decay shortly downstream of the inlet
302 as well as close to the turbines. At inlet TI 's of 15%, 25% and 30%, only TI
303 of 7%, 10% and 10.5% respectively were realised at the locations of Turbines
304 2 and 3, corresponding to a 53%, 60% and 65.5% drop in turbulence inten-
305 sity. As seen in Figure 8, the results are consistent with the experimental
306 measurements.

307 Figure 9 shows that increasing the turbulence intensity, TI has little effect
308 on the mean C_P and C_T for the TI 's evaluated in this analysis, with less
309 than 3.5% difference. Previous studies [9], [10] have also shown that the
310 mean C_P and C_T are only slightly dependent on the turbulence intensity at
311 TSR values of $1 \leq \text{TSR} \leq 10$. The results show an increase of 2.0% in power
312 production when inlet TI is increased from 15% to 25% and a further 1.2%
313 from 25% to 30%.

314 Figure 10 shows the wake velocity for the investigated TI 's. The results
315 show similar near wake features, however there are visible differences in the
316 far wake features. Concerning the profiles of velocities calculated downstream
317 of the arrays in Figures 11, it can be seen that, large differences exist between
318 the different turbulence rates (seen more clearly at $x/D > 2$). The maximum
319 deficit was observed for the lowest turbulence rate in all locations with the
320 peak occurring at $x/D = 2.5$. The results suggest that turbulence intensity
321 has little influence on the near wake of the array, but helps to recover the
322 axial velocity in the wake. This finding is consistent with previous research
323 [10].

324 **4. Case Study 2: Multiple Full-scale Turbines in Varied Configu-**
325 **ration**

326 *4.1. Turbine arrangements*

327 A fourteen-turbine array with two different arrangements was also simu-
328 lated. The first is a 4 row arrangement whereby the lateral and longitudinal

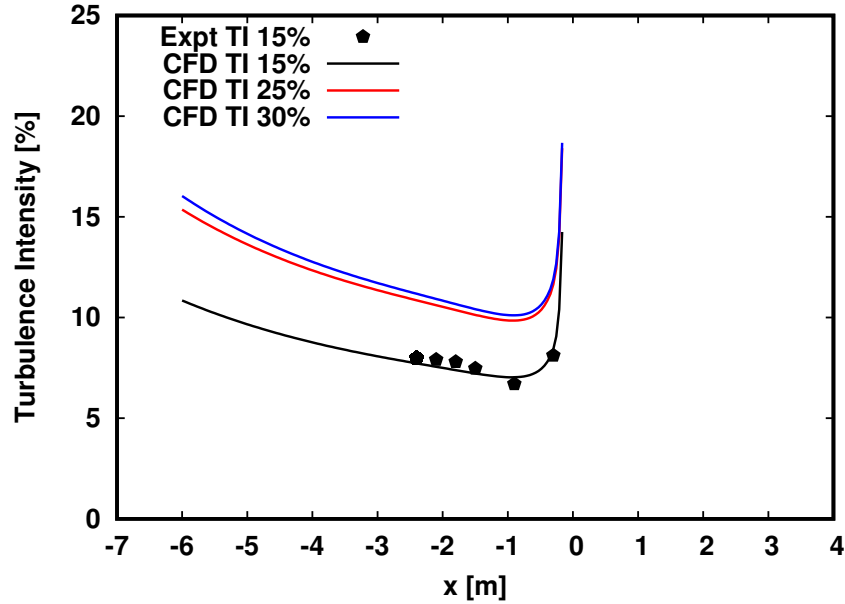


Figure 8: Turbulence intensities decay variation in the three array turbine, TSR = 7.

spacing are 3.0 diameters and 10.0 diameters respectively (regular formation), see top image in Figure 12. These are arbitrary values which have been chosen to reproduce reasonable turbine spacing that may be implemented in a real situation. The second arrangement presented in Figure 12, bottom image shows a different arrangement in which the lateral spacing between devices is increased to 4.0 diameters to maximise the flow acceleration between them (modified formation). The second and third rows have been moved so that they are one diameter away from the first and fourth rows such that the distance between the second and third row is 38.0 diameters. This serves two purposes, firstly the second and fourth rows will benefit from flow acceleration between upstream turbines to a greater extent. Secondly, such an arrangement will also facilitate a greater level of flow recovery before the flow interacts with the third and fourth rows. The turbines are fixed pitch variable speed, running at an optimal TSR of 3.0 based on the inlet velocity. Turbine rotational speed was set to be the same for the turbines, so that they have TSR of 3.0 relative to the inlet velocity. The turbines have a diameter of 10 m which is a reasonable representation of the scale of turbines likely to be deployed in nearshore environments. The chord length and chord twist angle characteristics of the blade are presented in Figure 13.

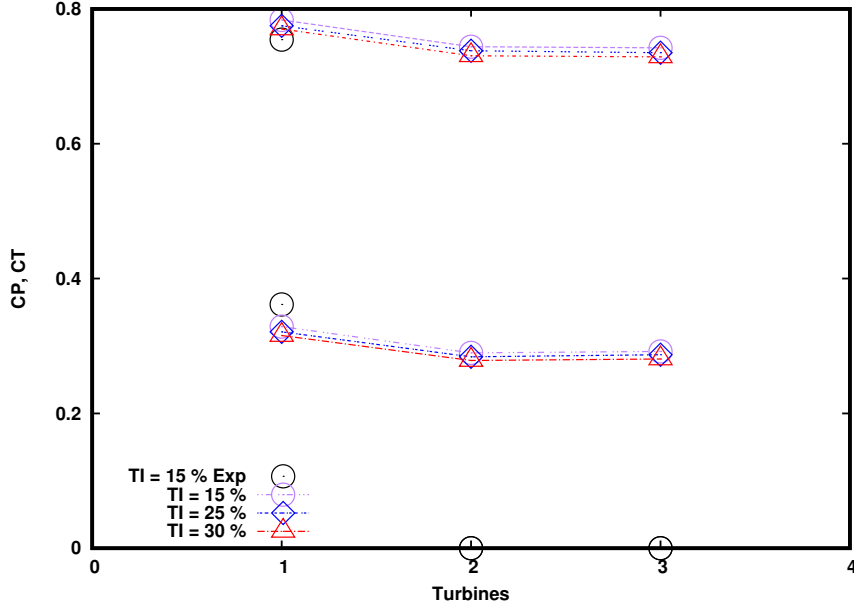


Figure 9: Comparison of coefficient of power C_P (bottom) and coefficient of thrust C_T (bottom) at different upstream turbulence intensities, $TSR = 7$.

348 The rotor geometry, and lift/drag characteristics, are also taken from [29].
 349 The NACA 4424 lift and drag curves are taken from [37] with chord-length
 350 Reynolds numbers varying between 0.2×10^6 (root) and 1.0×10^6 (tip).

351 4.2. Domain and boundary conditions

352 The inflow and outflow plane were located 30 D upstream of the front
 353 turbines and 60 D downstream of the rear turbines respectively. A cuboid
 354 computational domain is employed. The domain is 1200 metres in length
 355 (x-axis). The domain depth is 30 metres (z-axis), while the width is 300
 356 metres (y-axis). A uniform and steady velocity profile of 3.0 m/s, which is
 357 the nominal inflow velocity and turbulence intensities of 1%, 5% and 10%
 358 were applied at the inlet of the computation domain. This is applicable
 359 here as the turbine arrays are placed in a wide channel and therefore only
 360 extract a small fraction of the energy available to them. Future large-scale
 361 generation will undoubtedly require the deployment of hundreds of devices
 362 at high-energy locations. Such locations are fairly limited and hence, the
 363 devices are likely to be packed relatively closely to one another along the
 364 seabed. A high density of tidal turbines will cause excessive resistance to the

1
2
3
4
5
6
7
8
9
365 flow, or in effect an increase in the drag coefficient of the channel, causing a
366 reduction of flow velocities at the devices [38]. Under such circumstances, a
367 different turbine optimisation will be required than for a fixed upstream flow
368 [39], [40].

369 At the outlet boundary a zero gradient was applied. The nacelles and
370 bottom of the domain are set to zero velocity and wall functions used for k ,
371 ϵ , and nut . No roughness parameter was added and the bottom boundary
372 assumed a smooth wall. Five flow configurations, as illustrated in Table 5,
373 were also carried out.

Table 5: Simulation Flow Conditions

Yaw, β ($^\circ$)	$TurbulenceIntensity, TI$ (%)
0	1
0	5
0	10
2	1
8	1

374 *4.3. Grid Generation*

375 All grids were created utilizing both “blockMesh” and “snappyHexMesh”
376 in OpenFOAM version 6.0. The “blockMesh” utility is used to generate an
377 initial block (mesh domain) with size set to $1200\text{m} \times 300\text{m} \times 30\text{m}$ in x , y , and z
378 directions respectively which captures the domain extents. The discretisation
379 does not use any grading in this case thus “simpleGrading” is set to one.
380 Refinement of the mesh around the turbines and wake region is achieved
381 using “snappyHexMesh” utility. The wake region is defined as a cylinder
382 37.5 metre radius, extending from the rotor to 900 metres downstream, i.e.
383 to the domain outflow. The refinement level in this region is specified as level
384 2. The rotor assembly and bladebox is set with a refinement level of 4.

385 Mesh dependency of the simulations within the blade-box and wake re-
386 gions was assessed in [29] and [30] respectively with the turbine operating
387 close to an optimal design TSR of 3.0. Based on the recommendations in
388 these previous studies, subdivisions of $480 \times 120 \times 12$ with total element size
389 of approximately 25M representing a reasonable compromise in accuracy and
390 computational cost, was chosen to perform the remaining studies.

1
2
3
4
5
6
7
8
9
10
11
12
13
14
15
16
17
18
19
20
21
22
23
24
25
26
27
28
29
30
31
32
33
34
35
36
37
38
39
40
41
42
43
44
45
46
47
48
49
50
51
52
53
54
55
56
57
58
59
60
61
62
63
64
65

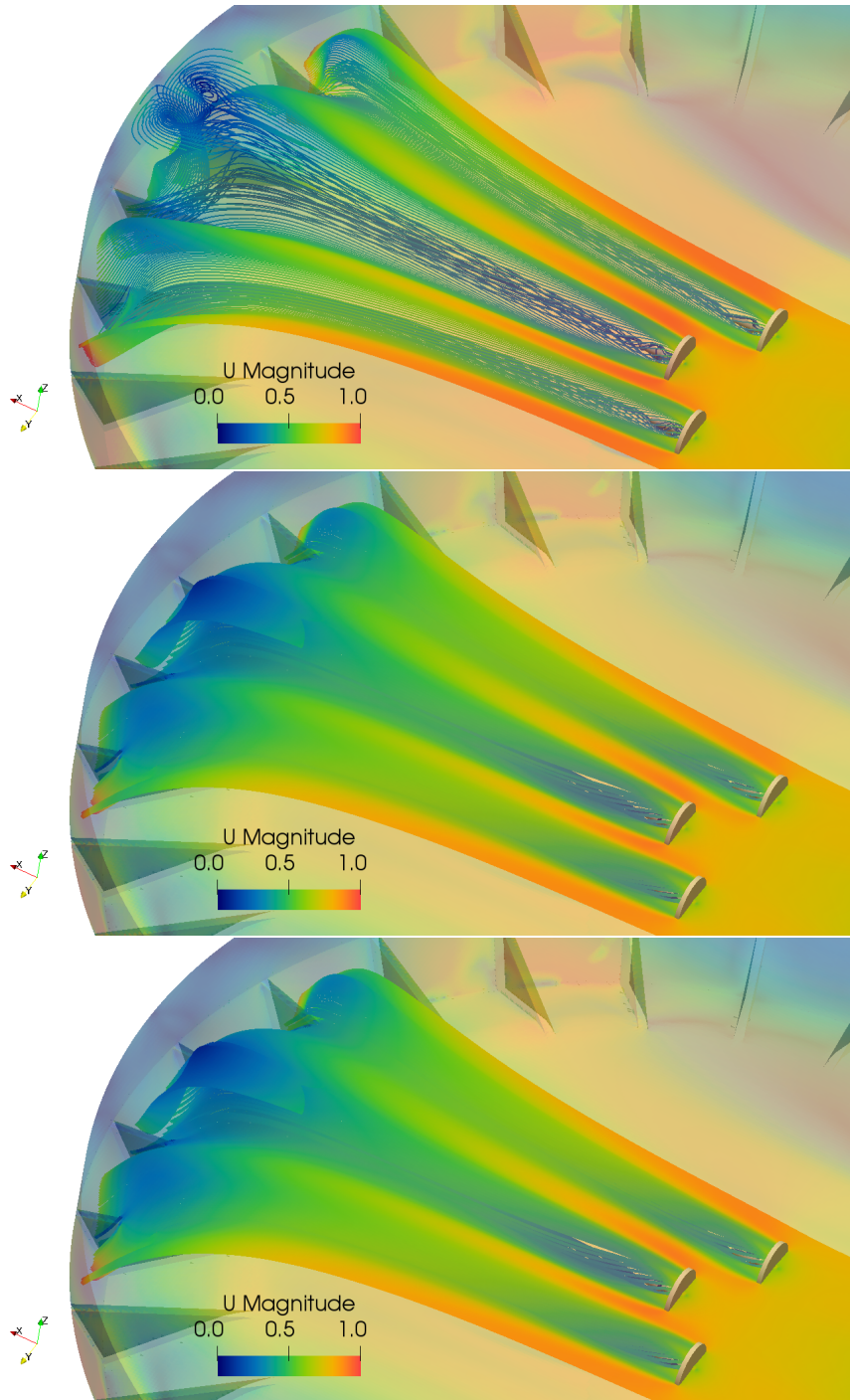
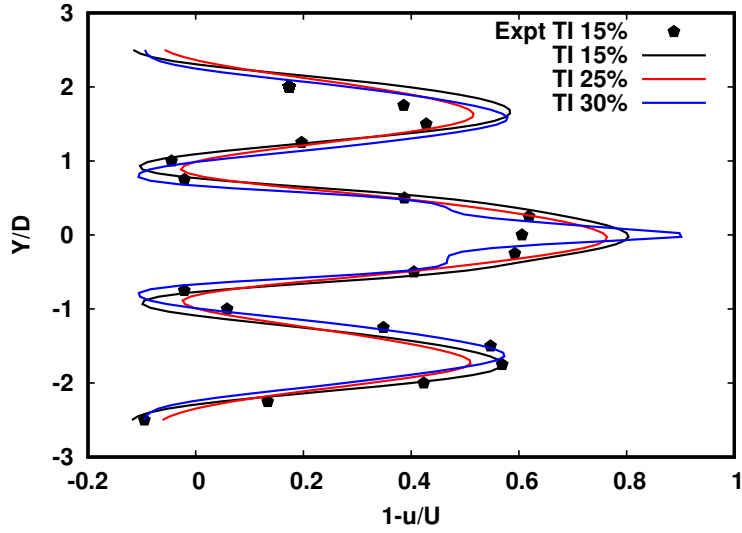
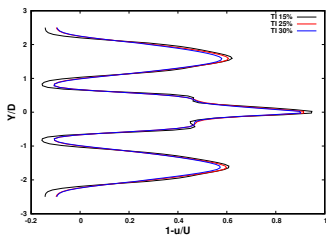


Figure 10: Wake velocity for the three turbine array at different upstream turbulence intensities. Top to bottom: $TI = 15\%$, $TI = 25\%$, $TI = 30\%$.

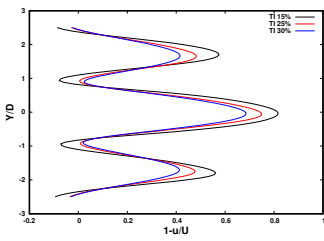
1
2
3
4
5
6
7
8
9
10
11
12
13
14
15
16
17
18
19
20
21
22
23
24
25
26
27
28
29
30
31
32
33
34
35
36
37
38
39
40
41
42
43
44
45
46
47
48
49
50
51
52
53
54
55
56
57
58
59
60
61
62
63
64
65



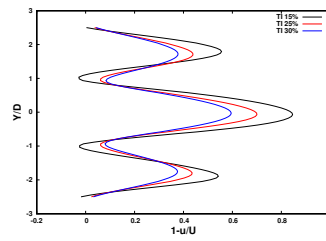
(a) $x/D = 2$



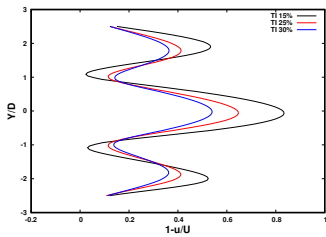
(b) $x/D = 1.0$



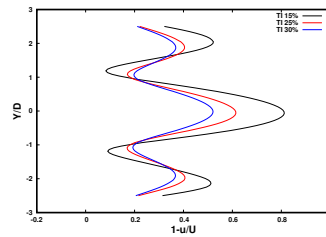
(c) $x/D = 2.5$



(d) $x/D = 3.5$



(e) $x/D = 4.5$



(f) $x/D = 5.0$

Figure 11: Transverse profiles of normalized downstream axial velocities at three different upstream turbulence intensities.

1
2
3
4
5
6
7
8
9
10
11
12
13
14
15
16
17
18
19
20
21
22
23
24
25
26
27
28
29
30
31
32
33
34
35
36
37
38
39
40
41
42
43
44
45
46
47
48
49
50
51
52
53
54
55
56
57
58
59
60
61
62
63
64
65

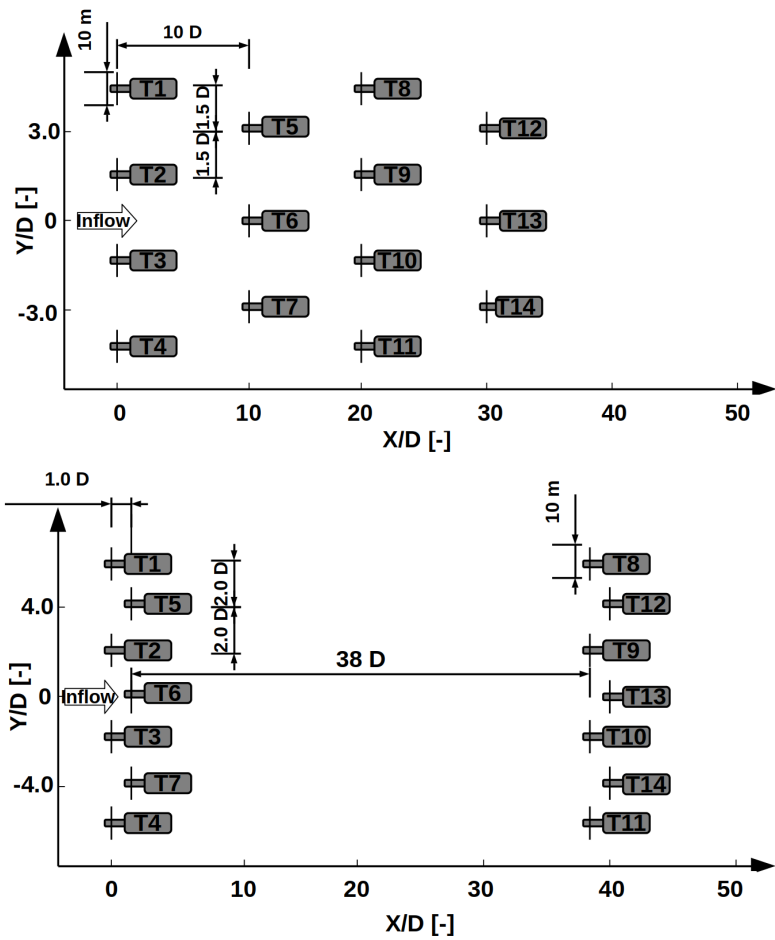


Figure 12: Schematics of the 14-turbine layout: (top) regular formation (bottom) modified formation including rotor numbers (not to scale).

1
2
3
4
5
6
7
8
9
10
11
12
13
14
15
16
17
18
19
20
21
22
23
24
25
26
27
28
29
30
31
32
33
34
35
36
37
38
39
40
41
42
43
44
45
46
47
48
49
50
51
52
53
54
55
56
57
58
59
60
61
62
63
64
65

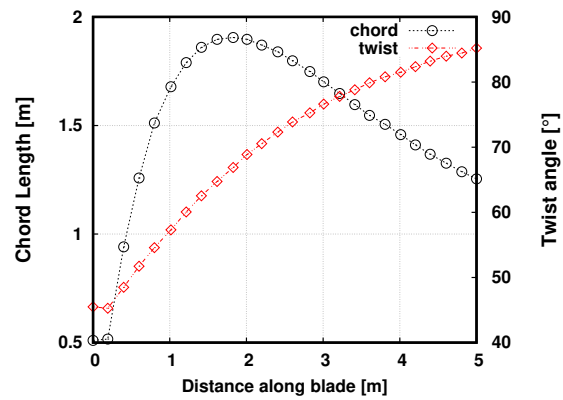


Figure 13: Chord length and twist characteristics of the blades used in the 14-turbine layout analysis.

1
2
3
4
5
6
7
8
9 391 *4.4. Results*

10 392 *4.4.1. Performance at different yaw angles*

11 393 This section presents the performance of both regular and modified array
12 394 configurations in straight flow conditions, with inlet turbulence defined by TI
13 395 = 1%. The individual devices within the arrays and the hydrodynamic flow
14 396 structures between the turbines are also evaluated. Figures 14 and 15 present
15 397 the coefficient of power, C_P , and thrust, C_T , for the two configurations at the
16 398 different yaw angles. C_P and C_T were also calculated based on the inflow
17 399 velocity and a fixed TSR. The computed power production at $\beta = 0^\circ$ for
18 400 the front four set of turbines in the modified formation was 1.826MW. At
19 401 $\beta = 2^\circ$ and 8° , the power production reduced to 1.767MW and 1.733MW
20 402 respectively, about 3% and 5% less than the $\beta = 0^\circ$ case. These values are
21 403 significantly less than the 0.06% and 1.0% reduction in C_P that would be
22 404 expected if yaw effects were only assumed to be a function of the decreased
23 405 projected swept area of the turbine. Similar tendencies were observed in the
24 406 regular formation.

25 407 There were however large differences in power in the second to fourth
26 408 sets of turbines, more especially turbines 8-14. Starting with the modified
27 409 formation at the higher yaw angle, turbines 8, 9 and 12 were not directly
28 410 affected by the wake of the front set of turbines (i.e turbines 1-7). The inflow
29 411 to these turbines were almost similar to freestream conditions (see also Figure
30 412 17). This resulted in an increase in their C_P values and a further increase
31 413 in C_P for turbine 12 which also took advantage of the bypass flow. All the
32 414 other turbines experienced some disturbances from the wake generated by
33 415 turbines 1-7 and resulted in reduced C_P values with a further decrease in
34 416 C_P in turbines 10 and 11 due to the reduced wake recovery and the smaller
35 417 recovery distance of the upstream turbines (5 and 6). In the $\beta = 2^\circ$ case, all
36 418 rear turbines with the exception of turbine 8 experienced disturbance from
37 419 the wake generated by turbines 1-7. Table 6 shows the computed power for
38 420 each row of turbines at $\beta = 0^\circ$, 2° and 8° . From these values, it can be seen
39 421 that apart from the third row of turbines, power production decreases with
40 422 increase in yaw angle.

41 423 Similar tendencies were also found in the regular formation. The pre-
42 424 dicted overall farm power was 5.32MW, 5.25MW, 3.64MW compared to
43 425 5.86MW, 5.83MW, 5.96MW in the modified formation at $\beta = 0^\circ$, 2° and
44 426 8° respectively. Although the overall farm power was higher in the modified
45 427 formation compared to the regular formation for the investigated yaw cases,

428 interestingly the highest power output was not necessarily obtained for the
 429 modified tidal farm at $\beta = 0^\circ$, but for $\beta = 8^\circ$ in this case. This shows
 430 that for larger tidal farms, the overall power output at yaw that can be ob-
 431 tained compared to the straight flow cases can either increase (or decrease)
 432 since the power output in rows further downstream depends on the orienta-
 433 tion in the first rows. The results also show that strong sensitivity of tidal
 434 farm power output to small variations of the inflow direction exists and this
 435 should be taken into account for optimal control as well as grid integration
 436 of tidal farms. Similar tendencies were observed in the coefficient of thrust
 437 C_T values in Figure 15 where C_T decreases as yaw angle increases due to the
 438 reduced axial component of the velocity rather than the spanwise component
 439 as thrust depends on the axial component.

440 Figures 16 and 17 show the calculated wake velocities for the two config-
 441 urations at the different yaw angles. The overall wake structure, wake width
 442 and expansion rates are similar for all three yaw angles. However, similar to
 443 the three turbine array, there is a slight increase in skewness in the wake and
 444 a decrease in the wake recovery distance at the highest yaw angle, seen more
 445 clearly in the Figure 16.

33 **Table 6:** Power for each row of turbines in the two layouts at different yaw angles, TI =
 34 1%

<i>Configuration</i>	<i>RowNo</i>	$\beta = 0^\circ$	$\beta = 2^\circ$	$\beta = 8^\circ$
Modified	1	1.826MW	1.767MW	1.733MW
Modified	2	1.487MW	1.438MW	1.408MW
Modified	3	1.411MW	1.502MW	1.585MW
Modified	4	1.141MW	1.128MW	1.240MW
Regular	1	1.798MW	1.753MW	1.724MW
Regular	2	1.459MW	1.358MW	0.371MW
Regular	3	1.206MW	1.399MW	1.048MW
Regular	4	0.855MW	0.740MW	0.497MW

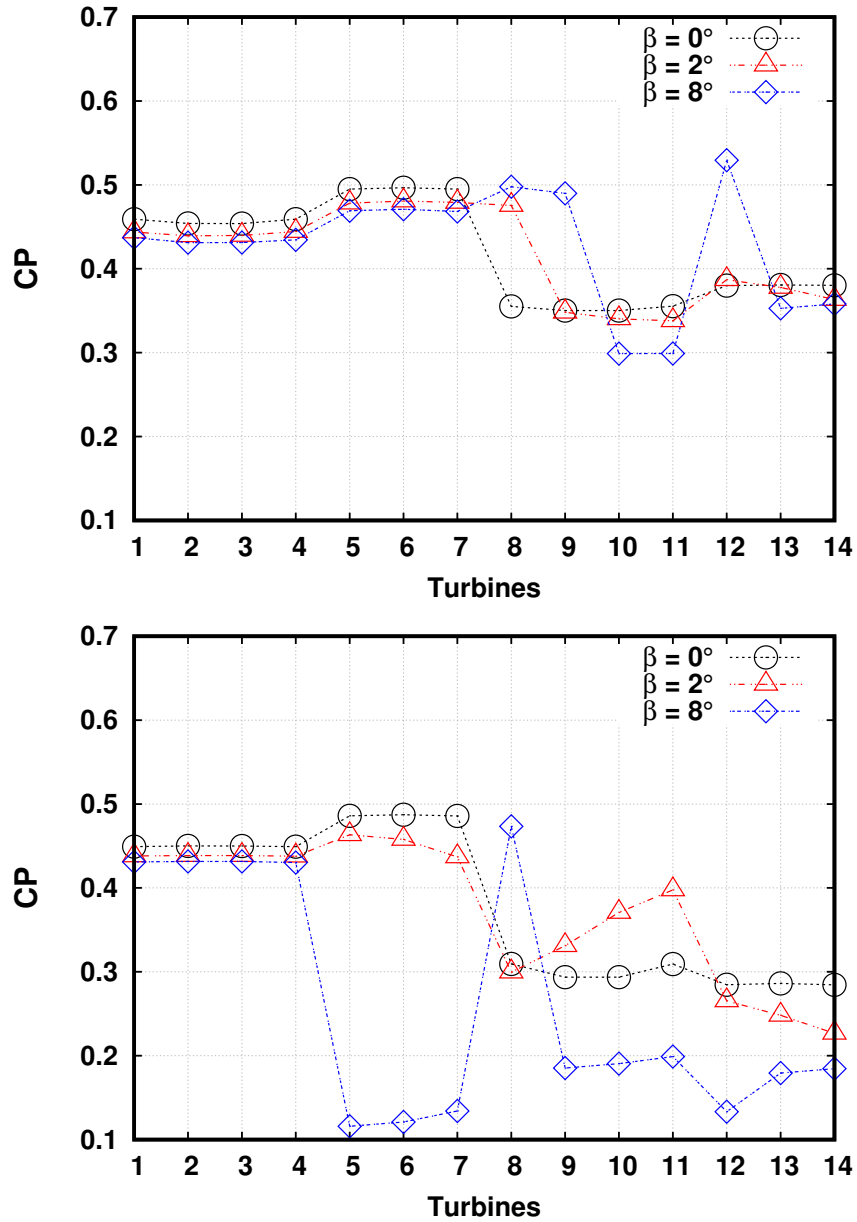


Figure 14: Comparison of coefficient of power C_P for the modified (top) and regular (bottom) configuration at different yaw angles, TI = 1%, TSR = 3.

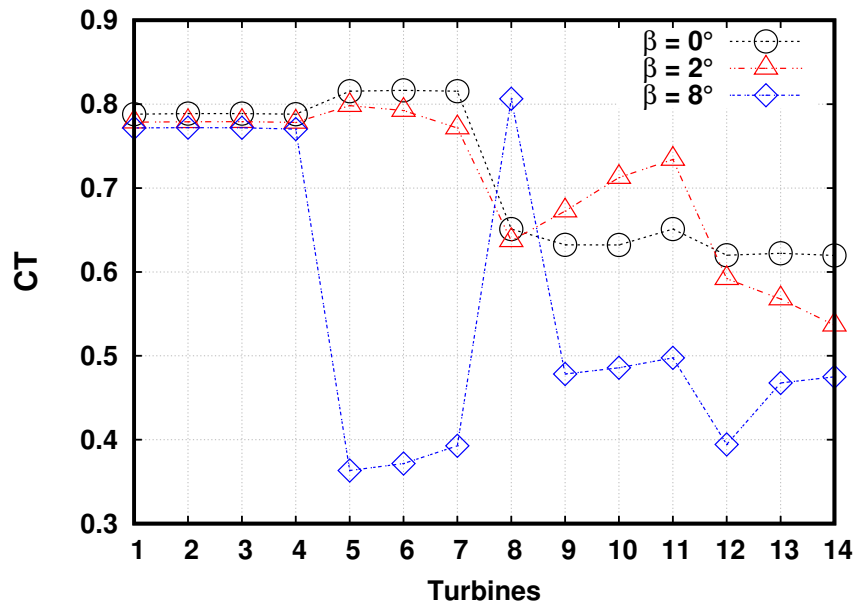
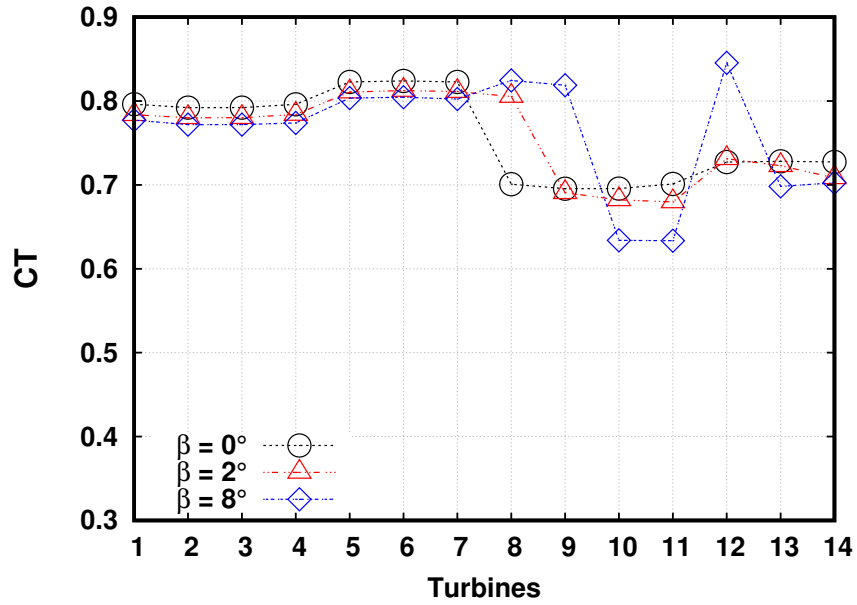


Figure 15: Comparison of coefficient of thrust C_T for the modified (top) and regular (bottom) configuration at different yaw angles, TI = 1%, TSR = 3.

1
2
3
4
5
6
7
8
9
10
11
12
13
14
15
16
17
18
19
20
21
22
23
24
25
26
27
28
29
30
31
32
33
34
35
36
37
38
39
40
41
42
43
44
45
46
47
48
49
50
51
52
53
54
55
56
57
58
59
60
61
62
63
64
65

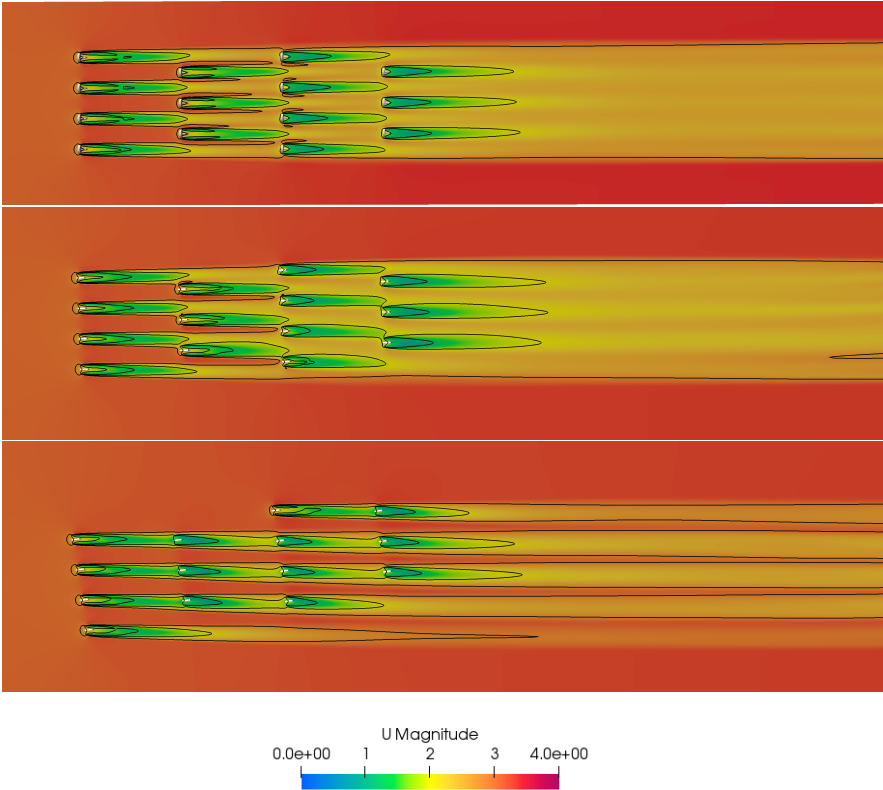


Figure 16: Wake velocity for the regular formation at different yaw angles. Top to bottom: $\beta = 0^\circ, 2^\circ, 8^\circ$, Isolines at 95% inlet velocity.

1
2
3
4
5
6
7
8
9
10
11
12
13
14
15
16
17
18
19
20
21
22
23
24
25
26
27
28
29
30
31
32
33
34
35
36
37
38
39
40
41
42
43
44
45
46
47
48
49
50
51
52
53
54
55
56
57
58
59
60
61
62
63
64
65

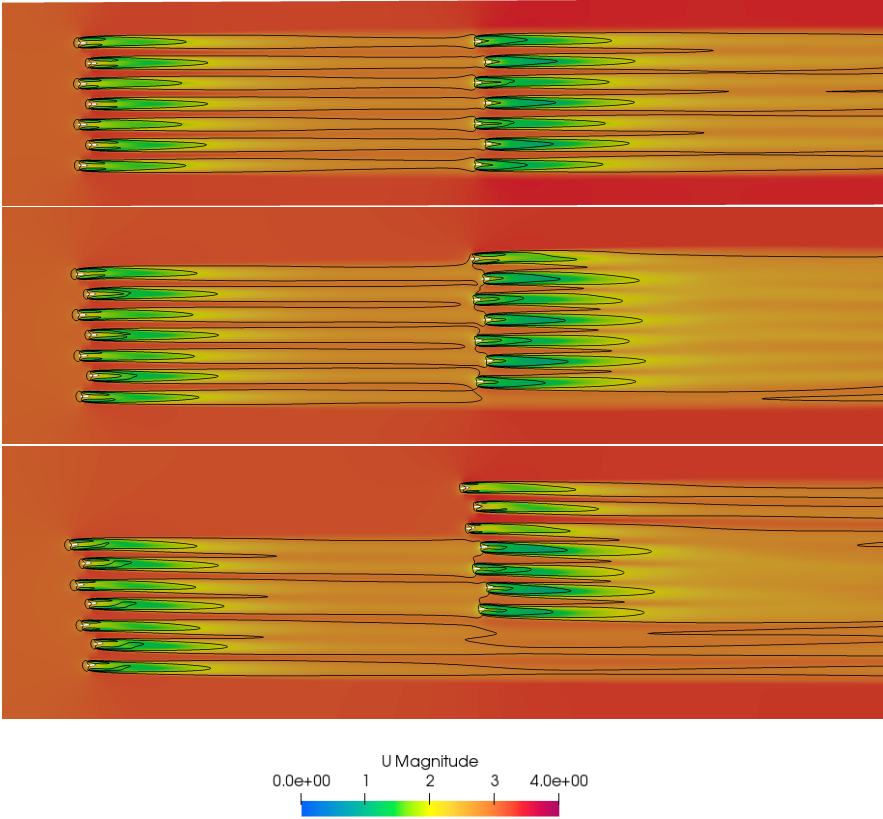


Figure 17: Wake velocity for the modified formation at different yaw angles. Top to bottom: $\beta = 0^\circ, 2^\circ, 8^\circ$, Isolines at 95% inlet velocity.

1
2
3
4
5
6
7
8
9
446 *4.4.2. Performance at different upstream turbulence intensities, TI 's*

447 Figures 18 and 19 present the results for power and thrust coefficients
448 for the two configurations at three different upstream turbulence intensities,
449 $TI = 1\%$, 5% and 10% at $\beta = 0^\circ$. Similar to the three turbine array, for
450 the front set of turbines in both configurations, TI has little effect on the
451 mean C_P and C_T for the TI 's evaluated in this analysis, with less than
452 3% difference. However, a closer inspection of the plots show some visible
453 differences, especially in the rear sets of turbines, where it appears that
454 increasing the turbulence intensity from 1% to 10% increases both C_P and
455 C_T .

456 Table 7 shows the computed power production for the first to fourth rows
457 of turbines for the modified formation at $TI = 1\%$, 5% and 10% . The results
458 show an increase of 11% in power production when inlet TI is increased to
459 5% and a further increase of 0.5% in the power production when inlet TI
460 is increased to 10% whilst in the regular formation, an increase of 4% in
461 power production is observed when inlet TI is increased to 5% and a further
462 increase of 7% when inlet TI is increased to 10% . Comparing both modified
463 and regular formations, these values corresponds to a 10.26% , 19.75% and
464 11.08% increase in overall farm power in the modified formation for $TI =$
465 1% , 5% and 10% respectively.

466 These results are very important especially as large arrays are likely to be
467 deployed in staggered arrangements to maximise the performance of down-
468 stream devices and the model results presented here indicate that TI influ-
469 ences downstream devices. It is also likely that the force fluctuations, hence
470 fatigue loads could also be affected, a factor that is relevant when optimising
471 turbine designs to increase reliability. The relatively low values of TI used
472 in the analysis will likely be found in strait channels without many features
473 that will increase turbulence levels.

474 Figures 20-21 show TI influence on the wake velocities for the two con-
475 figurations. Again, it can be seen that TI plays a major role in the wake
476 details. Both wake length and wake width increase with an increase in TI .
477 Near wake features were similar but recovery was more quicker in the higher
478 turbulence case. This is seen more clearly in Figure 20 where the wake of
479 the front set of turbines recovers quickly as it approaches the rear turbines
480 in the higher turbulence case. Turbulence intensity helps to recover the axial
481 velocity in the wake and the width of the wake increases with turbulence
482 intensity in the far wake, meaning that the arrays will have a wider wake

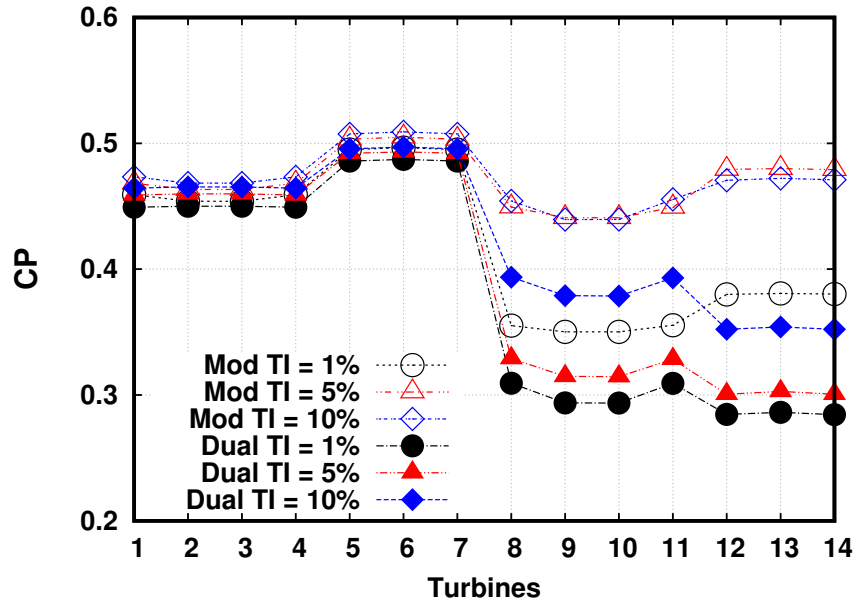


Figure 18: Comparison of coefficient of power C_P for the modified (hollow points) and regular formation (solid points) at three different upstream turbulence intensities.

483 when operating in turbulent environments.

Table 7: Power for each row of turbines in the two layouts at different turbulence intensities.

<i>Configuration</i>	<i>RowNo</i>	TI = 1%	TI = 5%	TI = 10%
Modified	1	1.826MW	1.863MW	1.883MW
Modified	2	1.487MW	1.511MW	1.542MW
Modified	3	1.411MW	1.780MW	1.789MW
Modified	4	1.141MW	1.438MW	1.414MW
Regular	1	1.798MW	1.837MW	1.859MW
Regular	2	1.459MW	1.477MW	1.488MW
Regular	3	1.206MW	1.287MW	1.544MW
Regular	4	0.855MW	0.904MW	1.059MW

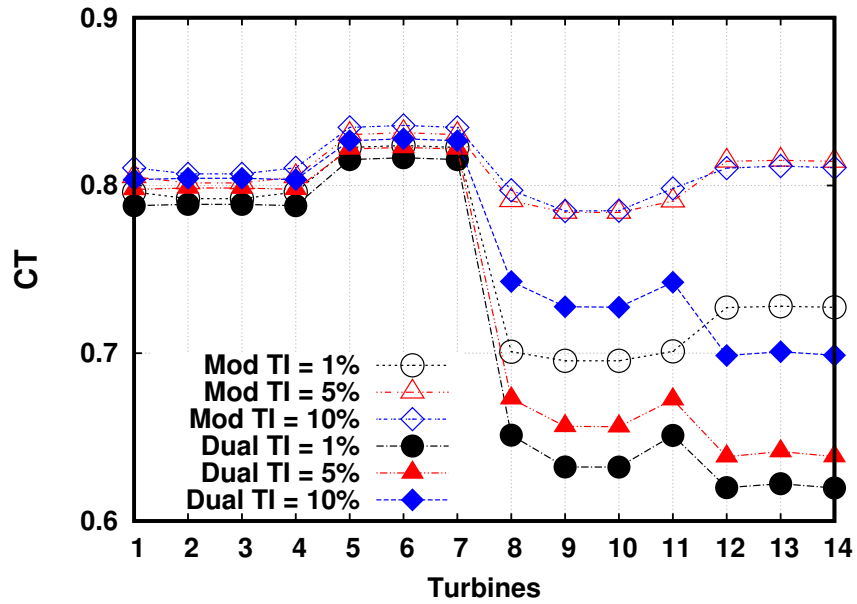


Figure 19: Comparison of coefficient of thrust C_T for the modified (hollow points) and regular formation (solid points) at three different upstream turbulence intensities.

1
2
3
4
5
6
7
8
9
10
11
12
13
14
15
16
17
18
19
20
21
22
23
24
25
26
27
28
29
30
31
32
33
34
35
36
37
38
39
40
41
42
43
44
45
46
47
48
49
50
51
52
53
54
55
56
57
58
59
60
61
62
63
64
65

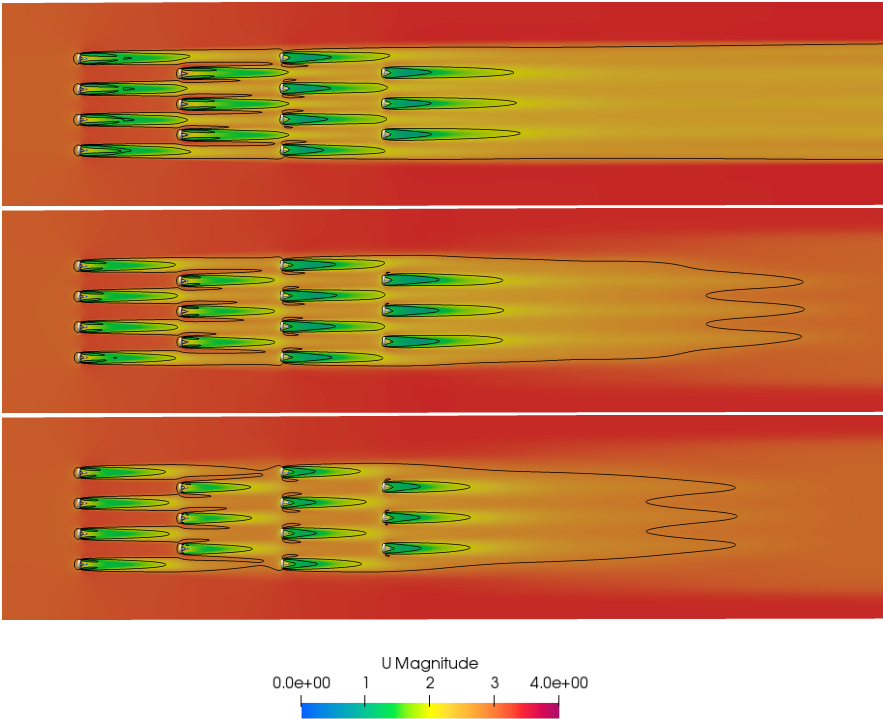


Figure 20: Wake velocity for the regular formation at three different upstream turbulence intensities. Top to bottom: TI = 1%, 5%, 10%, Isolines at 95% inlet velocity.

1
2
3
4
5
6
7
8
9
10
11
12
13
14
15
16
17
18
19
20
21
22
23
24
25
26
27
28
29
30
31
32
33
34
35
36
37
38
39
40
41
42
43
44
45
46
47
48
49
50
51
52
53
54
55
56
57
58
59
60
61
62
63
64
65

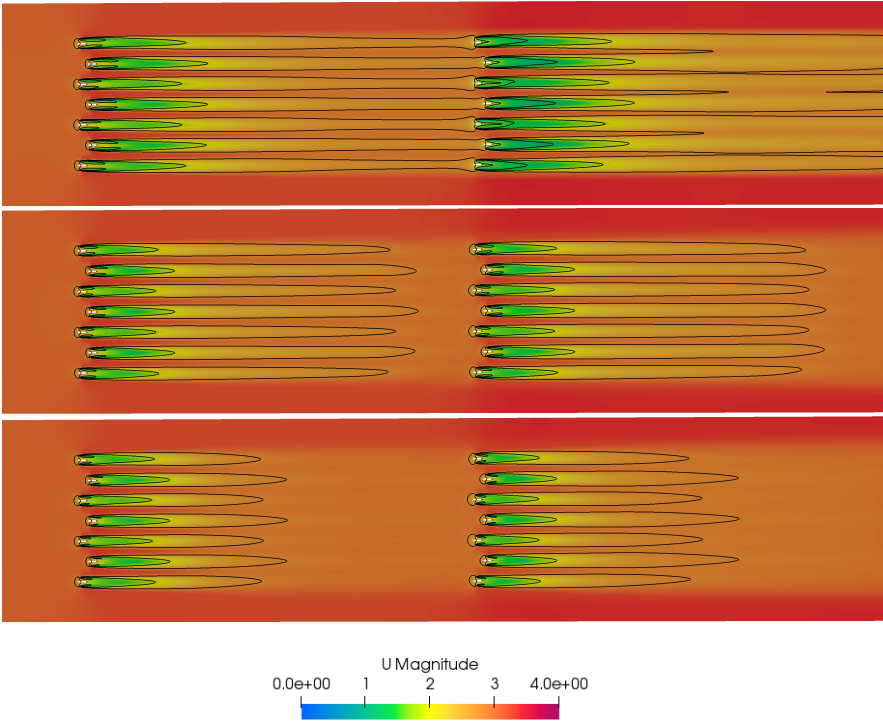


Figure 21: Wake velocity for the modified formation at three different upstream turbulence intensities. Top to bottom: TI = 1%, 5%, 10%, Isolines at 95% inlet velocity.

1
2
3
4
5
6
7
8
9 484 **5. Summary**

10
11 485 This paper introduces modelling techniques for better understanding of
12 486 the performance variations and wake effects of two different tidal stream ar-
13 487 ray configurations. First, a three turbine array was modelled, followed by a
14 488 fourteen turbine array with standard hypothetical staggered arrangement of
15 489 four rows with constant lateral and longitudinal spacing of 3.0 and 10.0 diam-
16 490 eters respectively. The array layout was then altered by moving the second
17 491 and third rows so they are 1D from the first and fourth rows. A performance
18 492 study was conducted by comparing the thrust and power coefficients under
19 493 varying effects of yaw angles and upstream inflow turbulence. A summary of
20 494 the important findings are outlined below:

21
22
23
24
25 495 *5.1. Yawed flow*

26 496 *5.1.1. Three turbine array*

- 27
28 497 • The performance characteristics for the straight flow in the three tur-
29 498 bines array are in close agreement with previous studies [26].
- 30
31
32 499 • Power and thrust decreased as yaw was increased.
- 33
34 500 • Yaw was found to have minimal effect on the individual wakes, however
35 501 small increase in skewness and decrease in recovery was found at the
36 502 higher yaw angle compared to the straight flow case.
- 37
38 503 • Yaw resulted in a shift in the wake plots. However, the profile of the
39 504 primary turbine show similar behaviour with the straight flow in the
40 505 near wake. Interestingly, for the two upstream turbines, the plots also
41 506 show that $\beta = 0^\circ$ has the largest velocity deficit for turbine 3 whereas
42 507 it has the smallest velocity deficit for turbine 2 in the near wake. It
43 508 is possible that this might be a feature of the complex tank velocity
44 509 rather than yaw.

45
46
47
48
49 510 *5.1.2. Fourteen turbine array*

- 50
51 511 • Compared to the regular staggered configuration at $\beta = 0^\circ$, the total
52 512 power output of the modified array was ncreased by over 10%. Wake
53 513 recovery to freestream was also better in the modified formation com-
54 514 pared to the regular staggered configuration.

1
2
3
4
5
6
7
8
9
10
11
12
13
14
15
16
17
18
19
20
21
22
23
24
25
26
27
28
29
30
31
32
33
34
35
36
37
38
39
40
41
42
43
44
45
46
47
48
49
50
51
52
53
54
55
56
57
58
59
60
61
62
63
64
65

- 515 • Lateral spacing between devices in straight flow conditions affected the
516 rate of flow recovery downstream. It was shown that for lateral spacing
517 of 4D there was faster downstream recovery compared to the 3D. This
518 is relevant in the context of large arrays where further devices may be
519 placed downstream.
- 520 • Similar to the three turbine array, power and thrust coefficient decrease
521 with increase in yaw angle in the front set of turbines. However, the
522 results are non-linear with the move away from optimal TSR in com-
523 bination with reduced upstream U to the rear turbines.
- 524 • Depending on the yaw angle, most of the individual devices downstream
525 were directly affected by the wakes of the upstream devices, resulting
526 in reduced power and thrust. However, few of the devices experienced
527 inflow conditions similar to the freestream resulting in power and thrust
528 increases.
- 529 • Strong sensitivity of tidal-farm power exists even to small variations
530 of inflow direction. This is relevant for optimal control as well as grid
531 intergration of tidal farms.

532 *5.2. Upstream turbulence intensities: Three and Fourteen turbine array*

- 533 • Turbulence intensity was found to decay rapidly shortly downstream
534 of the inlet which is consistent with experimental data.
- 535 • Turbulence intensity helps in recovery of axial velocity in the wake.
- 536 • Wake width increases with turbulence intensity in the far wake, mean-
537 ing that arrays will have a wider wake when operating in turbulent
538 environments.
- 539 • Turbulence intensity had little effect on the thrust and power of the
540 front set of devices in the array. It is important to stress that each of
541 these results have been obtained using a fixed TSR and a time averaged
542 representation of the flow. It is likely that using the local TSR's at the
543 turbines as well as a transient model could influence the results.

1
2
3
4
5
6
7
8
9
544 **6. Conclusions and Future Work**

545 In conclusion, an efficient method for simulating tidal stream energy con-
546 verter rotor response to realistic inflow and turbulence intensity conditions
547 and capturing the subsequent impact to farfield flow structure using a GAD-
548 CFD approach has been demonstrated. Model validation against experi-
549 mental testing has been conducted and the results show that large array
550 layouts influence on the flow around a downstream device is complex both in
551 straight and yawed flow and would be difficult to characterise using simple
552 empirical relationship. The results could help understand/improve array con-
553 figurations. Further validation of the model would be recommended as more
554 experimental data becomes available and the model improved to account for
555 more complex flow details. However, the study provides confidence that the
556 approach can be applied to a range of scenarios; both laboratory scale, and
557 large scale deployments in both the marine and wind environments.

558 Due to the computational efficiency, such an approach, especially when
559 compared to fully resolved turbine geometry models, makes the GAD-CFD
560 technique suitable for modelling arrays consisting of a large number of rotors
561 and for conducting multiple model runs under varying tidal and machine-
562 operating-point conditions. It is therefore appropriate to also consider the
563 model for studying tidal stream arrays and their interaction with respect to
564 local topography and power control.

565 Since tidal energy could play an important role in decarbonising electricity
566 generation it is important to have access to efficient and accurate engineering
567 tools such as the one developed here (which sits between highly detailed blade
568 resolved models and larger scale oceanographic and atmospheric models).
569 Improved modelling will reduce the technical risk of operating these devices
570 in the highly energetic marine environment thus increasing economic viability
571 of the sector.

572 Future work should focus on improving the model to account for changing
573 lift and drag characteristics at higher levels of free stream turbulence. As
574 turbulence levels increase, the quantity of lift and drag changes, as does the
575 stall point relative to angle of attack, and post stall features significantly
576 change. The model could also be combined with turbine control algorithms
577 that consider power capping through stall or pitch control to enable the study
578 of rotors. Other factors that will also affect device performance in natural
579 environments such as bathymetric effects and bottom roughness need to be
580 included as this will assist in improving existing methods for performance

1
2
3
4
5
6
7
8
9
10
11
12
13
14
15
16
17
18
19
20
21
22
23
24
25
26
27
28
29
30
31
32
33
34
35
36
37
38
39
40
41
42
43
44
45
46
47
48
49
50
51
52
53
54
55
56
57
58
59
60
61
62
63
64
65

581 prediction.

582 Beyond this immediate application the developers seek to develop and
583 incorporate more realistic bathymetry characterisations, which is expected
584 to be an important factor in real-world turbine array operation. It is the
585 authors intention to publish the implementation of the model to enable such
586 studies to take place.

587 **Acknowledgements**

588 This work was supported by the SELKIE project funded by the Euro-
589 pean Regional Development Fund through the Ireland Wales Cooperation
590 programme.

1
2
3
4
5
6
7
8
9
591 **References**

- 592 [1] A. Bahaj, A. Molland, J. Chaplin and W. Batten, "Marine current en-
593 ergy conversion: the dawn of a new era in electricity production," *Philos*
594 *Trans A Math Phys Eng Sci.* vol. 371, p. 20120500, 2013.
- 595 [2] The Crown Estate, "UK Wave and Tidal Key Re-
596 source Areas Project," *Tech. Rep. Version 2.* 2018.
597 <http://www.thecrownestate.co.uk/>, Retrieved: May 2018.
- 598 [3] M. Piano, S. P. Neill, M. J. Lewis, P. E. Robins, M. R. Hashemi,
599 A. G. Davies, S. L. Ward and M. J. Roberts, "Tidal stream resource
600 assessment uncertainty due to flow asymmetry and turbine yaw mis-
601 alignment," *Energy.* vol. 114, pp. 1363-1375, 2017.
- 602 [4] M. Adaramola and P. Krogstad, "Experimental investigation of wake
603 effects on wind turbine performance," *Renewable Energy.* vol. 36, pp.
604 2078-2086, 2011.
- 605 [5] P. W. Galloway, L. E. Myers and A. S. Bahaj, "Experimental and nu-
606 merical results of rotor power and thrust of a tidal turbine operating at
607 yaw and in waves," *In: World renewable energy congress.* Linkoping,
608 Sweden: May 8-13, 2011.
- 609 [6] P. W. Galloway, L. E. Myers and A. S. Bahaj, "Quantifying wave and
610 yaw effects on a scale tidal stream turbine," *Renewable Energy.* vol. 63,
611 pp. 297-307, 2014.
- 612 [7] F. Maganga, G. Germain, K. King, G. Pinon and E. Rivoalen, "Ex-
613 perimental study to determine flow characteristic effects on marine cur-
614 rent turbine behaviour," *Proc of the Euro Wave and Tidal Energy Conf.*
615 2009.
- 616 [8] C. Zhang, J. Zhang, A. Angeloudis, Y. Zhou, S. Kramer and M. Piggott,
617 "Physical modelling of tidal stream turbine wake structures under yaw
618 conditions," *Energies.* vol. 16, pp. 1742, 2023.
- 619 [9] P. Modali, N. S. Kolekar and A. Banerjee, "Performance and Wake
620 Characteristics of a Tidal Turbine under Yaw," *Int J. of Marine Eng.*
621 vol. 1, pp. 41-50, 2018.
- 622 [10] W. Tian, J. VanZwieten, P. Pyakurel and Y. Li, "Influences of yaw
623 angle and turbulence intensity on the performance of a 20 kW in-stream
624 hydrokinetic turbine," *Energy.* vol. 111, pp. 104-116, 2016.
- 625 [11] C. Tongchitpakdee, S. Benjanirat and L. Sankar, "Numerical simulation
626 of the aerodynamics of horizontal axis wind turbines under yawed flow
627 conditions," *J. Sol Energy Eng.* vol. 127, pp. 464-474, 2005.

- 1
2
3
4
5
6
7
8
9
10
11
12
13
14
15
16
17
18
19
20
21
22
23
24
25
26
27
28
29
30
31
32
33
34
35
36
37
38
39
40
41
42
43
44
45
46
47
48
49
50
51
52
53
54
55
56
57
58
59
60
61
62
63
64
65
- 628 [12] T. O’Doherty, A. Mason-Jones, D. M. O’Doherty, C. Byrne, I. Owen
629 and Y. X. Wang, “Experimental and computational analysis of a model
630 horizontal axis tidal turbine,” *Proc of the Euro Wave and Tidal Energy
631 Conf.* 2009.
- 632 [13] D. O’Doherty, A. Mason-Jones, T. O’Doherty, C. Byrne, I. Owen and
633 W. Wang, “Considerations of improved tidal stream turbine perfor-
634 mance using double rows of contra-rotating blades,” *Proc of the Euro
635 Wave and Tidal Energy Conf.* 2009.
- 636 [14] J. McNaughton, S. Rolfo, D. Apsley, I. Afgan, T. Stallad and P. Stansby,
637 “Turbulent flow and loading on a tidal stream turbine by LES and
638 RANS,” *Int J of Heat and Fluid Flow.* vol. 75, pp. 96-108, 2013.
- 639 [15] M. Howland, J. Bossuyt, M. Tossas, J. Meyers and C. Meneveau, “Wake
640 structure in actuator disk models of wind turbines in yaw under uniform
641 inflow conditions,” *J of Renewable and Sustainable Energy.* vol. 8, 2016.
642
- 643 [16] R. Baratchi, T. L. Jeans and A. G. Gerber, “Actuator line simulation
644 of a tidal turbine in straight and yawed flows,” *Int J. of Marine Eng.*
645 vol. 19, pp. 235-255, 2017.
- 646 [17] A. Bahaj, A. Molland, J. Chaplin and W. Batten, “Power and thrust
647 measurements of marine current turbines under various hydrodynamic
648 flow conditions in a cavitation tunnel and a towing tank,” *Renew. En-
649 ergy.* vol. 32, pp. 407-426, 2007.
- 650 [18] Z. Gao, Y. Li, W. Tongguang, S. Wenzhong, Z. Xiaobo, S. Prbsting,
651 D. Li and R. Li, “Modelling the nacelle wake of a horizontal-axis wind
652 turbine under different yaw conditions,” *Renewable Energy.* vol. 172,
653 pp. 263-275, 2021.
- 654 [19] C. Schulz, P. Letzgus, T. Lutz and E. Kramer, “CFD study on the
655 impact of yawed inflow on loads, power and near wake of a generic wind
656 turbine,” *Wind energy.* vol. 20, pp. 253-268, 2017.
- 657 [20] R. Malki, A. Williams, I. Masters, M. Togneri and T. N. Croft, “A
658 coupled blade element momentum-Computational fluid dynamics model
659 for evaluating tidal stream turbine performance,” *Applied Mathematical
660 Modelling.* vol. 37, pp. 3006-3020, 2013.
- 661 [21] S. Turnock, A. Phillips and R. Nicholls-Lee, “Modelling tidal current
662 turbine wakes using a coupled RANS-BEMT approach as a tool for
663 analysing power capture of arrays of turbines,” *Ocean Eng.* vol. 38, pp.
664 1300-1307, 2011.

- 1
2
3
4
5
6
7
8
9
10
11
12
13
14
15
16
17
18
19
20
21
22
23
24
25
26
27
28
29
30
31
32
33
34
35
36
37
38
39
40
41
42
43
44
45
46
47
48
49
50
51
52
53
54
55
56
57
58
59
60
61
62
63
64
65
- 665 [22] A. Olczak, T. Stallard, T. Feng and T. Stansby, "Comparison of a RANS
666 blade element model for tidal turbine arrays with laboratory scale mea-
667 surements of wake velocity and rotor thrust," *J. Fluids Struct.* vol. 64,
668 pp. 87-106, 2014.
- 669 [23] M. Edmunds, A. Williams and I. Masters, "Power Shedding from Stall
670 and Pitch Controlled Tidal Stream Turbines.," *Proc of 11th Euro Wave
671 and Tidal Eng Conf.* 2017.
- 672 [24] M. Edmunds, I. Masters, A. Banerjee, A. Williams and J. H. VanZwi-
673 eten, "A Spatially Nonlinear Generalised Actuator Disk Model for the
674 Simulation of Horizontal Axis Wind and Tidal Turbines," *Energy.* vol.
675 194, 2020.
- 676 [25] C. Badoe, M. Edmunds, A. Nambiar, A. Williams, B. Sellar, A. Kiprakis
677 and I. Masters, "Robust Validation of a Generalised Actuator Disk CFD
678 Model for Tidal Turbine Analysis using the FloWave Ocean Energy Re-
679 search Facility," *Renewable Energy.* vol. 190, pp. 232-250, 2022.
- 680 [26] D. Noble, S. Draycott, A. Nambiar, B. Sellar, B. Steynor and
681 A. Kiprakis, "Experimental Assessment of Flow, Performance, and
682 Loads for Tidal Turbines in a Closely-Spaced Array," *Energies.* 2020.
- 683 [27] D. Noble, T. Davey, H.C.M. Smith, P. Kaklis, A. Robinson and T. Bruce,
684 "Characterisation of spatial variation in currents generated in the
685 FloWave Ocean Energy Research Facility," *Proc of 11th Euro Wave and
686 Tidal Eng Conf.* 2015.
- 687 [28] D.R.J. Sutherland, D. Noble, T. Davey, J. Steynor, T.A.D. Davey and
688 T. Bruce, "Characterisation of Current and Turbulence in the FloWave
689 Ocean Energy Research Facility," *Ocean Eng.* vol. 139, pp. 103-115,
690 2017.
- 691 [29] R. Malki, I. Masters, A. Williams and T. N. Croft, "Planning tidal
692 stream turbine array layouts using a coupled blade element momentum-
693 computational fluid dynamics model," *Renewable energy.* vol. 63, pp.
694 46-54, 2014.
- 695 [30] M. Edmunds, A. Williams, I. Masters and T. N. Croft, "An enhanced
696 disk averaged CFD model for the simulation of horizontal axis tidal
697 turbines," *Renewable energy.* vol. 101, pp. 67-81, 2017.
- 698 [31] H. G. Weller, G. Tabor, H. Jasak and C. Fureby, "A tensorial ap-
699 proach to computational continuum mechanics using object-oriented
700 techniques," *Comp in Phys.* vol. 12, pp. 620-631, 1998.
- 701 [32] G. S. Payne, T. Stallard and R. Martinez, "Design and manufacture of a
702 bed supported tidal turbine model for blade and shaft load measurement

1
2
3
4
5
6
7
8
9
10
11
12
13
14
15
16
17
18
19
20
21
22
23
24
25
26
27
28
29
30
31
32
33
34
35
36
37
38
39
40
41
42
43
44
45
46
47
48
49
50
51
52
53
54
55
56
57
58
59
60
61
62
63
64
65

703 in turbulent flow and waves,” *Renewable energy*. vol. 107, pp. 312-326,
704 2017.

705 [33] C. Badoe, X. Li, A. Williams and I. Masters, “Computational Fluid Dy-
706 namics Modelling of Tidal Turbine Arrays in a Demonstration Site,” *Proc*
707 *of the Int Conf on Renewable Energies Offshore (RENEW 2022)*. 2022.

708

709 [34] C. Badoe, X. Li, S. Armstrong, A. Williams and I. Masters, “Tidal
710 stream turbine arrays in a demonstration site using GAD-CFD mod-
711 els,” *Proc of the 9th Conf on Comp Methods in Marine Eng (Marine*
712 *2021)*. 2021.

713 [35] T. Ebdon, T. O’Doherty, A. Mason-Jones and D. M. O’Doherty, “Sim-
714 ulating marine current turbine wakes with advanced turbulence mod-
715 els,” *Proc of the 3rd Asian Wave and Tidal Energy Conference*. 2016.

716

717 [36] W. M. J. Batten, M. E. Harrison and A. S. Bahaj, “Accuracy of the
718 actuator disc-RANS approach for predicting the performance and wake
719 of tidal turbines,” *Phil Trans of the Royal Soc A: Maths, Phys and Eng*
720 *Sci*. 2013.

721 [37] I. Abbott and A. Von Doenhoff, “Theory of Wing Sections, Including a
722 Summary of Airfoil Data, no. 1 in Dover Books on Aeronautical Engi-
723 neering Series,” *Dover Publications*. 1959.

724 [38] C. Garrett and P. Cummins, “The power potential of tidal currents in
725 channels,” *Proc Royal Soc A*. vol. 461, pp. 2563-2572, 2005.

726 [39] R. Vennell, “Tuning turbines in a tidal channel,” *J Fluid Mech*. vol.
727 663, pp. 253-267, 2010.

728 [40] R. Vennell, “Tuning tidal turbines in-concert to maximise farm effi-
729 ciency,” *J Fluid Mech*. vol. 671, pp. 587-604, 2011.

Output of a tidal farm in yawed flow and varying turbulence using GAD-CFD

Charles E. Badoe, Xiaorong Li, Alison J. Williams[†] and Ian Masters

Energy and Environment Research Group, Zienkiewicz Centre for Computational Engineering, College of Engineering, Bay Campus, Swansea University, SA1 8EN, Wales, UK.

[†] *Corresponding author: alison.j.williams@swansea.ac.uk*

Abstract

Tidal stream turbine arrays will be subject to a range of flow conditions throughout the tidal cycle and it is important for developers to have an understanding of the impact of these on array performance when planning site design. A generalised actuator disk-computational fluid dynamics (GAD-CFD) model is used to conduct simulations on a three and fourteen turbine array arranged in two different configurations. Firstly, simulations of both arrays are conducted in straight flow conditions to understand the hydrodynamics around devices and evaluate their performance. Performance predictions for the three turbine array in straight flow conditions are in close agreement with previous studies. In the fourteen turbine array, wake recovery to free-stream conditions was better in the modified formation compared to the regular formation and the total power output was increased by over 10%. The influence of yaw angle and upstream TI (turbulence intensity) on both array performance was also studied. Strong sensitivity of overall farm power and thrust was found to exist in small variations in yaw angle. However, the overall wake structures were similar irrespective of the yaw angle.

Finally, simulations of different turbulence intensities showed rapid decay shortly downstream of the inlet. In all arrays, turbulence intensity had little effect on the thrust and power of the upstream set of devices for the considered TI range but greatly influenced the individual downstream devices.

Keywords: FloWave, GAD-CFD, Blade Element Momentum, Tidal Energy, Tidal Turbine, Horizontal Axis Turbine

1. Introduction

Tidal stream power generation is currently undergoing rapid progressing as a reliable form of renewable energy due to the predictability of tidal periods and magnitudes [1]. A number of sites across the world are being identified and tidal current turbines installed in small arrays to generate and export electricity to local networks [2]. However, a lot of the sites that have been identified for installation of these devices exhibits some degree of misalignment in incident flow, more especially in nearshore environments where bathymetric and seabed frictional effects are significant. Misalignment in incident flow or yawed inflow may also occur due to turbine support structures and the presence of upstream bluff bodies [3]. When a tidal current turbine experiences misalignment in incident flow or yawed inflow, the flow of water is no longer aligned with the turbine and crossflow is developed across the turbine plane. This will alter the turbine's thrust and power as well as changing the effective direction of the turbine race. The net side-force due to the turbine will vary more than during straight flow conditions. Wake behaviour will also vary compared to straight flow conditions. Yaw misalignment effects therefore play an important role and quantification of a turbine's performance and wake details under such condition is essential for the design layout of a tidal farm for maximizing the power output [4].

A number of experimental studies have been conducted to improve understanding of yawed inflow influence on tidal turbines. For example, Galloway et al. [5] studied the power and thrust performance of a scaled tidal current turbine operating at yaw and in waves in a tow tank. The authors observed that less power and rotor thrust was captured by the turbine and resulted in reduced performance as yaw angle increased. Galloway et al. [6] followed on his earlier work by conducting experiments to study the cyclic loading and fatigue effects due to dynamic yaw on a rotor caused by wave-current interaction. They found that yaw angles below 7.5 degrees had negligible effect on the rotor. Maganga et al. [7] conducted experimental studies to quantify the effects of flow characteristics (yaw and velocity gradient) on the performance and loading on a tidal turbine. The authors observed that the turbine's performance was sensitive to the quality of the incoming flow and a misalignment of a fixed turbine can cause significant losses. Zhang et al [8] studied the effects of a turbine operating under varying yaw conditions. Their results showed that increasing yaw angle results in a decrease in the turbine's streamwise force and an increase in spanwise force. Velocity distri-

1
2
3
4
5
6
7
8
9
10
11
12
13
14
15
16
17
18
19
20
21
22
23
24
25
26
27
28
29
30
31
32
33
34
35
36
37
38
39
40
41
42
43
44
45
46
47
48
49
50
51
52
53
54
55
56
57
58
59
60
61
62
63
64
65

butions also showed that the wake deflection and velocity deficit recovery rate increased at a rate proportional to the yaw angle. Modali et al [9] studied turbine performance and wake deflection within $\pm 15^\circ$ yawed conditions and showed that when an upstream turbine is yawed, the downstream turbine can extract more than 50% higher energy in a staggered layout than in an aligned layout. All of the above experimental work provides an opportunity to evaluate the performance of the tidal devices in a relatively low-cost, controlled laboratory environment, which can also be used to complement and validate numerical models.

Computational fluid dynamics (CFD) has also been used, through a number of approaches to study the performance and wake details of tidal devices under yawed inflow conditions. Each approach has advantages and disadvantages, with the main balance being a trade off between detailed simulation of the physics and the computational time and resources required to achieve a result. At the smallest and most detailed scale, fully resolved tidal current turbine geometry models have been used to provide insight into the development of the wake structures downstream of a device [10], [11], [12]. Turbulence was resolved using either Reynolds-averaged Navier-Stokes [13] or Large Eddy Simulations [14]. However, these approaches require small time steps due to restrictions imposed by explicitly solving the turbine flow, thus placing a high demand on computation. As such, they are not feasible when considering simulation of large arrays of full-scale turbines. In addition, high computational cost restricts simulation of a wide range of incident environmental conditions, which are known, for tidal energy sites, to be highly variable resulting from complex combinations of waves, currents and turbulence. Computations of this nature are often performed using momentum source models.

Momentum source models are able to compute the force distributions along the rotor blades, and determine the overall performance of a turbine. Significantly lower computational requirements and fast processing time can be exploited where many analyses are required. Howland et al. [15] used an actuator disk model, to investigate wake deflections of a turbine under yawed conditions. Their findings suggest that when a turbine is yawed for the benefit of downstream turbines, the curled shape of the wake and its asymmetry must be taken into account since this affects how much of it interacts with the downstream turbines. Baratchi et al. [16] used an actuator line method to study the performance and wake of the tidal turbine in both straight and yawed flow. Their results showed good agreement with the measurements

1
2
3
4
5
6
7
8
9
10
11
12
13
14
15
16
17
18
19
20
21
22
23
24
25
26
27
28
29
30
31
32
33
34
35
36
37
38
39
40
41
42
43
44
45
46
47
48
49
50
51
52
53
54
55
56
57
58
59
60
61
62
63
64
65

76 published in [17]. Gao et al. [18] coupled an actuator line method to large
77 eddy simulations to study the wake characteristics of a turbine under various
78 yaw conditions. They showed that wake skew exacerbates the instability of
79 the tip vortex and causes the wake region to narrow. At lower yaw angles,
80 nacelle vortex radially diffuses and blends with the tip vortex in the far wake
81 whilst at higher yaw angles, the nacelle vortex intercepts the tip vortex in
82 the near wake due to the different spatial distribution of thrust.

83 Despite the valuable insight from these experimental and numerical stud-
84 ies, there is still a gap in the performance and wake details of tidal current
85 turbines in arrays as most of these studies were carried out for either one or
86 two turbines. The wake generated by for example, the front set of turbines
87 in a large tidal turbine farm can cause disturbance to the rear set of turbines
88 in straight flow conditions and significantly increase in angled incoming flow
89 conditions [19]. Very large computational resources are also needed to cap-
90 ture and understand such flow detail. There are also open questions about
91 the wake details, for example, its propagation and extent of recovery in yaw
92 conditions.

93 One particular area of research which has gained momentum in recent
94 years and has been used to compute multiple tidal current turbines in arrays
95 is the Blade Element Theory combined with Computational Fluid Dynamics
96 simulation techniques (BEM-CFD) [20], [21]. The BEM-CFD models utilises
97 radially varying set of turbine blade characteristics, distributed uniformly in
98 an axial direction. Hence, computational cells at the same radius from the
99 turbine centre have the same properties, however, as the flow varies from cell
100 to cell, the resultant forces on the fluid also vary. The model can allow the
101 local environment to be simulated providing a comprehensive study of a tidal
102 farm and wake at a reduced computational cost [22]. The application of tip
103 loss corrections and downwash pertinent to a CFD type model representa-
104 tion takes the BEM-CFD approach further. This extension, the Generalised
105 Actuator Disk (GAD-CFD), has provided confidence when applied to labo-
106 ratory scale flume studies [23]. The GAD-CFD model includes new improved
107 features such as a more concise downwash distribution computation, varia-
108 tion of foil section, application of tip radius correction, variation of lift/drag
109 curves with Reynolds number and surface roughness. The use of analytical
110 methods to successfully and effectively predict the distribution of lift towards
111 the tip of finite wing, have been demonstrated to produce reasonable esti-
112 mates of thrust and power [24]. Allowing for the variation of foil section
113 shape within the model adds to the refinements including the distribution

1
2
3
4
5
6
7
8
9
10
11
12
13
14
15
16
17
18
19
20
21
22
23
24
25
26
27
28
29
30
31
32
33
34
35
36
37
38
39
40
41
42
43
44
45
46
47
48
49
50
51
52
53
54
55
56
57
58
59
60
61
62
63
64
65

114 of forces along the foils. This helps produce slightly better characteristics
115 closer to the rotor hub, and also improved prediction in the stall region of
116 the TSR range. The benefit of the GAD-CFD approach, with respect to
117 computational cost, is unequivocal and allows us to move into the realms of
118 array interaction modelling and site design at a more reasonable level of cost
119 [25].

120 In this work, the effectiveness of the GAD-CFD approach in accurately
121 capturing fluid-machine interaction for multiple tidal energy converters sub-
122 ject to yawed flow conditions is assessed. The GAD-CFD model is first used
123 to simulate a three-turbine array in straight flow, $\beta = 0^\circ$, and the results
124 compared with physical tank-testing conducted at the FloWave facility [26],
125 [27], [28]. Additional simulations are then conducted at yawed angles, $\beta =$
126 4° and 8° to study yaw effects. A second simulation is conducted to further
127 assess the performance of the approach, in terms of the capacity to model
128 multiple full-scale turbines in more varied configuration. The current work
129 extends our previous work in [29], [30] to provide a better understanding of
130 the influence of rotor spacing on the hydrodynamics around devices, leading
131 to optimised performance for large arrays.

132 Finally, as turbulence intensity also impacts the fluid-machine interac-
133 tions associated with the turbine energy production, simulations under straight
134 flow conditions with varying incoming turbulence intensities are also per-
135 formed and analyzed. This demonstrates how the GAD-CFD tool can be
136 useful to developers in real projects.

137

2. Numerical Methodology

2.1. Governing equations

The OpenFOAM toolbox [31] is utilised for the model implementation. The OpenFOAM toolkit provides a range of standard solvers which can be modified for use with the additional turbine physics. The additional GAD source terms are implemented in the steady state Reynolds Averaged Navier Stokes (RANS) “simpleFoam” solver. A more detailed description of the GAD-CFD model including the extended downwash distribution method and coupling strategy is presented in [24-25]. Within the assumption of an incompressible fluid, the set of equations may be written in the form:

$$\frac{\partial \bar{U}_i}{\partial x_i} = 0 \quad (1)$$

$$\frac{\partial \bar{U}_i}{\partial t} + \frac{\partial \bar{U}_i \bar{U}_j}{\partial x_j} = -\frac{1}{\rho} \frac{\partial \bar{P}}{\partial x_i} + \frac{\partial}{\partial x_j} \left(\nu \left(\frac{\partial \bar{U}_i}{\partial x_j} + \frac{\partial \bar{U}_j}{\partial x_i} \right) \right) - \frac{\partial \overline{u_i u_j}}{\partial x_j} + f_i, \quad (2)$$

where x_i represents the Cartesian coordinates (X, Y, Z), U_i is the Cartesian mean velocity components ($\bar{U}_x, \bar{U}_y, \bar{U}_z$) and f_i includes an additional source representing the disc rotor characteristics. The Reynolds stress is $\overline{u_i u_j}$ and must be modeled to close the governing equations by employing an appropriate turbulence model.

The k - ϵ RNG turbulence model [32] has been used for this work. In this model two equations are solved; k represents the energy contained within the turbulent fluctuations, and ϵ represents the dissipation rate of this energy. The equations for the transport of these variables are similar in form to the momentum equations. The model has been credible when applied to flows involving large rotating downstream wakes [33], [34] which is one of the key aspects of the present application. However, the models are also known to sometimes over-predict wake lengths, mainly due to the turbulence dissipation turbulent kinetic energy which can influence the loadings on downstream turbines [35].

3. Case Study 1: Three Turbine Array Turbine

3.1. Turbine arrangements

Using the GAD-CFD model, a three turbine array as shown in Figure 1 is simulated. The hubs of these two upstream turbines are 1 D upstream and

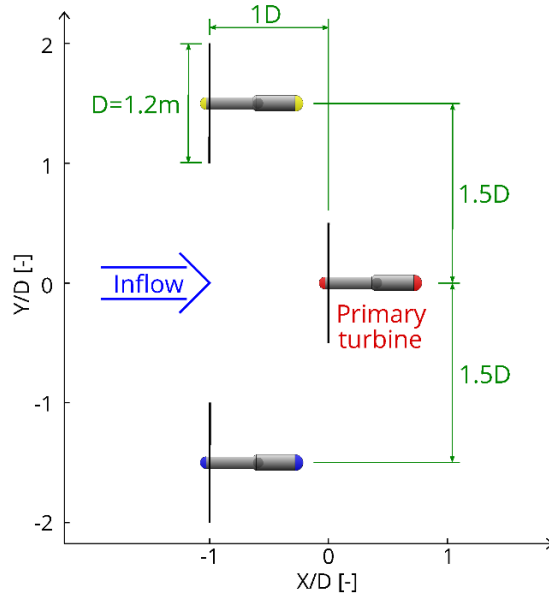


Figure 1: Schematics of the three-turbine array layout (not to scale). Turbine 1 denotes the primary turbine, Turbines 2 and 3 denote the right and left upstream turbines in the inflow direction respectively.

1.5 D either side of the primary turbine, giving a transverse separation of 3 D. This configuration was shown in [25] to accelerate the flow experienced by the rear turbine and improve its performance. Additionally, the front row being only 1 D in front of the primary turbine, means that the rear turbine is not in the wake of the front two turbines. The turbines are generic bed-mounted, fixed-pitch, three-bladed horizontal axis design. The turbine models are 1:15 scale, corresponding to an 18 m diameter prototype. Table 1 summarizes the principal dimensions of the turbines. Turbine rotational speed is set to be the same for all turbines, so that they have a tip speed ratio (TSR), of 7.0 relative to the inlet velocity. The turbine geometries were based on the NACA63812 and 63815 aerofoil sections and a separate CFD study was conducted to determine a set of lift and drag curves curves at a range of Reynolds numbers and turbulence levels required for these sections to use for this study. The chord-length Reynolds numbers vary between 0.5×10^5 (root) and 2.5×10^5 (tip). **Physical tank testing experiments have been conducted in straight flow conditions, $\beta = 0^\circ$. Full details of the experiments can be found in [26].**

Table 1: Three-turbine array dimensions

<i>Parameter</i>	<i>Dimension[m]</i>
Rotor diameter	1.2 (1D)
Nacelle length	1.03
Nacelle diameter, hub to tower	0.12
Nacelle diameter, beyond tower	0.16
Hub height	1.0 (0.83D)
Tower diameter	0.102
Distance from rotor plane to tower axis	0.486 (0.4D)

3.2. Domains and boundary condition

The entire flow field was considered as a result of asymmetry of the flow induced by the oblique motion and rotation induced by the turbines. Turbine yaw angle was achieved by keeping the inflow/domain fixed and rotating the turbines as per the required yaw angle. This technique was automated by employing a script which, when called upon, allows rotation of the turbines within the domain to the required yaw angle. The domain size represents the Flowave tank dimensions, see also Figure 2. The nominal inflow velocity of 0.8 m/s was set at the inlet. This corresponds to a full-scale flow speed of 3.1 m/s. Flow rates are set at the inlet vents. **In the physical tank testing experiments, the turbulence intensity at the turbine location was recorded to be approximately 7% for the flow velocity used [26].** The tank walls are set to zero velocity and wall functions used for k , ϵ , and nut . The top of the domain is set to a full slip condition representing the open fluid surface. The initial conditions are mapped to the boundary conditions in all but velocity. The initial velocity condition is set to zero. The kinematic viscosity ν of this problem is set to $1.6667e^{-6}m^2.s^{-1}$. No roughness parameter was added and the bottom boundary assumed a smooth wall. Table 2 summarizes the computational parameters adopted for this study. Five flow configurations have been investigated, as illustrated in Table 3.

3.3. Grid Generation

The grids were created utilizing both blockMesh and snappyHexMesh in OpenFOAM. First, an initial structured hexahedral background mesh consisting of a block topology structure was generated which captures the domain extents of thirty metres square and four metres deep. The domain is

1
2
3
4
5
6
7
8
9
10
11
12
13
14
15
16
17
18
19
20
21
22
23
24
25
26
27
28
29
30
31
32
33
34
35
36
37
38
39
40
41
42
43
44
45
46
47
48
49
50
51
52
53
54
55
56
57
58
59
60
61
62
63
64
65

Table 2: Computational Parameters

<i>Parameter</i>	<i>Settings</i>
Computing	Astute Linux Cluster ^a
Mesh type	Unstructured hexahedral
Turbulence model	<i>k</i> - ϵ RNG
Pressure velocity coupling	SIMPLE
y^+ average (nacelle)	30
Grad (U) scheme	Gauss linear
Convergence criteria	RMS residual $< 10^{-3}$

Note: Run type and Parallel run (14 partitions run on $2 \times$ dual core nodes). ^a <http://enhpc-wiki.swan.ac.uk>.

Table 3: Simulation Flow Conditions

<i>Yaw, β ($^\circ$)</i>	<i>Turbulence Intensity, TI (%)</i>
0	15
0	25
0	30
4	15
8	15

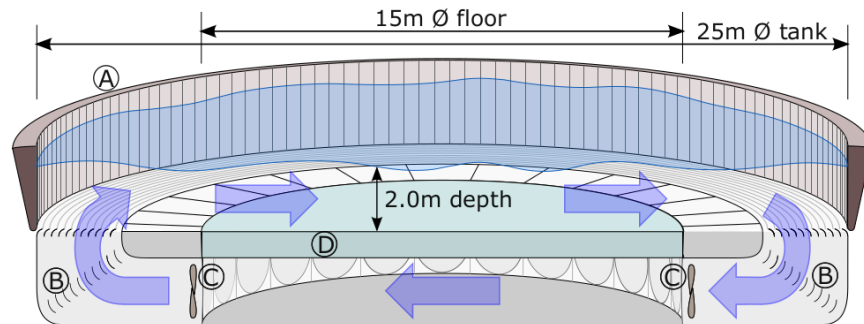


Figure 2: Sectional schematic of FloWave basin showing: (A) wavemaker paddles around circumference; (B) turning vanes and flow conditioning filters; (C) current drive impeller units; (D) buoyant raisable floor (15 mØ) below test area [27].

209 then subdivided using divisions defined in Table 4. With reference to Figure
 210 3, refinement of the mesh around the turbines and wake region is achieved
 211 using the snappyHexMesh utility. The wake region is defined as a cylinder
 212 0.7 metre radius, extending from the rotor to 9 metres downstream, i.e. to
 213 the domain outflow. The refinement level in this region is specified as level
 214 2, the base cell/mesh is subdivided twice in this region (Note 2 in Figure 3).
 215 The rotor assembly and bladebox is set with a refinement level of 5, i.e. Note
 216 5 in Figure 3. The region around the rotor assembly (Note 3 in Figure 3) is
 217 set at level 3 up to 0.1 metres from the assembly. A reasonable level of detail
 218 of the nacelle and support is included in the model as shown in Figure 3.

219 For the mesh independence study an examination of the coefficients of
 220 power, C_P and coefficients of thrust C_T is performed for a single rotor in
 221 straight inflow conditions, $\beta = 0^\circ$. It can be seen in Figure 4 that the
 222 coefficients tend to not change significantly after mesh density G4. Based
 223 on the study, mesh G4 (see Table 4), representing a reasonable compromise
 224 in accuracy and computational cost, was chosen to perform the remaining
 225 studies.

226 3.4. Results

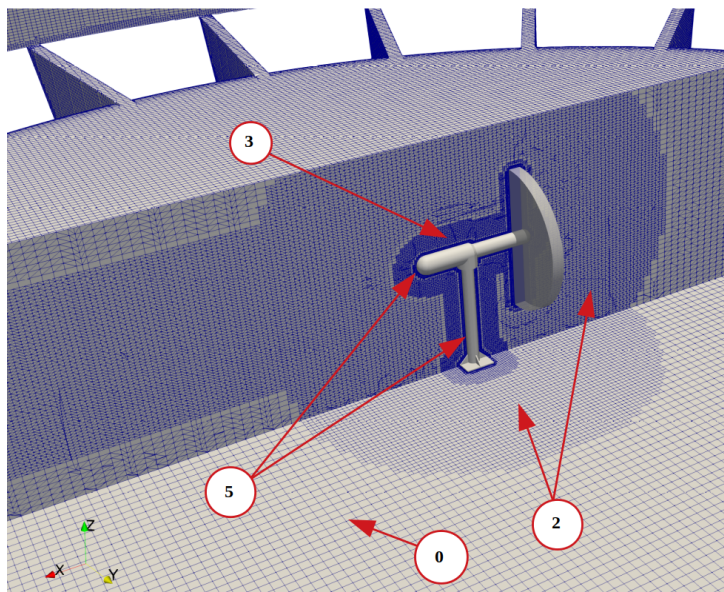
227 3.4.1. Performance at different yaw angles

228 The tidal stream configuration performances at yaw was quantified by
 229 comparing the yaw results with the straight flow cases. Two yawed inflow
 230 cases were considered, i.e. $\beta = 4^\circ$ and 8° . As already pointed out, the turbines
 231 have been fully tested experimentally at $\beta = 0^\circ$ and the results have been

1
2
3
4
5
6
7
8
9
10
11
12
13
14
15
16
17
18
19
20
21
22
23
24
25
26
27
28
29
30
31
32
33
34
35
36
37
38
39
40
41
42
43
44
45
46
47
48
49
50
51
52
53
54
55
56
57
58
59
60
61
62
63
64
65

Table 4: Table of initial mesh subdivisions for the set of meshes studied. The total cell count is post refinement using the snappyHexMesh utility

<i>Mesh</i>	<i>Subdivisions</i>	<i>Total no of cells</i>
G1	100×100×30	95686
G2	200×200×60	766968
G3	300×300×90	2590032
G4	400×400×120	6146016
G5	500×500×150	11998116
G6	600×600×180	20740456



(a)

Figure 3: Mesh topology generated using a combination of “blockMesh” and “snappy-HexMesh” utilities. Note 0 shows the outer/base distribution of cells, while Note 2 shows the level 2 refinements made in the wake region. Note 3 identifies the assembly area refinement, and Note 5 identifies the level 5 assembly region.

232 included for comparison purpose. Figure 5 demonstrates the performance
 233 of all turbines in the array model in terms of C_P and C_T at $TSR = 7$.
 234 Compared to the experiment, GAD-CFD predicts the thrust and power of
 235 the primary rotor (Turbine 1) within 3.5% and 9.5% respectively for $\beta =$
 236 0° . The GAD-CFD model only reports thrust acting directly on the rotor,

1
2
3
4
5
6
7
8
9
10
11
12
13
14
15
16
17
18
19
20
21
22
23
24
25
26
27
28
29
30
31
32
33
34
35
36
37
38
39
40
41
42
43
44
45
46
47
48
49
50
51
52
53
54
55
56
57
58
59
60
61
62
63
64
65

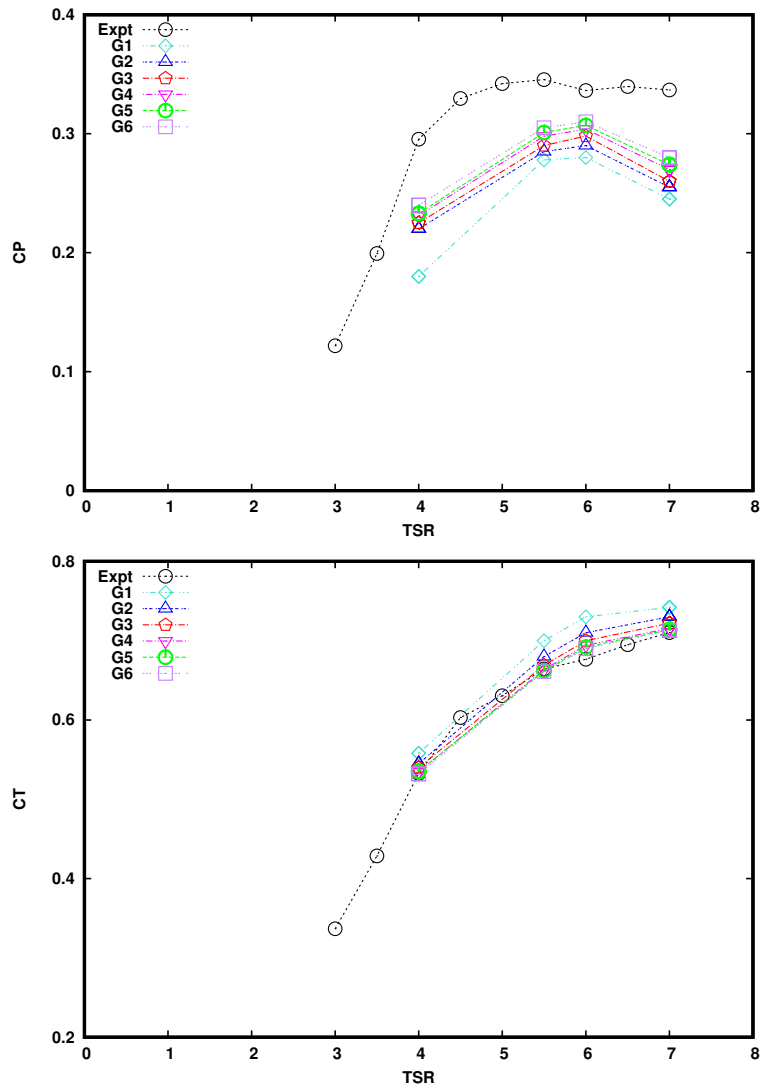


Figure 4: Coefficients of power, C_P (top) and thrust, C_T (bottom) plotted against mesh number from coarsest (G1) to finest (G6).

237 thus a correction needs to be calculated considering the fluid drag acting
238 on the assembly. This issue has been examined in [30] and demonstrated
239 good correlation for the combined results of thrust. RANS based models
240 including the GAD-CFD model are known to under-predict how much of the
241 energy exerted on the turbine will be converted into rotation on the blades

1
2
3
4
5
6
7
8
9
10
11
12
13
14
15
16
17
18
19
20
21
22
23
24
25
26
27
28
29
30
31
32
33
34
35
36
37
38
39
40
41
42
43
44
45
46
47
48
49
50
51
52
53
54
55
56
57
58
59
60
61
62
63
64
65

242 and hence useful power. This has also been reported by [35], [36]. C_P under
243 prediction may also be attributed to variations in local flow directions at
244 the blades and numerical rounding in the model. With this in mind the
245 thrust and power characteristics correlate well and show a similar trend to
246 the observations of the experimental results (see also Figure 4). Compared
247 to the other turbines, the primary rotor (Turbine 1) also produces the most
248 power. This is because it benefits from the accelerated approaching flow
249 from the two upstream turbines (Turbines 2 and 3). Having higher velocities
250 approaching the turbine can result in an increase in the extractable power.

251 The trend in both power and thrust curves for the different angles of
252 yaw are also identical. C_P and C_T decreases as yaw angle increases. This
253 is because as the incoming flow is no longer aligned to the turbine blades, a
254 crossflow is developed across the turbine plane and as the yaw angle increases,
255 the axial component of the velocity reduces, leading to less lift and hence
256 torque. Another problem regarding the reduction in C_P with increase in
257 yaw angle may be attributed to the separation of the nacelle and the flow in
258 the vicinity of the rotor. As yaw increases, the separation at the nose of the
259 nacelle becomes greater. This causes the flow in the vicinity of the turbine to
260 be more turbulent. Lastly, the blockage by the turbines to the flow can be felt
261 upstream, leading to greater deficit in the wake region and a corresponding
262 decrease in power. **The overall power was reduced by 3.0% and 5.0% for $\beta =$**
263 **4° and 8° respectively compared to the $\beta = 0^\circ$ case. Additionally, the thrust**
264 **also reduced by 2.0% to 4.0% for $\beta = 4^\circ$ and 8° respectively compared to the**
265 **$\beta = 0^\circ$ case.** Figure 6 shows the differences in the wake structure structure
266 for the various yaw angles. There is a slight increase in the skewness in
267 the wake as well as a slight decrease in the recovery distance as yaw angle
268 increases. This has also been reported by [10] at a similar TSR value. As
269 the wake propagates downstream, it also deviates slightly from the direction
270 of yaw.

271 Line samples of the velocities were taken downstream (Figure 7) of the
272 primary rotor to capture the fluid characteristics exiting the array for the
273 different yaw angles. The samples were taken at six x/D locations. Results
274 for the $\beta = 0^\circ$ case demonstrates that the wakefield generated by the array
275 compares well with experimental values. For yaw influence, the profiles are
276 different for turbines 2 and 3 compared to the primary turbine in the near
277 wake, i.e $x/D \leq 2.5$. In turbines 2 and 3, there is a shift in the profiles
278 compared to the $\beta = 0^\circ$ profile. However, for the primary turbine (or tur-
279 bine 1), the profiles show similar behaviour. **When tidal arrays experience**

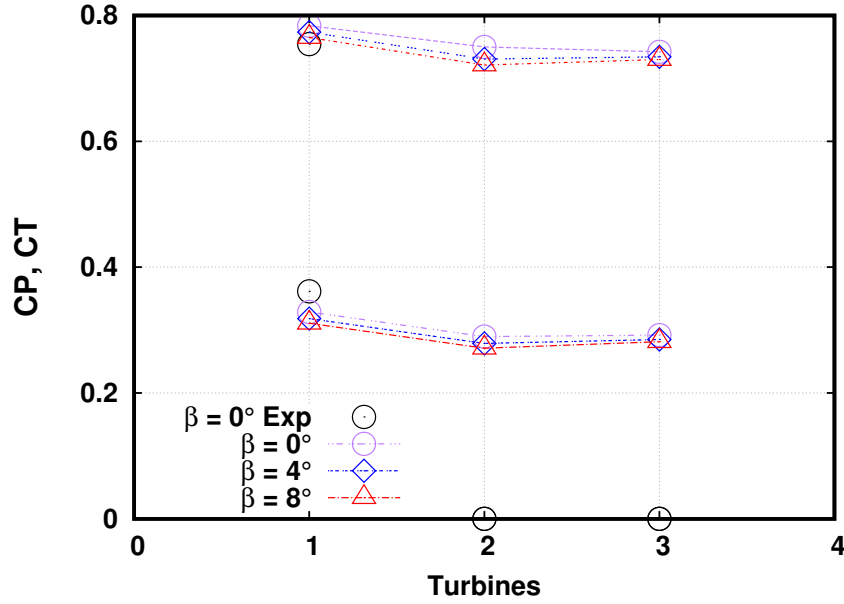


Figure 5: Comparison of coefficient of power C_P (bottom) and coefficient of thrust C_T (bottom) at different yaw angles, $TI = 15\%$, $TSR = 7$.

280 misalignment in flow conditions, the net sideforce will vary more than dur-
 281 ing straight ahead conditions resulting in a decrease in effective inflow angle,
 282 especially to a downstream turbine. At the same time an upstream turbine
 283 can block and straighten the flow to the downstream turbine, leading to a
 284 recovery in effective inflow angle to the downstream turbine. It is possible
 285 that the blockage by the two upstream turbines may have contributed to the
 286 behaviour of the primary turbine profile. Interestingly, for the two upstream
 287 turbines, the plots also show that $\beta = 0^\circ$ has the largest velocity deficit for
 288 turbine 3 whereas it has the smallest velocity deficit for turbine 2.

289 At $x/D > 2.5$ (Figures 7d-f, see also Figure 6), the peak velocity deficits
 290 in the combined or individual wakes is higher for $\beta = 0^\circ$ compared to the
 291 yaw cases. This may be as a results of the higher turbulence levels in the
 292 yawed flow cases.

1
2
3
4
5
6
7
8
9
10
11
12
13
14
15
16
17
18
19
20
21
22
23
24
25
26
27
28
29
30
31
32
33
34
35
36
37
38
39
40
41
42
43
44
45
46
47
48
49
50
51
52
53
54
55
56
57
58
59
60
61
62
63
64
65

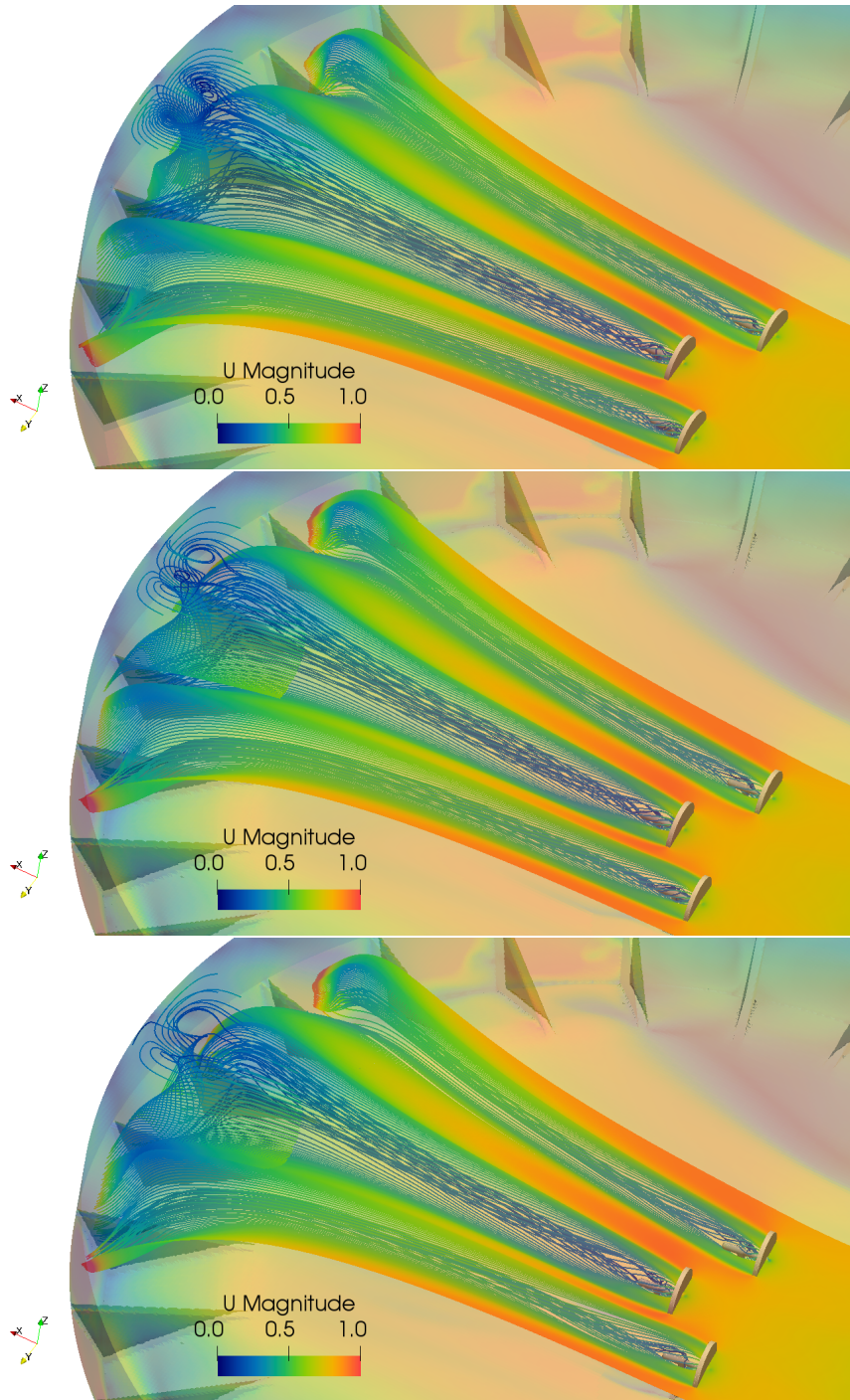


Figure 6: Wake velocity for the three turbine array at different yaw angles. Top to bottom: $\beta = 0^\circ, 4^\circ, 8^\circ$. Note: Increase in yaw angle is in a clockwise direction.

1
2
3
4
5
6
7
8
9
10
11
12
13
14
15
16
17
18
19
20
21
22
23
24
25
26
27
28
29
30
31
32
33
34
35
36
37
38
39
40
41
42
43
44
45
46
47
48
49
50
51
52
53
54
55
56
57
58
59
60
61
62
63
64
65

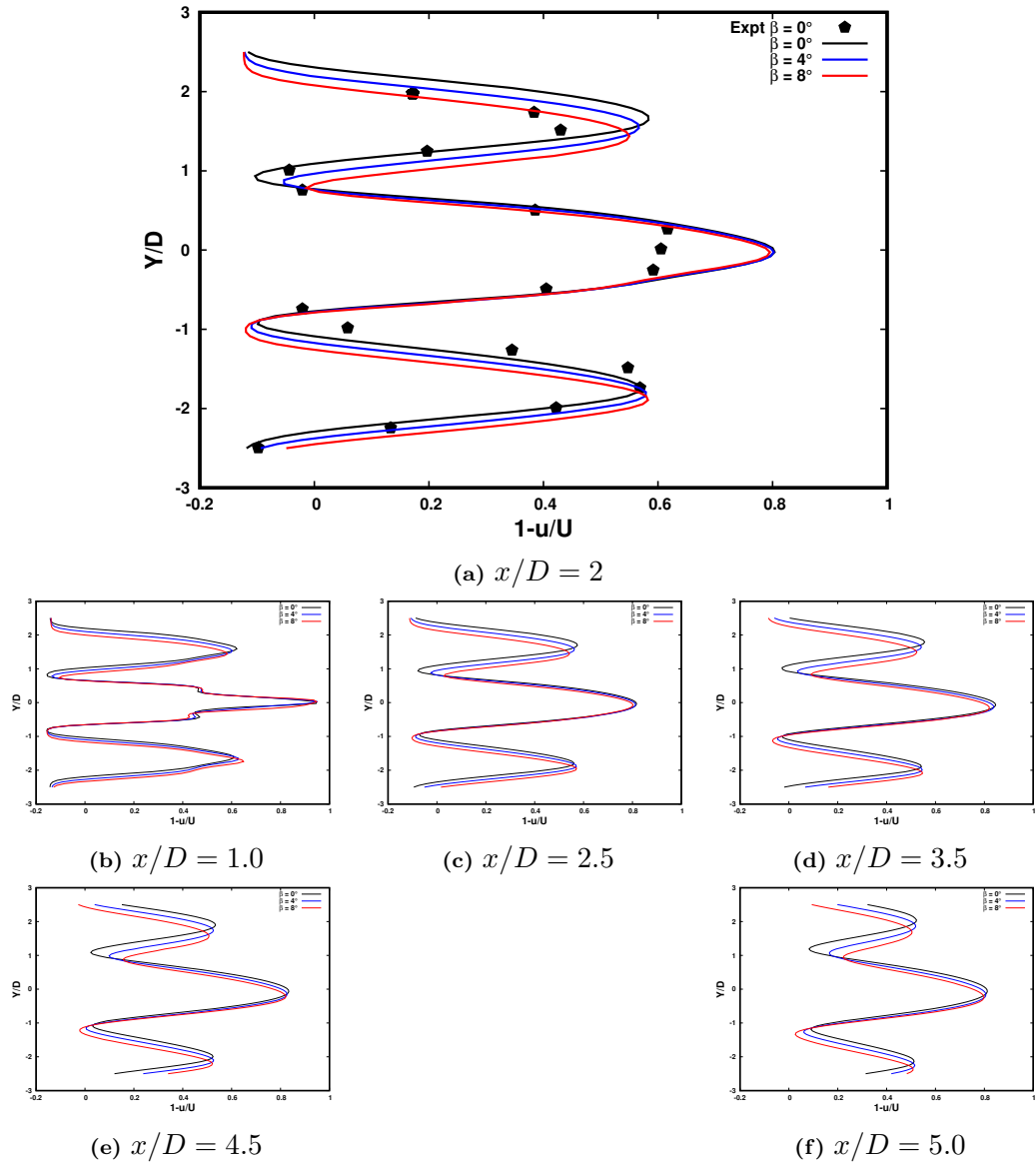


Figure 7: Transverse profiles of normalized downstream axial velocities at three different yaw angles, $\beta = 0^\circ, 4^\circ, 8^\circ$.

1
2
3
4
5
6
7
8
9
293 *3.4.2. Performance at different upstream turbulence intensities, TI 's*

294 Interaction of turbulence with tidal turbines is important if accurate fa-
295 tigue predictions are to be made and turbine reliability optimised. To con-
296 sider the effects of turbulence intensity, the three turbine array is compared
297 with three inlet turbulence intensities, TI 's of 15%, 25% and 30% at $\beta = 0^\circ$.
298 Figure 8 shows turbulence intensity decay variation as they progress down-
299 stream to the turbines. The two upstream turbines (Turbines 2 and 3) are
300 located at $x = -1.2$ m whilst the located of the primary turbine (Turbine 1)
301 is at $x = 0$ m. The plot shows a rapid decay shortly downstream of the inlet
302 as well as close to the turbines. At inlet TI 's of 15%, 25% and 30%, only TI
303 of 7%, 10% and 10.5% respectively were realised at the locations of Turbines
304 2 and 3, corresponding to a 53%, 60% and 65.5% drop in turbulence inten-
305 sity. As seen in Figure 8, the results are consistent with the experimental
306 measurements.

307 Figure 9 shows that increasing the turbulence intensity, TI has little effect
308 on the mean C_P and C_T for the TI 's evaluated in this analysis, with less
309 than 3.5% difference. Previous studies [9], [10] have also shown that the
310 mean C_P and C_T are only slightly dependent on the turbulence intensity at
311 TSR values of $1 \leq \text{TSR} \leq 10$. The results show an increase of 2.0% in power
312 production when inlet TI is increased from 15% to 25% and a further 1.2%
313 from 25% to 30%.

314 Figure 10 shows the wake velocity for the investigated TI 's. The results
315 show similar near wake features, however there are visible differences in the
316 far wake features. Concerning the profiles of velocities calculated downstream
317 of the arrays in Figures 11, it can be seen that, large differences exist between
318 the different turbulence rates (seen more clearly at $x/D > 2$). The maximum
319 deficit was observed for the lowest turbulence rate in all locations with the
320 peak occuring at $x/D = 2.5$. The results suggest that turbulence intensity
321 has little influence on the near wake of the array, but helps to recover the
322 axial velocity in the wake. This finding is consistent with previous research
323 [10].

324 **4. Case Study 2: Multiple Full-scale Turbines in Varied Configu-**
325 **ration**

326 *4.1. Turbine arrangements*

327 A fourteen-turbine array with two different arrangements was also simu-
328 lated. The first is a 4 row arrangement whereby the lateral and longitudinal

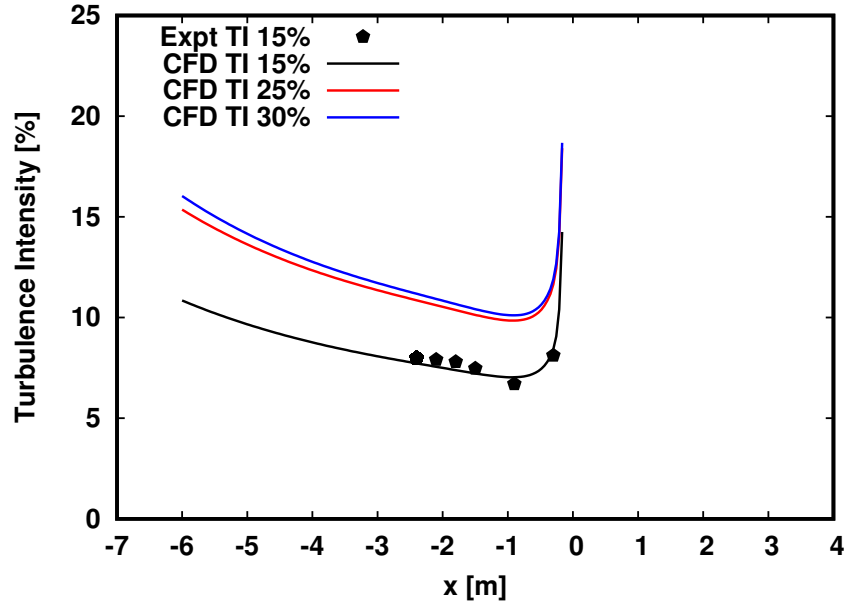


Figure 8: Turbulence intensities decay variation in the three array turbine, TSR = 7.

spacing are 3.0 diameters and 10.0 diameters respectively (regular formation), see top image in Figure 12. These are arbitrary values which have been chosen to reproduce reasonable turbine spacing that may be implemented in a real situation. The second arrangement presented in Figure 12, bottom image shows a different arrangement in which the lateral spacing between devices is increased to 4.0 diameters to maximise the flow acceleration between them (modified formation). The second and third rows have been moved so that they are one diameter away from the first and fourth rows such that the distance between the second and third row is 38.0 diameters. This serves two purposes, firstly the second and fourth rows will benefit from flow acceleration between upstream turbines to a greater extent. Secondly, such an arrangement will also facilitate a greater level of flow recovery before the flow interacts with the third and fourth rows. The turbines are fixed pitch variable speed, running at an optimal TSR of 3.0 based on the inlet velocity. Turbine rotational speed was set to be the same for the turbines, so that they have TSR of 3.0 relative to the inlet velocity. The turbines have a diameter of 10 m which is a reasonable representation of the scale of turbines likely to be deployed in nearshore environments. The chord length and chord twist angle characteristics of the blade are presented in Figure 13.

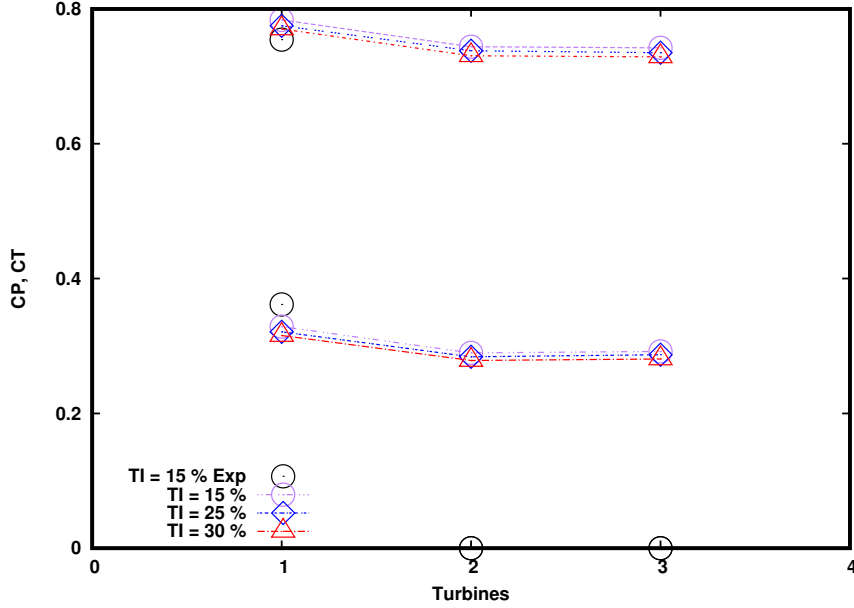


Figure 9: Comparison of coefficient of power C_P (bottom) and coefficient of thrust C_T (bottom) at different upstream turbulence intensities, $TSR = 7$.

348 The rotor geometry, and lift/drag characteristics, are also taken from [29].
 349 The NACA 4424 lift and drag curves are taken from [37] with chord-length
 350 Reynolds numbers varying between 0.2×10^6 (root) and 1.0×10^6 (tip).

351 4.2. Domain and boundary conditions

352 The inflow and outflow plane were located 30 D upstream of the front
 353 turbines and 60 D downstream of the rear turbines respectively. A cuboid
 354 computational domain is employed. The domain is 1200 metres in length
 355 (x-axis). The domain depth is 30 metres (z-axis), while the width is 300
 356 metres (y-axis). **A uniform and steady velocity profile of 3.0 m/s, which is**
 357 **the nominal inflow velocity and turbulence intensities of 1%, 5% and 10%**
 358 **were applied at the inlet of the computation domain.** This is applicable
 359 here as the turbine arrays are placed in a wide channel and therefore only
 360 extract a small fraction of the energy available to them. Future large-scale
 361 generation will undoubtedly require the deployment of hundreds of devices
 362 at high-energy locations. Such locations are fairly limited and hence, the
 363 devices are likely to be packed relatively closely to one another along the
 364 seabed. A high density of tidal turbines will cause excessive resistance to the

1
2
3
4
5
6
7
8
9
365 flow, or in effect an increase in the drag coefficient of the channel, causing a
366 reduction of flow velocities at the devices [38]. Under such circumstances, a
367 different turbine optimisation will be required than for a fixed upstream flow
368 [39], [40].

369 At the outlet boundary a zero gradient was applied. The nacelles and
370 bottom of the domain are set to zero velocity and wall functions used for k ,
371 ϵ , and nut . No roughness parameter was added and the bottom boundary
372 assumed a smooth wall. Five flow configurations, as illustrated in Table 5,
373 were also carried out.

Table 5: Simulation Flow Conditions

Yaw, β ($^\circ$)	$TurbulenceIntensity, TI$ (%)
0	1
0	5
0	10
2	1
8	1

374 *4.3. Grid Generation*

375 All grids were created utilizing both “blockMesh” and “snappyHexMesh”
376 in OpenFOAM version 6.0. The “blockMesh” utility is used to generate an
377 initial block (mesh domain) with size set to $1200\text{m} \times 300\text{m} \times 30\text{m}$ in x , y , and z
378 directions respectively which captures the domain extents. The discretisation
379 does not use any grading in this case thus “simpleGrading” is set to one.
380 Refinement of the mesh around the turbines and wake region is achieved
381 using “snappyHexMesh” utility. The wake region is defined as a cylinder
382 37.5 metre radius, extending from the rotor to 900 metres downstream, i.e.
383 to the domain outflow. The refinement level in this region is specified as level
384 2. The rotor assembly and bladebox is set with a refinement level of 4.

385 Mesh dependency of the simulations within the blade-box and wake re-
386 gions was assessed in [29] and [30] respectively with the turbine operating
387 close to an optimal design TSR of 3.0. Based on the recommendations in
388 these previous studies, subdivisions of $480 \times 120 \times 12$ with total element size
389 of approximately 25M representing a reasonable compromise in accuracy and
390 computational cost, was chosen to perform the remaining studies.

1
2
3
4
5
6
7
8
9
10
11
12
13
14
15
16
17
18
19
20
21
22
23
24
25
26
27
28
29
30
31
32
33
34
35
36
37
38
39
40
41
42
43
44
45
46
47
48
49
50
51
52
53
54
55
56
57
58
59
60
61
62
63
64
65

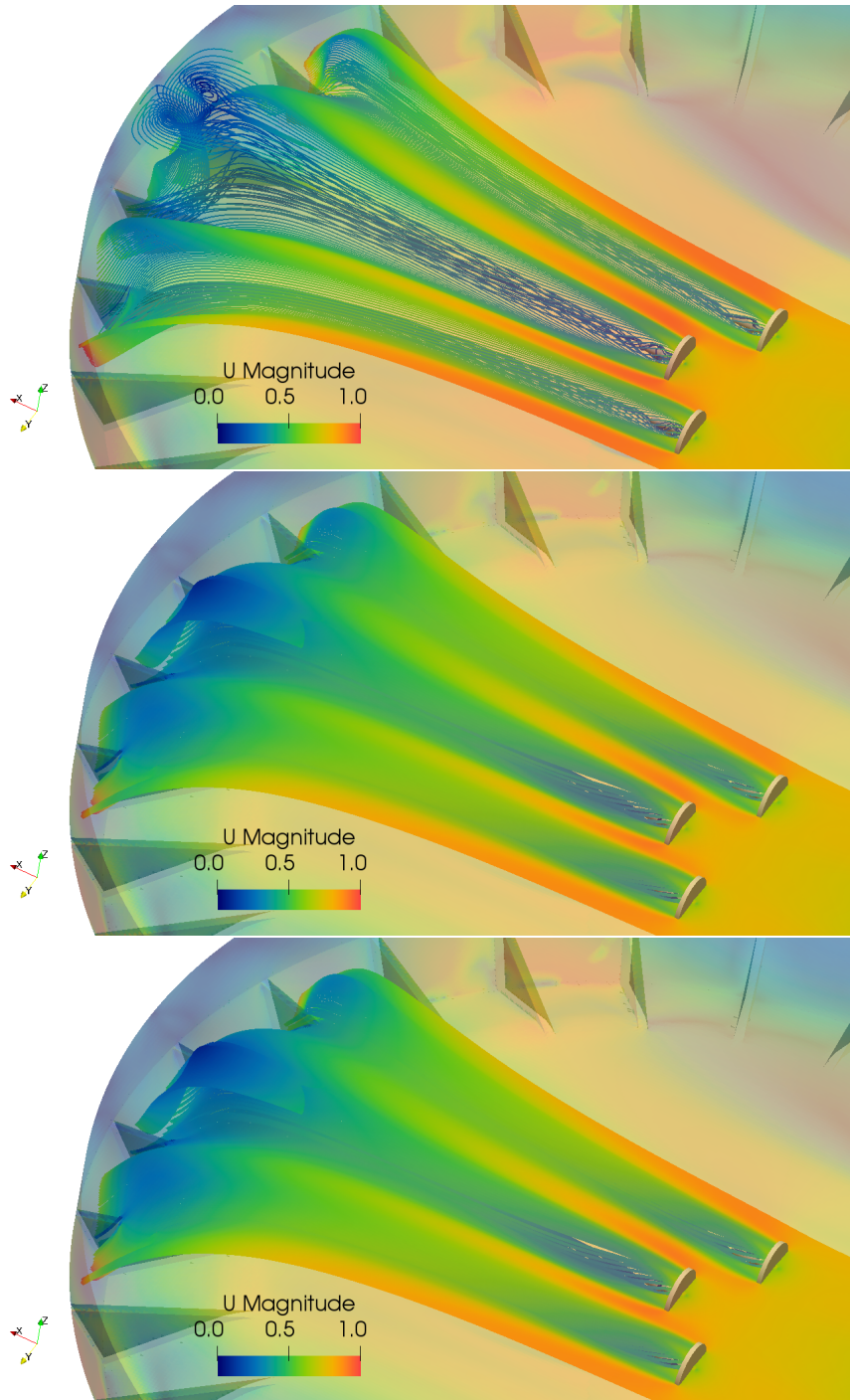
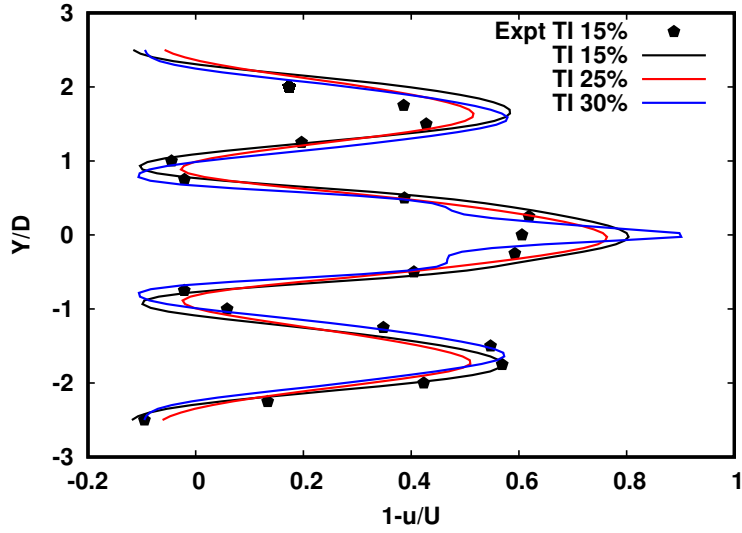
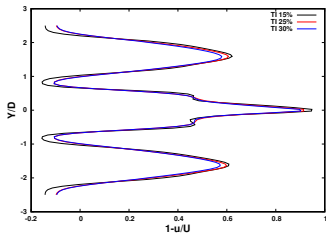


Figure 10: Wake velocity for the three turbine array at different upstream turbulence intensities. Top to bottom: $TI = 15\%$, $TI = 25\%$, $TI = 30\%$.

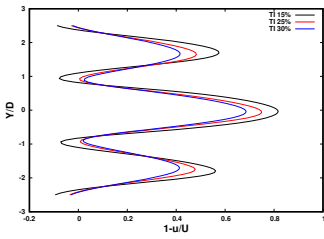
1
2
3
4
5
6
7
8
9
10
11
12
13
14
15
16
17
18
19
20
21
22
23
24
25
26
27
28
29
30
31
32
33
34
35
36
37
38
39
40
41
42
43
44
45
46
47
48
49
50
51
52
53
54
55
56
57
58
59
60
61
62
63
64
65



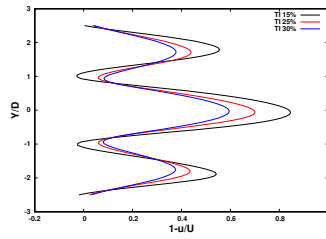
(a) $x/D = 2$



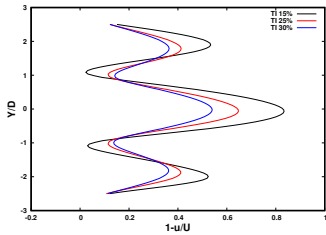
(b) $x/D = 1.0$



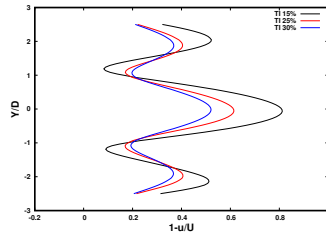
(c) $x/D = 2.5$



(d) $x/D = 3.5$



(e) $x/D = 4.5$



(f) $x/D = 5.0$

Figure 11: Transverse profiles of normalized downstream axial velocities at three different upstream turbulence intensities.

1
2
3
4
5
6
7
8
9
10
11
12
13
14
15
16
17
18
19
20
21
22
23
24
25
26
27
28
29
30
31
32
33
34
35
36
37
38
39
40
41
42
43
44
45
46
47
48
49
50
51
52
53
54
55
56
57
58
59
60
61
62
63
64
65

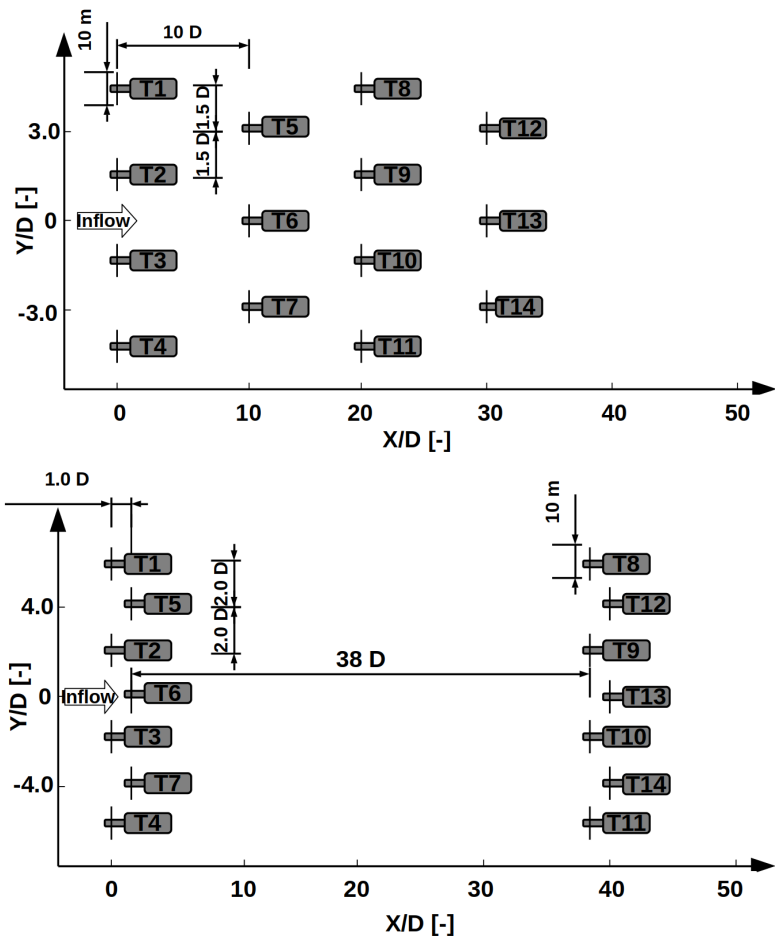


Figure 12: Schematics of the 14-turbine layout: (top) regular formation (bottom) modified formation including rotor numbers (not to scale).

1
2
3
4
5
6
7
8
9
10
11
12
13
14
15
16
17
18
19
20
21
22
23
24
25
26
27
28
29
30
31
32
33
34
35
36
37
38
39
40
41
42
43
44
45
46
47
48
49
50
51
52
53
54
55
56
57
58
59
60
61
62
63
64
65

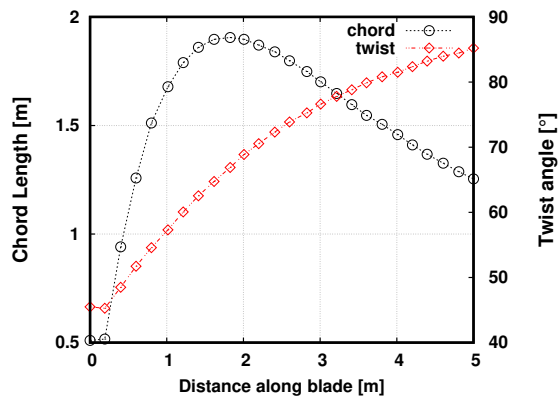


Figure 13: Chord length and twist characteristics of the blades used in the 14-turbine layout analysis.

1
2
3
4
5
6
7
8
9 391 *4.4. Results*

10 392 *4.4.1. Performance at different yaw angles*

11
12 393 This section presents the performance of both regular and modified array
13 394 configurations in straight flow conditions, with inlet turbulence defined by TI
14 395 = 1%. The individual devices within the arrays and the hydrodynamic flow
15 396 structures between the turbines are also evaluated. Figures 14 and 15 present
16 397 the coefficient of power, C_P , and thrust, C_T , for the two configurations at the
17 398 different yaw angles. C_P and C_T were also calculated based on the inflow
18 399 velocity and a fixed TSR. The computed power production at $\beta = 0^\circ$ for
19 400 the front four set of turbines in the modified formation was 1.826MW. At
20 401 $\beta = 2^\circ$ and 8° , the power production reduced to 1.767MW and 1.733MW
21 402 respectively, about 3% and 5% less than the $\beta = 0^\circ$ case. These values are
22 403 significantly less than the 0.06% and 1.0% reduction in C_P that would be
23 404 expected if yaw effects were only assumed to be a function of the decreased
24 405 projected swept area of the turbine. Similar tendencies were observed in the
25 406 regular formation.

26
27
28
29
30 407 There were however large differences in power in the second to fourth
31 408 sets of turbines, more especially turbines 8-14. Starting with the modified
32 409 formation at the higher yaw angle, turbines 8, 9 and 12 were not directly
33 410 affected by the wake of the front set of turbines (i.e turbines 1-7). The inflow
34 411 to these turbines were almost similar to freestream conditions (see also Figure
35 412 17). This resulted in an increase in their C_P values and a further increase
36 413 in C_P for turbine 12 which also took advantage of the bypass flow. All the
37 414 other turbines experienced some disturbances from the wake generated by
38 415 turbines 1-7 and resulted in reduced C_P values with a further decrease in
39 416 C_P in turbines 10 and 11 due to the reduced wake recovery and the smaller
40 417 recovery distance of the upstream turbines (5 and 6). In the $\beta = 2^\circ$ case, all
41 418 rear turbines with the exception of turbine 8 experienced disturbance from
42 419 the wake generated by turbines 1-7. Table 6 shows the computed power for
43 420 each row of turbines at $\beta = 0^\circ$, 2° and 8° . From these values, it can be seen
44 421 that apart from the third row of turbines, power production decreases with
45 422 increase in yaw angle.

46
47
48
49
50 423 Similar tendencies were also found in the regular formation. The pre-
51 424 dicted overall farm power was 5.32MW, 5.25MW, 3.64MW compared to
52 425 5.86MW, 5.83MW, 5.96MW in the modified formation at $\beta = 0^\circ$, 2° and
53 426 8° respectively. Although the overall farm power was higher in the modified
54 427 formation compared to the regular formation for the investigated yaw cases,
55
56
57
58
59
60
61
62
63
64
65

428 interestingly the highest power output was not necessarily obtained for the
 429 modified tidal farm at $\beta = 0^\circ$, but for $\beta = 8^\circ$ in this case. This shows
 430 that for larger tidal farms, the overall power output at yaw that can be ob-
 431 tained compared to the straight flow cases can either increase (or decrease)
 432 since the power output in rows further downstream depends on the orienta-
 433 tion in the first rows. The results also show that strong sensitivity of tidal
 434 farm power output to small variations of the inflow direction exists and this
 435 should be taken into account for optimal control as well as grid integration
 436 of tidal farms. Similar tendencies were observed in the coefficient of thrust
 437 C_T values in Figure 15 where C_T decreases as yaw angle increases due to the
 438 reduced axial component of the velocity rather than the spanwise component
 439 as thrust depends on the axial component.

440 Figures 16 and 17 show the calculated wake velocities for the two config-
 441 urations at the different yaw angles. The overall wake structure, wake width
 442 and expansion rates are similar for all three yaw angles. However, similar to
 443 the three turbine array, there is a slight increase in skewness in the wake and
 444 a decrease in the wake recovery distance at the highest yaw angle, seen more
 445 clearly in the Figure 16.

33 **Table 6:** Power for each row of turbines in the two layouts at different yaw angles, TI =
 34 1%

<i>Configuration</i>	<i>RowNo</i>	$\beta = 0^\circ$	$\beta = 2^\circ$	$\beta = 8^\circ$
Modified	1	1.826MW	1.767MW	1.733MW
Modified	2	1.487MW	1.438MW	1.408MW
Modified	3	1.411MW	1.502MW	1.585MW
Modified	4	1.141MW	1.128MW	1.240MW
Regular	1	1.798MW	1.753MW	1.724MW
Regular	2	1.459MW	1.358MW	0.371MW
Regular	3	1.206MW	1.399MW	1.048MW
Regular	4	0.855MW	0.740MW	0.497MW

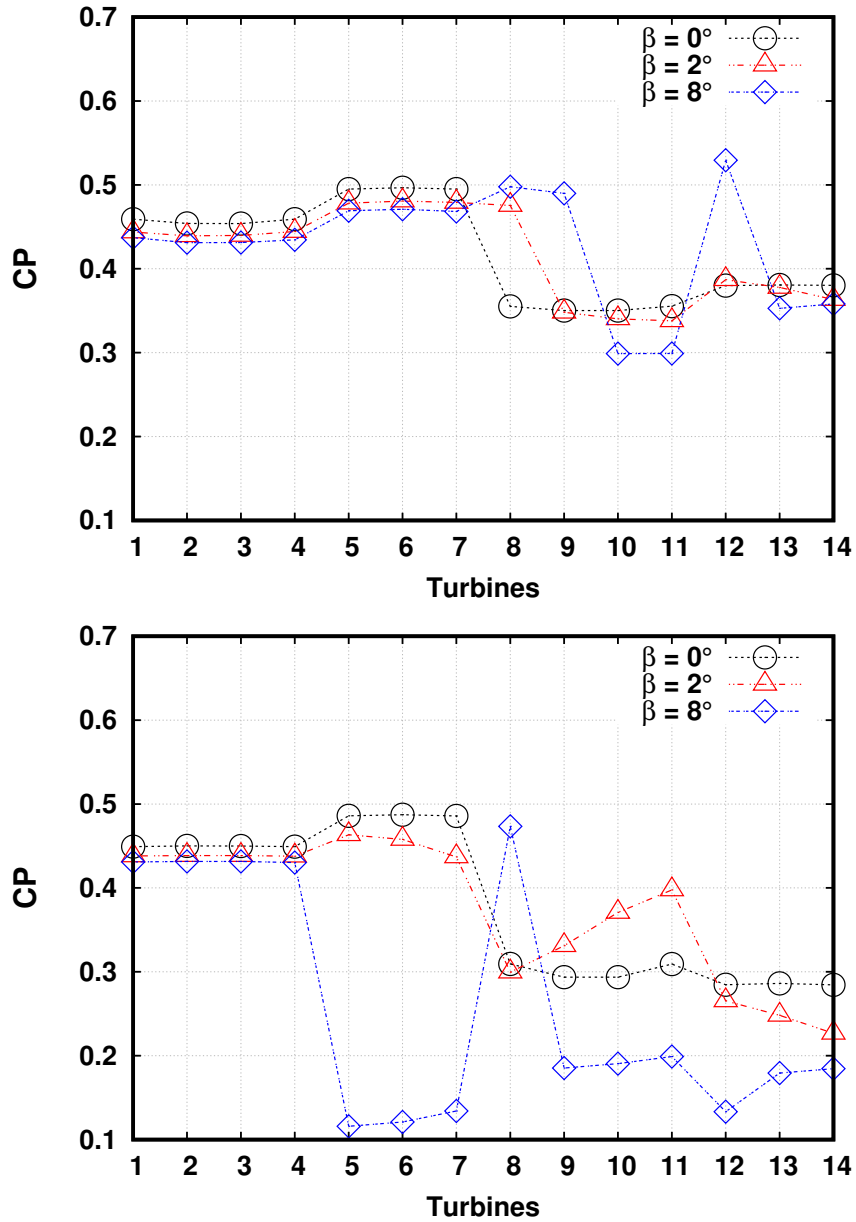


Figure 14: Comparison of coefficient of power C_P for the modified (top) and regular (bottom) configuration at different yaw angles, TI = 1%, TSR = 3.

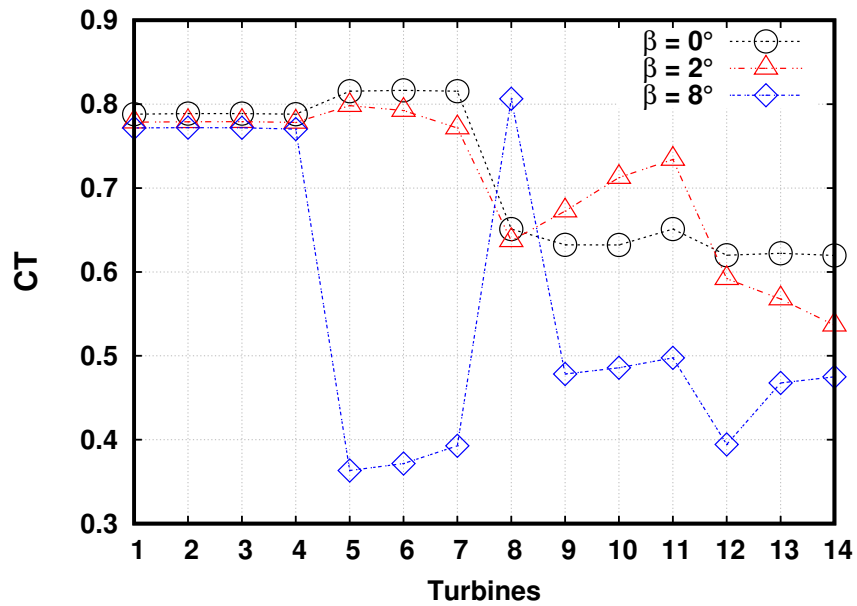
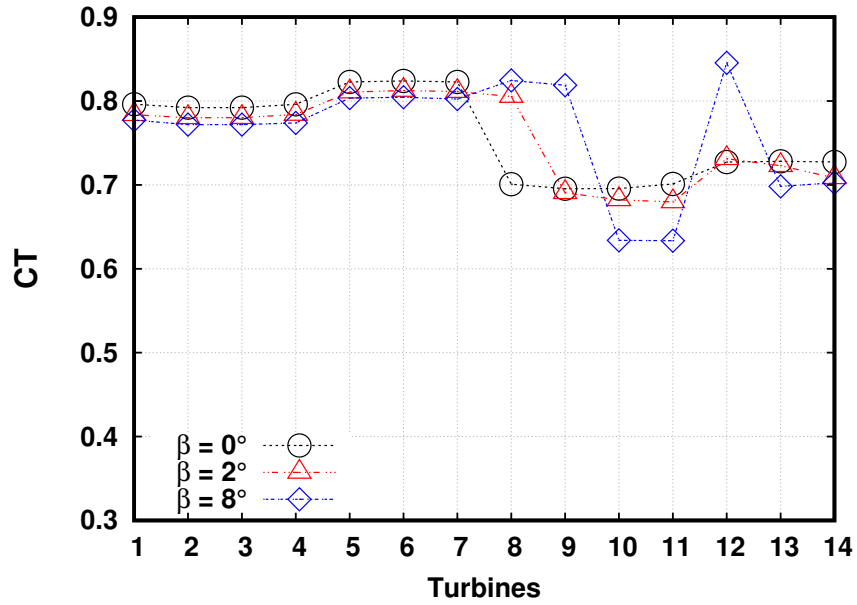


Figure 15: Comparison of coefficient of thrust C_T for the modified (top) and regular (bottom) configuration at different yaw angles, TI = 1%, TSR = 3.

1
2
3
4
5
6
7
8
9
10
11
12
13
14
15
16
17
18
19
20
21
22
23
24
25
26
27
28
29
30
31
32
33
34
35
36
37
38
39
40
41
42
43
44
45
46
47
48
49
50
51
52
53
54
55
56
57
58
59
60
61
62
63
64
65

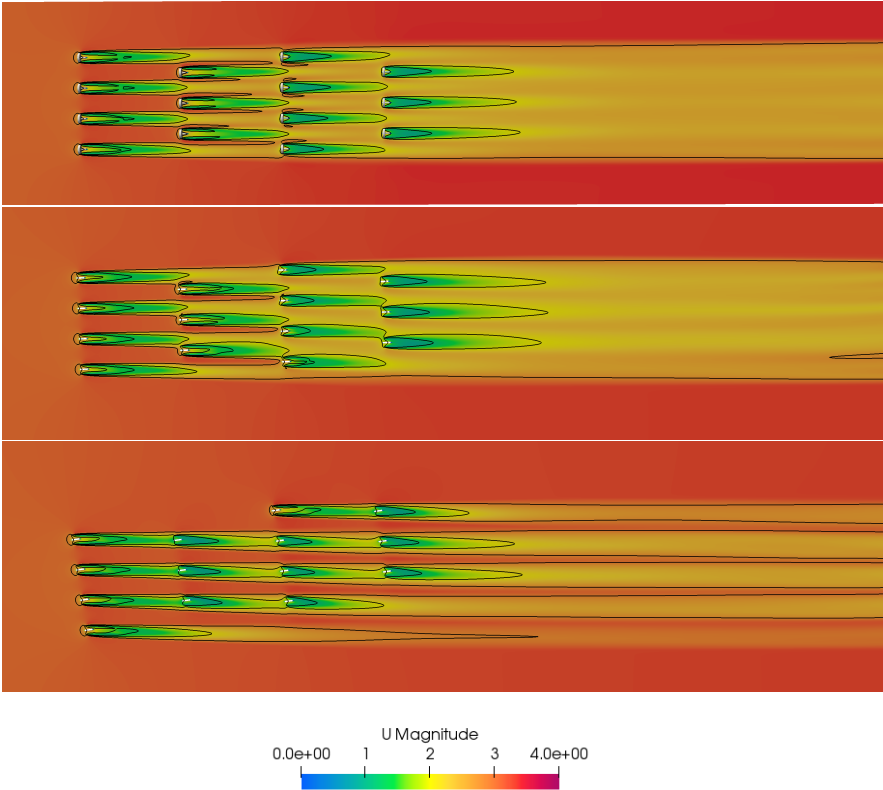


Figure 16: Wake velocity for the regular formation at different yaw angles. Top to bottom: $\beta = 0^\circ, 2^\circ, 8^\circ$, Isolines at 95% inlet velocity.

1
2
3
4
5
6
7
8
9
10
11
12
13
14
15
16
17
18
19
20
21
22
23
24
25
26
27
28
29
30
31
32
33
34
35
36
37
38
39
40
41
42
43
44
45
46
47
48
49
50
51
52
53
54
55
56
57
58
59
60
61
62
63
64
65

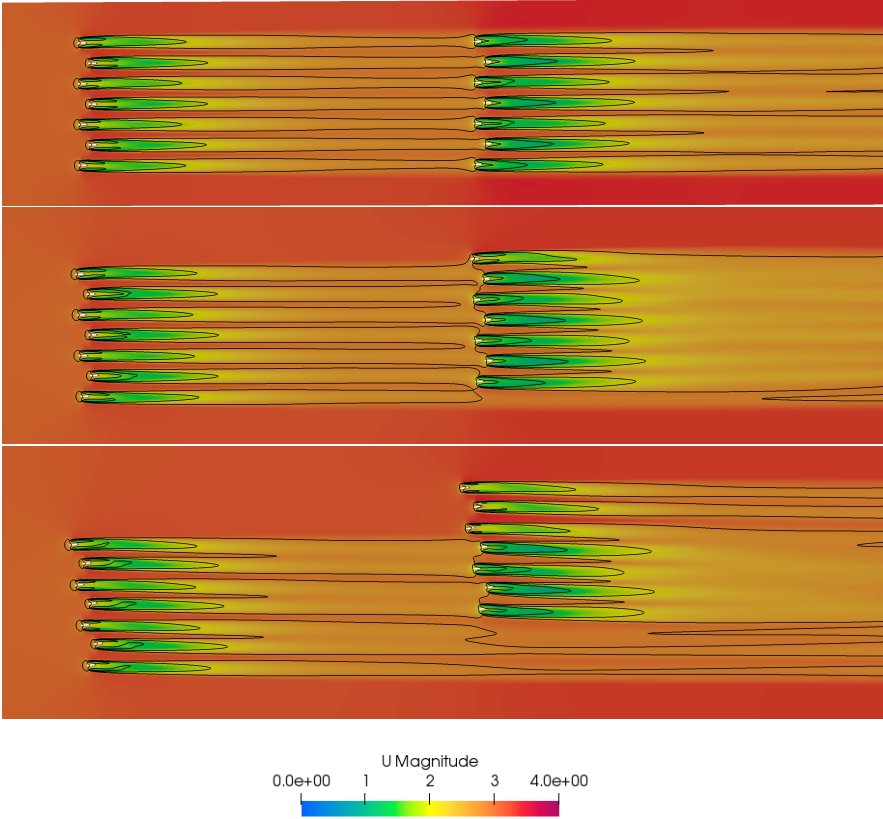


Figure 17: Wake velocity for the modified formation at different yaw angles. Top to bottom: $\beta = 0^\circ, 2^\circ, 8^\circ$, Isolines at 95% inlet velocity.

1
2
3
4
5
6
7
8
9 446 *4.4.2. Performance at different upstream turbulence intensities, TI 's*

10 447 Figures 18 and 19 present the results for power and thrust coefficients
11 448 for the two configurations at three different upstream turbulence intensities,
12 449 $TI = 1\%$, 5% and 10% at $\beta = 0^\circ$. Similar to the three turbine array, for
13 450 the front set of turbines in both configurations, TI has little effect on the
14 451 mean C_P and C_T for the TI 's evaluated in this analysis, with less than
15 452 3% difference. However, a closer inspection of the plots show some visible
16 453 differences, especially in the rear sets of turbines, where it appears that
17 454 increasing the turbulence intensity from 1% to 10% increases both C_P and
18 455 C_T .

19 456 Table 7 shows the computed power production for the first to fourth rows
20 457 of turbines for the modified formation at $TI = 1\%$, 5% and 10% . The results
21 458 show an increase of 11% in power production when inlet TI is increased to
22 459 5% and a further increase of 0.5% in the power production when inlet TI
23 460 is increased to 10% whilst in the regular formation, an increase of 4% in
24 461 power production is observed when inlet TI is increased to 5% and a further
25 462 increase of 7% when inlet TI is increased to 10% . Comparing both modified
26 463 and regular formations, these values corresponds to a 10.26% , 19.75% and
27 464 11.08% increase in overall farm power in the modified formation for $TI =$
28 465 1% , 5% and 10% respectively.

29 466 These results are very important especially as large arrays are likely to be
30 467 deployed in staggered arrangements to maximise the performance of down-
31 468 stream devices and the model results presented here indicate that TI influ-
32 469 ences downstream devices. It is also likely that the force fluctuations, hence
33 470 fatigue loads could also be affected, a factor that is relevant when optimising
34 471 turbine designs to increase reliability. The relatively low values of TI used
35 472 in the analysis will likely be found in strait channels without many features
36 473 that will increase turbulence levels.

37 474 Figures 20-21 show TI influence on the wake velocities for the two con-
38 475 figurations. Again, it can be seen that TI plays a major role in the wake
39 476 details. Both wake length and wake width increase with an increase in TI .
40 477 Near wake features were similar but recovery was more quicker in the higher
41 478 turbulence case. This is seen more clearly in Figure 20 where the wake of
42 479 the front set of turbines recovers quickly as it approaches the rear turbines
43 480 in the higher turbulence case. Turbulence intensity helps to recover the axial
44 481 velocity in the wake and the width of the wake increases with turbulence
45 482 intensity in the far wake, meaning that the arrays will have a wider wake

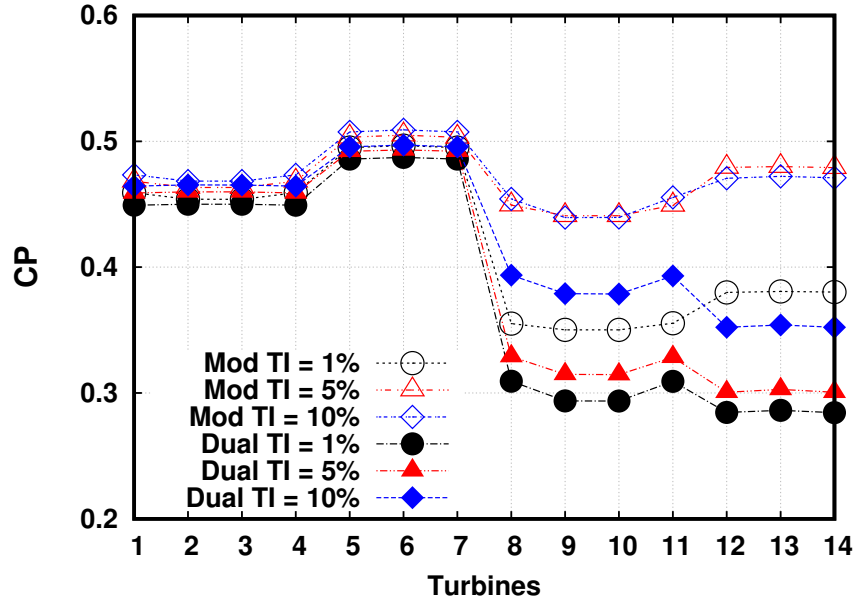


Figure 18: Comparison of coefficient of power C_P for the modified (hollow points) and regular formation (solid points) at three different upstream turbulence intensities.

483 when operating in turbulent environments.

Table 7: Power for each row of turbines in the two layouts at different turbulence intensities.

<i>Configuration</i>	<i>RowNo</i>	TI = 1%	TI = 5%	TI = 10%
Modified	1	1.826MW	1.863MW	1.883MW
Modified	2	1.487MW	1.511MW	1.542MW
Modified	3	1.411MW	1.780MW	1.789MW
Modified	4	1.141MW	1.438MW	1.414MW
Regular	1	1.798MW	1.837MW	1.859MW
Regular	2	1.459MW	1.477MW	1.488MW
Regular	3	1.206MW	1.287MW	1.544MW
Regular	4	0.855MW	0.904MW	1.059MW

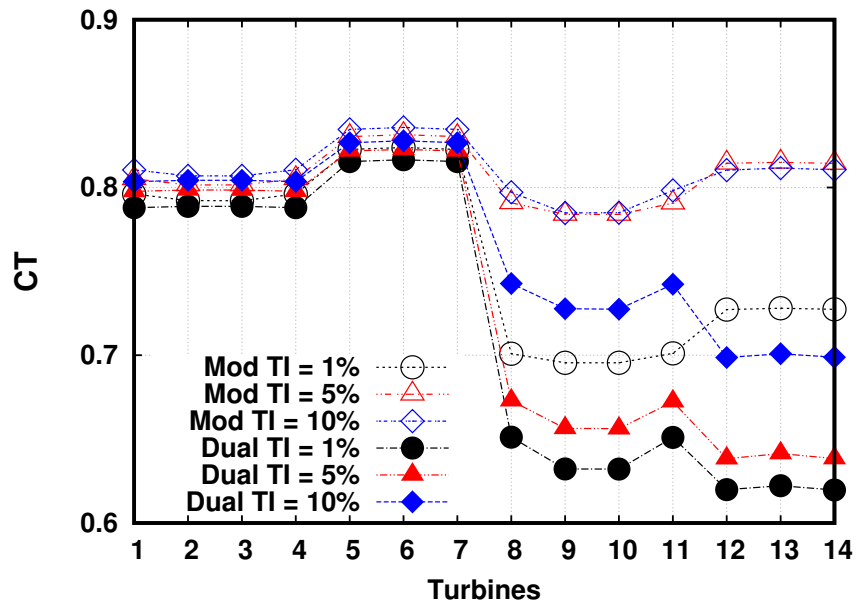


Figure 19: Comparison of coefficient of thrust C_T for the modified (hollow points) and regular formation (solid points) at three different upstream turbulence intensities.

1
2
3
4
5
6
7
8
9
10
11
12
13
14
15
16
17
18
19
20
21
22
23
24
25
26
27
28
29
30
31
32
33
34
35
36
37
38
39
40
41
42
43
44
45
46
47
48
49
50
51
52
53
54
55
56
57
58
59
60
61
62
63
64
65

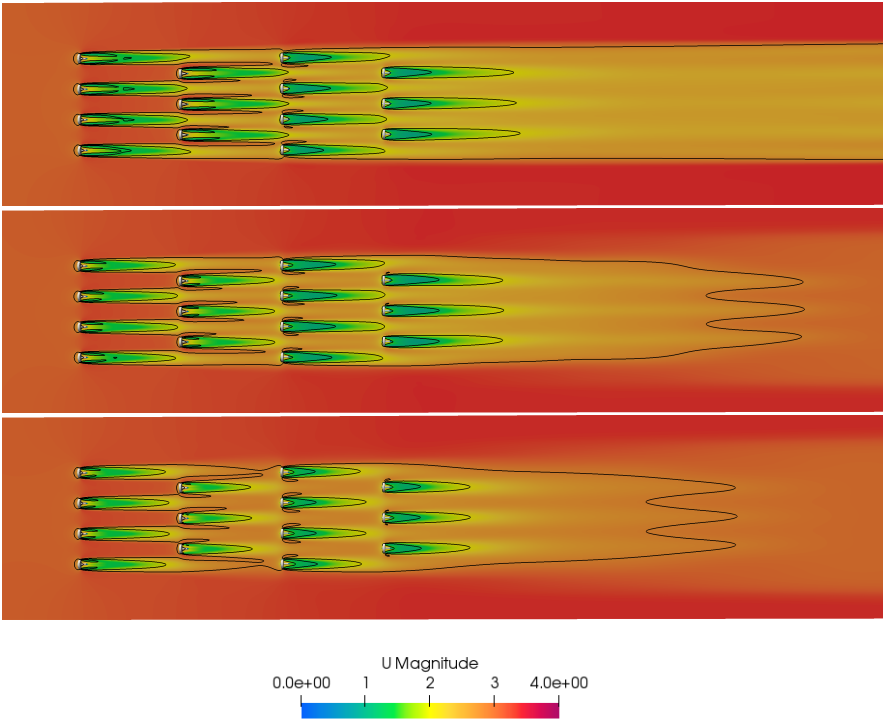


Figure 20: Wake velocity for the regular formation at three different upstream turbulence intensities. Top to bottom: TI = 1%, 5%, 10%, Isolines at 95% inlet velocity.

1
2
3
4
5
6
7
8
9
10
11
12
13
14
15
16
17
18
19
20
21
22
23
24
25
26
27
28
29
30
31
32
33
34
35
36
37
38
39
40
41
42
43
44
45
46
47
48
49
50
51
52
53
54
55
56
57
58
59
60
61
62
63
64
65

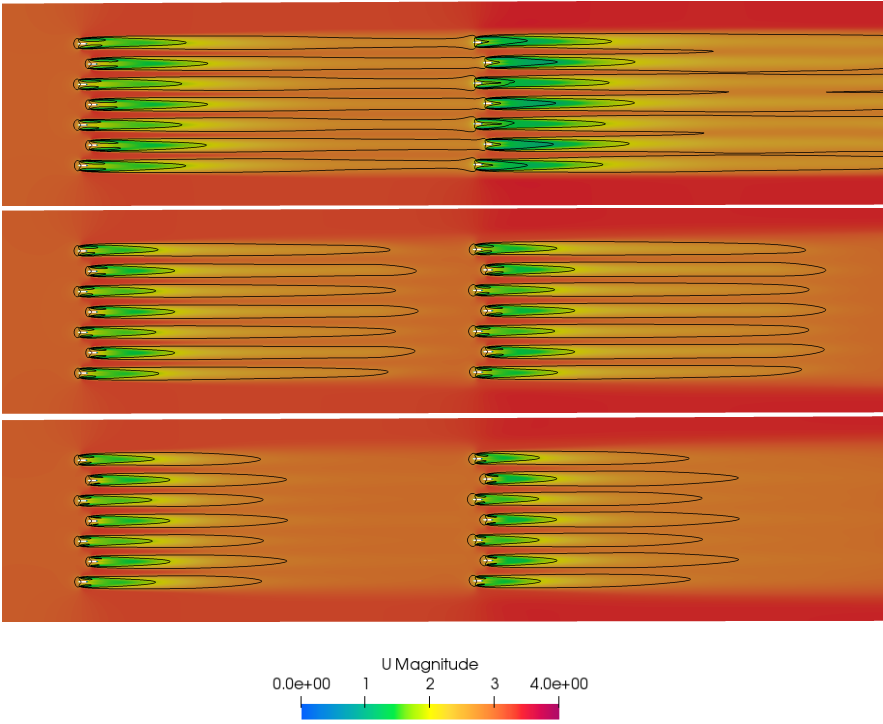


Figure 21: Wake velocity for the modified formation at three different upstream turbulence intensities. Top to bottom: TI = 1%, 5%, 10%, Isolines at 95% inlet velocity.

5. Summary

This paper introduces modelling techniques for better understanding of the performance variations and wake effects of two different tidal stream array configurations. First, a three turbine array was modelled, followed by a fourteen turbine array with standard hypothetical staggered arrangement of four rows with constant lateral and longitudinal spacing of 3.0 and 10.0 diameters respectively. The array layout was then altered by moving the second and third rows so they are 1D from the first and fourth rows. A performance study was conducted by comparing the thrust and power coefficients under varying effects of yaw angles and upstream inflow turbulence. A summary of the important findings are outlined below:

5.1. Yawed flow

5.1.1. Three turbine array

- The performance characteristics for the straight flow in the three turbines array are in close agreement with previous studies [26].
- **Power and thrust decreased as yaw was increased.**
- Yaw was found to have minimal effect on the individual wakes, however small increase in skewness and decrease in recovery was found at the higher yaw angle compared to the straight flow case.
- Yaw resulted in a shift in the wake plots. However, the profile of the primary turbine show similar behaviour with the straight flow in the near wake. Interestingly, for the two upstream turbines, the plots also show that $\beta = 0^\circ$ has the largest velocity deficit for turbine 3 whereas it has the smallest velocity deficit for turbine 2 in the near wake. It is possible that this might be a feature of the complex tank velocity rather than yaw.

5.1.2. Fourteen turbine array

- **Compared to the regular staggered configuration at $\beta = 0^\circ$, the total power output of the modified array was increased by over 10%. Wake recovery to freestream was also better in the modified formation compared to the regular staggered configuration.**

1
2
3
4
5
6
7
8
9
10
11
12
13
14
15
16
17
18
19
20
21
22
23
24
25
26
27
28
29
30
31
32
33
34
35
36
37
38
39
40
41
42
43
44
45
46
47
48
49
50
51
52
53
54
55
56
57
58
59
60
61
62
63
64
65

- 515 • Lateral spacing between devices in straight flow conditions affected the
516 rate of flow recovery downstream. It was shown that for lateral spacing
517 of 4D there was faster downstream recovery compared to the 3D. This
518 is relevant in the context of large arrays where further devices may be
519 placed downstream.
- 520 • Similar to the three turbine array, power and thrust coefficient decrease
521 with increase in yaw angle in the front set of turbines. However, the
522 results are non-linear with the move away from optimal TSR in com-
523 bination with reduced upstream U to the rear turbines.
- 524 • Depending on the yaw angle, most of the individual devices downstream
525 were directly affected by the wakes of the upstream devices, resulting
526 in reduced power and thrust. However, few of the devices experienced
527 inflow conditions similar to the freestream resulting in power and thrust
528 increases.
- 529 • Strong sensitivity of tidal-farm power exists even to small variations
530 of inflow direction. This is relevant for optimal control as well as grid
531 intergration of tidal farms.

532 *5.2. Upstream turbulence intensities: Three and Fourteen turbine array*

- 533 • Turbulence intensity was found to decay rapidly shortly downstream
534 of the inlet which is consistent with experimental data.
- 535 • Turbulence intensity helps in recovery of axial velocity in the wake.
- 536 • Wake width increases with turbulence intensity in the far wake, mean-
537 ing that arrays will have a wider wake when operating in turbulent
538 environments.
- 539 • Turbulence intensity had little effect on the thrust and power of the
540 front set of devices in the array. It is important to stress that each of
541 these results have been obtained using a fixed TSR and a time averaged
542 representation of the flow. It is likely that using the local TSR's at the
543 turbines as well as a transient model could influence the results.

1
2
3
4
5
6
7
8
9
544 **6. Conclusions and Future Work**

545 In conclusion, an efficient method for simulating tidal stream energy con-
546 verter rotor response to realistic inflow and turbulence intensity conditions
547 and capturing the subsequent impact to farfield flow structure using a GAD-
548 CFD approach has been demonstrated. Model validation against experi-
549 mental testing has been conducted and the results show that large array
550 layouts influence on the flow around a downstream device is complex both in
551 straight and yawed flow and would be difficult to characterise using simple
552 empirical relationship. The results could help understand/improve array con-
553 figurations. Further validation of the model would be recommended as more
554 experimental data becomes available and the model improved to account for
555 more complex flow details. However, the study provides confidence that the
556 approach can be applied to a range of scenarios; both laboratory scale, and
557 large scale deployments in both the marine and wind environments.

558 Due to the computational efficiency, such an approach, especially when
559 compared to fully resolved turbine geometry models, makes the GAD-CFD
560 technique suitable for modelling arrays consisting of a large number of rotors
561 and for conducting multiple model runs under varying tidal and machine-
562 operating-point conditions. It is therefore appropriate to also consider the
563 model for studying tidal stream arrays and their interaction with respect to
564 local topography and power control.

565 Since tidal energy could play an important role in decarbonising electricity
566 generation it is important to have access to efficient and accurate engineering
567 tools such as the one developed here (which sits between highly detailed blade
568 resolved models and larger scale oceanographic and atmospheric models).
569 Improved modelling will reduce the technical risk of operating these devices
570 in the highly energetic marine environment thus increasing economic viability
571 of the sector.

572 Future work should focus on improving the model to account for changing
573 lift and drag characteristics at higher levels of free stream turbulence. As
574 turbulence levels increase, the quantity of lift and drag changes, as does the
575 stall point relative to angle of attack, and post stall features significantly
576 change. The model could also be combined with turbine control algorithms
577 that consider power capping through stall or pitch control to enable the study
578 of rotors. Other factors that will also affect device performance in natural
579 environments such as bathymetric effects and bottom roughness need to be
580 included as this will assist in improving existing methods for performance

1
2
3
4
5
6
7
8
9
10
11
12
13
14
15
16
17
18
19
20
21
22
23
24
25
26
27
28
29
30
31
32
33
34
35
36
37
38
39
40
41
42
43
44
45
46
47
48
49
50
51
52
53
54
55
56
57
58
59
60
61
62
63
64
65

581 prediction.

582 Beyond this immediate application the developers seek to develop and
583 incorporate more realistic bathymetry characterisations, which is expected
584 to be an important factor in real-world turbine array operation. It is the
585 authors intention to publish the implementation of the model to enable such
586 studies to take place.

587 **Acknowledgements**

588 This work was supported by the SELKIE project funded by the Euro-
589 pean Regional Development Fund through the Ireland Wales Cooperation
590 programme.

1
2
3
4
5
6
7
8
9
591 **References**

- 592 [1] A. Bahaj, A. Molland, J. Chaplin and W. Batten, "Marine current en-
593 ergy conversion: the dawn of a new era in electricity production," *Philos*
594 *Trans A Math Phys Eng Sci.* vol. 371, p. 20120500, 2013.
- 595 [2] The Crown Estate, "UK Wave and Tidal Key Re-
596 source Areas Project," *Tech. Rep. Version 2.* 2018.
597 <http://www.thecrownestate.co.uk/>, Retrieved: May 2018.
- 598 [3] M. Piano, S. P. Neill, M. J. Lewis, P. E. Robins, M. R. Hashemi,
599 A. G. Davies, S. L. Ward and M. J. Roberts, "Tidal stream resource
600 assessment uncertainty due to flow asymmetry and turbine yaw mis-
601 alignment," *Energy.* vol. 114, pp. 1363-1375, 2017.
- 602 [4] M. Adaramola and P. Krogstad, "Experimental investigation of wake
603 effects on wind turbine performance," *Renewable Energy.* vol. 36, pp.
604 2078-2086, 2011.
- 605 [5] P. W. Galloway, L. E. Myers and A. S. Bahaj, "Experimental and nu-
606 merical results of rotor power and thrust of a tidal turbine operating at
607 yaw and in waves," *In: World renewable energy congress.* Linkoping,
608 Sweden: May 8-13, 2011.
- 609 [6] P. W. Galloway, L. E. Myers and A. S. Bahaj, "Quantifying wave and
610 yaw effects on a scale tidal stream turbine," *Renewable Energy.* vol. 63,
611 pp. 297-307, 2014.
- 612 [7] F. Maganga, G. Germain, K. King, G. Pinon and E. Rivoalen, "Ex-
613 perimental study to determine flow characteristic effects on marine cur-
614 rent turbine behaviour," *Proc of the Euro Wave and Tidal Energy Conf.*
615 2009.
- 616 [8] C. Zhang, J. Zhang, A. Angeloudis, Y. Zhou, S. Kramer and M. Piggott,
617 "Physical modelling of tidal stream turbine wake structures under yaw
618 conditions," *Energies.* vol. 16, pp. 1742, 2023.
- 619 [9] P. Modali, N. S. Kolekar and A. Banerjee, "Performance and Wake
620 Characteristics of a Tidal Turbine under Yaw," *Int J. of Marine Eng.*
621 vol. 1, pp. 41-50, 2018.
- 622 [10] W. Tian, J. VanZwieten, P. Pyakurel and Y. Li, "Influences of yaw
623 angle and turbulence intensity on the performance of a 20 kW in-stream
624 hydrokinetic turbine," *Energy.* vol. 111, pp. 104-116, 2016.
- 625 [11] C. Tongchitpakdee, S. Benjanirat and L. Sankar, "Numerical simulation
626 of the aerodynamics of horizontal axis wind turbines under yawed flow
627 conditions," *J. Sol Energy Eng.* vol. 127, pp. 464-474, 2005.

- 1
2
3
4
5
6
7
8
9
10
11
12
13
14
15
16
17
18
19
20
21
22
23
24
25
26
27
28
29
30
31
32
33
34
35
36
37
38
39
40
41
42
43
44
45
46
47
48
49
50
51
52
53
54
55
56
57
58
59
60
61
62
63
64
65
- 628 [12] T. O’Doherty, A. Mason-Jones, D. M. O’Doherty, C. Byrne, I. Owen
629 and Y. X. Wang, “Experimental and computational analysis of a model
630 horizontal axis tidal turbine,” *Proc of the Euro Wave and Tidal Energy
631 Conf.* 2009.
- 632 [13] D. O’Doherty, A. Mason-Jones, T. O’Doherty, C. Byrne, I. Owen and
633 W. Wang, “Considerations of improved tidal stream turbine perfor-
634 mance using double rows of contra-rotating blades,” *Proc of the Euro
635 Wave and Tidal Energy Conf.* 2009.
- 636 [14] J. McNaughton, S. Rolfo, D. Apsley, I. Afgan, T. Stallad and P. Stansby,
637 “Turbulent flow and loading on a tidal stream turbine by LES and
638 RANS,” *Int J of Heat and Fluid Flow.* vol. 75, pp. 96-108, 2013.
- 639 [15] M. Howland, J. Bossuyt, M. Tossas, J. Meyers and C. Meneveau, “Wake
640 structure in actuator disk models of wind turbines in yaw under uniform
641 inflow conditions,” *J of Renewable and Sustainable Energy.* vol. 8, 2016.
642
- 643 [16] R. Baratchi, T. L. Jeans and A. G. Gerber, “Actuator line simulation
644 of a tidal turbine in straight and yawed flows,” *Int J. of Marine Eng.*
645 vol. 19, pp. 235-255, 2017.
- 646 [17] A. Bahaj, A. Molland, J. Chaplin and W. Batten, “Power and thrust
647 measurements of marine current turbines under various hydrodynamic
648 flow conditions in a cavitation tunnel and a towing tank,” *Renew. En-
649 ergy.* vol. 32, pp. 407-426, 2007.
- 650 [18] Z. Gao, Y. Li, W. Tongguang, S. Wenzhong, Z. Xiaobo, S. Prbsting,
651 D. Li and R. Li, “Modelling the nacelle wake of a horizontal-axis wind
652 turbine under different yaw conditions,” *Renewable Energy.* vol. 172,
653 pp. 263-275, 2021.
- 654 [19] C. Schulz, P. Letzgus, T. Lutz and E. Kramer, “CFD study on the
655 impact of yawed inflow on loads, power and near wake of a generic wind
656 turbine,” *Wind energy.* vol. 20, pp. 253-268, 2017.
- 657 [20] R. Malki, A. Williams, I. Masters, M. Togneri and T. N. Croft, “A
658 coupled blade element momentum-Computational fluid dynamics model
659 for evaluating tidal stream turbine performance,” *Applied Mathematical
660 Modelling.* vol. 37, pp. 3006-3020, 2013.
- 661 [21] S. Turnock, A. Phillips and R. Nicholls-Lee, “Modelling tidal current
662 turbine wakes using a coupled RANS-BEMT approach as a tool for
663 analysing power capture of arrays of turbines,” *Ocean Eng.* vol. 38, pp.
664 1300-1307, 2011.

- 1
2
3
4
5
6
7
8
9
10
11
12
13
14
15
16
17
18
19
20
21
22
23
24
25
26
27
28
29
30
31
32
33
34
35
36
37
38
39
40
41
42
43
44
45
46
47
48
49
50
51
52
53
54
55
56
57
58
59
60
61
62
63
64
65
- 665 [22] A. Olczak, T. Stallard, T. Feng and T. Stansby, "Comparison of a RANS
666 blade element model for tidal turbine arrays with laboratory scale mea-
667 surements of wake velocity and rotor thrust," *J. Fluids Struct.* vol. 64,
668 pp. 87-106, 2014.
- 669 [23] M. Edmunds, A. Williams and I. Masters, "Power Shedding from Stall
670 and Pitch Controlled Tidal Stream Turbines.," *Proc of 11th Euro Wave
671 and Tidal Eng Conf.* 2017.
- 672 [24] M. Edmunds, I. Masters, A. Banerjee, A. Williams and J. H. VanZwi-
673 eten, "A Spatially Nonlinear Generalised Actuator Disk Model for the
674 Simulation of Horizontal Axis Wind and Tidal Turbines," *Energy.* vol.
675 194, 2020.
- 676 [25] C. Badoe, M. Edmunds, A. Nambiar, A. Williams, B. Sellar, A. Kiprakis
677 and I. Masters, "Robust Validation of a Generalised Actuator Disk CFD
678 Model for Tidal Turbine Analysis using the FloWave Ocean Energy Re-
679 search Facility," *Renewable Energy.* vol. 190, pp. 232-250, 2022.
- 680 [26] D. Noble, S. Draycott, A. Nambiar, B. Sellar, B. Steynor and
681 A. Kiprakis, "Experimental Assessment of Flow, Performance, and
682 Loads for Tidal Turbines in a Closely-Spaced Array," *Energies.* 2020.
- 683 [27] D. Noble, T. Davey, H.C.M. Smith, P. Kaklis, A. Robinson and T. Bruce,
684 "Characterisation of spatial variation in currents generated in the
685 FloWave Ocean Energy Research Facility," *Proc of 11th Euro Wave and
686 Tidal Eng Conf.* 2015.
- 687 [28] D.R.J. Sutherland, D. Noble, T. Davey, J. Steynor, T.A.D. Davey and
688 T. Bruce, "Characterisation of Current and Turbulence in the FloWave
689 Ocean Energy Research Facility," *Ocean Eng.* vol. 139, pp. 103-115,
690 2017.
- 691 [29] R. Malki, I. Masters, A. Williams and T. N. Croft, "Planning tidal
692 stream turbine array layouts using a coupled blade element momentum-
693 computational fluid dynamics model," *Renewable energy.* vol. 63, pp.
694 46-54, 2014.
- 695 [30] M. Edmunds, A. Williams, I. Masters and T. N. Croft, "An enhanced
696 disk averaged CFD model for the simulation of horizontal axis tidal
697 turbines," *Renewable energy.* vol. 101, pp. 67-81, 2017.
- 698 [31] H. G. Weller, G. Tabor, H. Jasak and C. Fureby, "A tensorial ap-
699 proach to computational continuum mechanics using object-oriented
700 techniques," *Comp in Phys.* vol. 12, pp. 620-631, 1998.
- 701 [32] G. S. Payne, T. Stallard and R. Martinez, "Design and manufacture of a
702 bed supported tidal turbine model for blade and shaft load measurement

1
2
3
4
5
6
7
8
9
10
11
12
13
14
15
16
17
18
19
20
21
22
23
24
25
26
27
28
29
30
31
32
33
34
35
36
37
38
39
40
41
42
43
44
45
46
47
48
49
50
51
52
53
54
55
56
57
58
59
60
61
62
63
64
65

703 in turbulent flow and waves,” *Renewable energy*. vol. 107, pp. 312-326,
704 2017.

705 [33] C. Badoe, X. Li, A. Williams and I. Masters, “Computational Fluid Dy-
706 namics Modelling of Tidal Turbine Arrays in a Demonstration Site,” *Proc*
707 *of the Int Conf on Renewable Energies Offshore (RENEW 2022)*. 2022.

708

709 [34] C. Badoe, X. Li, S. Armstrong, A. Williams and I. Masters, “Tidal
710 stream turbine arrays in a demonstration site using GAD-CFD mod-
711 els,” *Proc of the 9th Conf on Comp Methods in Marine Eng (Marine*
712 *2021)*. 2021.

713 [35] T. Ebdon, T. O’Doherty, A. Mason-Jones and D. M. O’Doherty, “Sim-
714 ulating marine current turbine wakes with advanced turbulence mod-
715 els,” *Proc of the 3rd Asian Wave and Tidal Energy Conference*. 2016.

716

717 [36] W. M. J. Batten, M. E. Harrison and A. S. Bahaj, “Accuracy of the
718 actuator disc-RANS approach for predicting the performance and wake
719 of tidal turbines,” *Phil Trans of the Royal Soc A: Maths, Phys and Eng*
720 *Sci*. 2013.

721 [37] I. Abbott and A. Von Doenhoff, “Theory of Wing Sections, Including a
722 Summary of Airfoil Data, no. 1 in Dover Books on Aeronautical Engi-
723 neering Series,” *Dover Publications*. 1959.

724 [38] C. Garrett and P. Cummins, “The power potential of tidal currents in
725 channels,” *Proc Royal Soc A*. vol. 461, pp. 2563-2572, 2005.

726 [39] R. Vennell, “Tuning turbines in a tidal channel,” *J Fluid Mech*. vol.
727 663, pp. 253-267, 2010.

728 [40] R. Vennell, “Tuning tidal turbines in-concert to maximise farm effi-
729 ciency,” *J Fluid Mech*. vol. 671, pp. 587-604, 2011.



Click here to access/download

LaTeX Source Files

Latex_files.zip

